"Polymeric Ionic Liquids Based on Asymmetrically *N*-substituted Polybenzimidazoles for Gas Permeation Studies"

Thesis submitted to AcSIR

For the Award of the Degree of

DOCTOR OF PHILOSOPHY

In

CHEMICAL SCIENCES

By

Sayali Vinayak Shaligram
(Registration Number: 10CC11J26057)

Under the guidance of
Dr. Ulhas K. Kharul

POLYMER SCIENCE AND ENGINEERING DIVISION
CSIR-NATIONAL CHEMICAL LABORATORY
PUNE-411008, INDIA

December 2015

सीएसआयआर–राष्ट्रीय रासायनिक प्रयोगशाला
(वैज्ञानिक तथा औद्योगिक अनुसंधान परिषद)
डॉ. होमी भाभा मार्ग, पुणे – 411 008. भारत
CSIR-NATIONAL CHEMICAL LABORATORY
(Council of Scientific & Industrial Research)
Dr. Homi Bhabha Road, Pune - 411008. India

Certificate

This is to certify that the work reported in this Ph.D. thesis entitled "**Polymeric Ionic Liquids Based on Asymmetrically *N*-substituted Polybenzimidazoles for Gas Permeation Studies**" submitted by **Ms. Sayali V. Shaligram** to Academy of Scientific and Innovative Research (AcSIR) in the fulfillment of the requirements for the award of the Degree of **Doctor of Philosophy in Chemical Sciences**, embodies original research work under my supervision. I further certify that this work has not been submitted to any other University or Institution in part or full for the award of any degree or diploma. Research material obtained from other sources has been duly acknowledged in the thesis. Any text, illustration, table etc., used in the thesis from other sources, have been duly cited and acknowledged.

Research Guide

Dr. Ulhas Kharul

Communications Channels
NCL Level DID : 2590
NCL Board No. : +91-20-25902000
Four PRI Lines : +91-20-25902000
FAX
Director's Office : +91-20-25902601
COA's Office : +91-20-25902660
SPO's Office : +91 20 25902664
WEBSITE
www.ncl-india.org

Declaration by the Candidate

I declare that the thesis entitled "**Polymeric Ionic Liquids Based on Asymmetrically *N*-substituted Polybenzimidazoles for Gas Permeation Studies**" is my own work conducted under the supervision of Dr. U. K. Kharul, at Polymer Science and Engineering Division, National Chemical Laboratory, Pune. I further declare that to the best of my knowledge, this thesis does not contain any part of work, which has been submitted for the award of any degree either of this University or any other University without proper citation.

Research Student

(Sayali Vinayak Shaligram)

Dedicated to my parents
Thank you for supporting all my decisions

Acknowledgements

The completion of Ph. D. dissertation was a long journey. It is aptly said that "Life is what happens" when you are completing your dissertation. I have finished my dissertation but not alone. I would have lost without the invaluable support of several. Without these supporters, especially the select few I'm about to mention, I may not have stood where I am today.

First and foremost, I would like to thank Dr. Ulhas Kharul, my research advisor. It's difficult for me to state my gratitude to him for accepting me in his research group and introducing me to the wonderful and exciting world of membrane science. He has not only taught me how to identify interesting directions in the academic research, prepare appealing figures, analyze and present data but also how to hold high research standards. I take this opportunity to express my deepest gratitude to Dr. P. P. Wadgaonkar who was always there to listen patiently and give valuable advice. Dr. Wadgaonkar was my co-advisor in the initial stages of my research work. The long discussions with him thought me how to question thoughts, express ideas scientifically and become an independent researcher. Knowing him, one can rarely stay untouched with his natural simplicity and infectious enthusiasm.

I am indebted to my DAC committee members: Dr. Ashish Lele, Dr. Rahul Banerjee, Dr. Ashutosh Kelkar and Dr. Prashant Kulkarni, for timely reviews as well as invaluable comments which helped in improving my work. I would like to thank Mr. K. V. Pandare, Dr. C. Ramesh, Dr. Rajmohan, Dr. Neelima Bulakh, Mrs. Dhoble, Mrs. Sangita, Mrs. Purvi, Mr. Saroj for their guidance in characterization facilities.

I want to give special thanks to my lab mates Harshal, Anita, Anand and Bishnu for their constant encouragement and without whom the lab would have been a lonely world to me. I truly enjoyed the discussions with them. I would like to thank Dr. Rupesh Bhavsar, Dr. Bhausaheb Tawade, Dr. Savita Varma, Dr. Prakash Sane for providing me early on with the lab fundamentals. I followed their every move in hopes of learning the fundamentals that I could apply to my project. At this stage I cannot forget my all other lab members Rahul, Bhavana, Sachin K., Ritesh, Sachin G., Dharmaraj, Anuja, Ashwini, Nilesh, Sagar, Vinaya, Manisha, Deepti, Sneha D., Nikita, Smita, Divya, Amay, Rishit, Majid, Sneha T., Prajakta, Varsha, Krishna, Bhushan, Sudhir, Ganesh, Prakash, Vasanti,

Madhur, Shlok, Shruthi, Shilpa, Kreeti, Deekshith, Deepika, Arun, Taran, Kiran, Rohit, Ramendra, Praveen, Prashant, Sagar Patil, Hemchandra ,Harsha, Godavari, Supriya, Kanhu, Shabeeb, Chetana, Vrushali, Sunil, Vijay, Jagdish, Bharat, Shraaddha, Indravadan, Deepshikha, Rupali, Aarti, Durgaprasad, Nitin, Abhijit, Amol, Nagnath, Sachin P., Sachin K., Samadhan, Kavita, Vikas, Deepak, Sachin S. and Uday. I would like to mention special thanks to Mr. Swaraj Singh for his assistance during my work. The group has been a source of friendship and good advice.

I cannot find the words to truly thank where my basic source of life energy resides: mother and father. They provided unconditional love and support throughout my PhD pursuit. They were my shining lights when it seemed like there was darkness. This degree is as much theirs as it is mine.

Sayali Vinayak Shaligram

Contents

*	List of Schemes	i
*	List of Figures	ii
*	List of Tables	ix

Chapter 1 Introduction and literature survey

1.1	**Need for CO_2 separation**	1
1.2	**Established methods for CO_2 separation**	2
	1.2.1 Absorption	3
	1.2.2 Adsorption	3
	1.2.3 Cryogenic distillation	3
	1.2.4 Membrane based separation	4
1.3	**Gas transport through nonporous polymeric membranes**	4
	1.3.1 Transport in rubbery polymers	7
	1.3.2 Transport in glassy polymers	7
1.4	**Factors effecting gas permeation properties in glassy polymers**	10
	1.4.1 Effect of polymer properties	
	1.4.2.1 Chain packing density	11
	1.4.2.2 Chain and subgroup mobility	12
	1.4.2.3 Polarity	12
	1.4.2.4 Crosslinking	12
	1.4.2.4 Crystallinity	12
	1.4.2 Effect of penetrant properties on permeability and permselectivity	13
	1.4.2.1 Condensability of gas molecules	13
	1.4.2.2 Size and shape of gas molecules	13
	1.4.3 Effects of operational conditions	14
	1.4.4 Effects of membrane preparation parameters	15
1.5	**Selected commercially relevant polymers for CO_2 separation**	16
	1.5.1 Polysulfones	17
	1.5.2 Cellulose acetates	17

1.5.3 PPO 18
1.5.4 Polyimides 18
1.6 Challenges in polymeric membrane materials for gas separation 19
1.6.1 Plasticization 19
1.6.2 Physical aging 20
1.6.3 Permeability/selectivity tradeoff (the upper bound) 20
1.7 Emerging membrane materials 22
1.7.1 Ionic Liquids (ILs) for CO_2 separation 23
1.7.2 CO_2 capture by room-temperature ionic liquids (RTILs) 24
1.7.3 CO_2 capture by task-specific ionic liquids (TSILs) 25
1.7.4 Supported ionic-liquid membranes (SILMs) for CO_2 separation 25
1.8 Polymeric Ionic Liquids 26
1.8.1 Synthesis of PILs 27
1.8.1.1 Polymerization of IL monomers 27
1.8.1.2 Chemical modification of existing polymers 27
1.9 Applications of PILs 28
1.10 CO_2 separation performance 29

Chapter 2 Scope and objectives 39

Chapter 3 Experimental

3.1 Monomers and materials
3.2 Synthesis 43
3.2.1 PBI Synthesis 43
3.2.2 *N*-Substitution of PBIs 44
3.3.3 *N*-Quaternization of *N*-Substituted PBIs 46
3.3.4 Anion exchange of *N*-Quaternized PILs 46
3.3 Polymer Characterizations 48
3.3.1 Solvent solubility, WAXD analysis and density 48
3.3.2 Spectral characterizations 48
3.3.3 Thermal characterizations 49
3.4 Membrane preparation 49

3.4.1 Dense membrane preparation 49
3.4.2 Ultrafiltration (UF) membrane preparation 49
3.4.3 TFC membrane preparation 50
3.5 Gas permeation analysis 50
3.5.1 Gas sorption 50
3.5.2 Permeation analysis 52
3.5.3 Estimation of diffusivity coefficient 54
3.6 Mixed gas permeation 54

Chapter 4 Variations in '*N*-substituent' of PILs in an asymmetric manner: Investigations on physical and gas permeation properties

4.1 Introduction 55
4.2 Synthesis of PILs and their characterization by spectroscopic techniques 55
4.3 Physical properties 60
4.3.1 Solvent solubility, WAXD analysis and density 61
4.3.2 Thermal stability of PILs 64
4.4 Gas sorption properties 67
4.4.1 Sorption parameters 70
4.4.2 Sorption coefficients 73
4.5 Gas permeation properties 73
4.5.1 Effects of variation in *N*-substituent of PIL 75
4.5.2 Effects of variation in anion
4.6 Effect of asymmetric substitution on gas permeation properties 76
4.7 Conclusions 82

Chapter 5 Incorporation of rigid polyaromatic substituents in PBI based PILs: Effects on gas permeation and nitroexplosive detection properties

5.1 Introduction 83

5.2. Synthesis of PILs and their characterization by spectroscopic techniques 84
5.3 Physical Properties 86
5.3.1 Solvent solubility, WAXD analysis and density 87
5.3.2 Thermal stability of PILs 88
5.4a Gas sorption 90
5.5a Gas permeability 93
5.5.1a Effects of variation in *N*-substituent 93
5.5.2a Effects of variation in the anion
5.5.3a Comparison with PBI based PILs and other common polymers 97
5.6a Conclusions 97
5.4b Optical properties 100
5.4.1b UV spectra 100
5.4.2b Fluorescence measurements 101
5.5b Solution state sensing properties of nitroaromatics 102
5.6b Solid state sensing properties of nitroaromatics 105
5.6.1b Fluorescence quenching in thin films 105
5.6.2b Reversibility of the quenching process 108
5.7b Conclusions 109

Chapter 6 Effect of bulky anions on physical and Gas Permeation Properties of PILs based on PBI

6.1 Introduction 110
6.2 Synthesis of PILs and their characterizations 110
6.3 Physical properties 111
6.3.1 Solvent solubility, WAXD analysis and density 111
6.3.2 Thermal stability of PILs 114
6.4 Gas sorption properties 115
6.4.1 Sorption parameters 115
6.4.2 Sorption coefficients 116
6.5 Gas permeation properties 118
6.6 Conclusions 120

Chapter 7 Polymeric ionic liquid membranes for separation of olefin/paraffin

7.1 Introduction 122
7.2 Dense membrane properties 123
7.3 UF membrane properties 126
7.4 Properties of thin film composite (TFC) membranes 126
7.4.1 Effect of UF support properties on gas permeance of TFC membrane 126
7.4.2 Effect of coating solution concentration 128
7.5 Mixed gas permeation properties 130
7.6 Conclusions 131

Chapter 8 Conclusions 132

References 136
Synopsis 145
List of publications 149

List of Schemes

Scheme No.	Description	Page No.
Scheme 3.1	Synthesis of PBI by condensation of DAB with aromatic dicarboxylic acids	44
Scheme 3.2	Synthesis of PILs with different substituents	45
Scheme 3.3	Anion exchange of PILs based on PBI-BuI and PBI-HFA	47
Scheme 3.4	Anion exchange of PILs based on PBI-BuI with bulky anions	47

List of Figures

Figure No.	Description	Page No.
Figure 1.1	Solvent absorption of CO_2	2
Figure 1.2	Simple membrane separation tube	4
Figure 1.3	Time-lag measurement of gas permeation	6
Figure 1.4	Schematic representation of gas diffusion through polymer matrix	8
Figure 1.5	Schematic representation of polymeric glassy state depicting the matrix and the microvoids [Tsujita (2003)]	8
Figure 1.6	Schematic representations of dual-mode sorption [Tsujita (2003)]	9
Figure 1.7	Plot of log *D* versus 1/FFV for diffusion of He, H_2 O_2, N_2, CO_2, and CH_4, in various polymers [Thran (1999)].	11
Figure 1.8	Effect of penetrant characteristics on diffusion and solubility selectivities [Koros (1992)]	14
Figure 1.9	Plasticization induced swelling of polymer chains	20
Figure 1.10	Relationship between hydrogen permeability and H_2/N_2 selectivity for rubbery (o) and glassy (●) polymers and the empirical upper bound relation [Robeson (1991)]	22
Figure 1.11	Commonly used anions and cations of ionic liquids.	24
Figure 3.1	Schematic of gas sorption equipment	51
Figure 3.2	Photograph of gas sorption equipment	52
Figure 3.3	Schematic of gas permeation equipment	53
Figure 3.4	Photograph of gas permeation equipment	53
Figure 4.1	^{1}H NMR spectra of disubstituted PBI-BuI	56
Figure 4.2	^{1}H NMR spectra of disubstituted PBI-HFA	57
Figure 4.3	^{1}H NMR spectra of PILs based on PBI-BuI.	57
Figure 4.4	^{1}H NMR spectra of PILs based on PBI-HFA.	58

Figure 4.5	FT-IR spectra of PILs based on PBI-BuI (a: PBI-BuI, b: [DBDMPBI-BuI][I], c: [DBDMPBI-BuI][BF_4], d: [DBDMPBI-BuI][Tf_2N], e: [DBDMPBI-BuI][HFB], f: [DBzDMPBI-BuI][I], g: [DBzDMPBI-BuI][BF_4], h: [DBzDMPBI-BuI][Tf_2N], i: [DBzDMPBI-BuI][HFB]).	59
Figure 4.6	FT-IR spectra of PILs based on PBI-HFA (a: PBI-HFA, b: [DBDMPBI-HFA][I], c: [DBDMPBI-HFA][BF_4], d: [DBDMPBI-HFA][Tf_2N], e: [DBDMPBI-HFA][HFB], f: [DBzDMPBI-HFA][I], g: [DBzDMPBI-HFA][BF_4], h: [DBzDMPBI-HFA][Tf_2N], i: [DBzDMPBI-HFA][HFB]).	60
Figure 4.7	WAXD pattern ofPILs based on PBI-BuI (a: PBI-BuI, b: [DBDMPBI-BuI][I], c: [DBDMPBI-BuI][BF_4], d: [DBDMPBI-BuI][Tf_2N], e: [DBDMPBI-BuI][HFB], f: [DBzDMPBI-BuI][I], g: [DBzDMPBI-BuI][BF_4], h: [DBzDMPBI-BuI][Tf_2N], i: [DBzDMPBI-BuI][HFB]).	62
Figure 4.8	WAXD pattern of PILs based on PBI-HFA (a: PBI-HFA, b: [DBDMPBI-HFA][I],c: [DBDMPBI-HFA][BF_4], d: [DBDMPBI-HFA][Tf_2N], e: [DBDMPBI-HFA][HFB],f: [DBzDMPBI-HFA][I], g: [DBzDMPBI-HFA][BF_4], h: [DBzDMPBI-HFA][Tf_2N],i: [DBzDMPBI-HFA][HFB]).	63
Figure 4.9	TG curves of PILs based on PBI-BuI (a: PBI-BuI, b: [DBDMPBI-BuI][I], c: [DBDMPBI-BuI][BF_4], d: [DBDMPBI-BuI][Tf_2N], e: [DBDMPBI-BuI][HFB], f: [DBzDMPBI-BuI][I], g: [DBzDMPBI-BuI][BF_4], h: [DBzDMPBI-BuI][Tf_2N], i: [DBzDMPBI-BuI][HFB]).	65
Figure 4.10	TG curves of PILs based on PBI-HFA (a: PBI-HFA, b: [DBDMPBI-HFA][I], c: [DBDMPBI-HFA][BF_4], d: [DBDMPBI-HFA][Tf_2N], e: [DBDMPBI-HFA][HFB], f: [DBzDMPBI-HFA][I], g: [DBzDMPBI-HFA][BF_4], h: [DBzDMPBI-HFA][Tf_2N], i: [DBzDMPBI-HFA][HFB]).	65
Figure 4.11	DMA curves (tan δ) of PILs as function of temperature (■: [DBDMPBI-BuI][Tf_2N], △: [DBzDMPBI-BuI][Tf_2N], □: [DBDMPBI-HFA][BF_4], ▼: [DBDMPBI-HFA][Tf_2N], ▲: [DBzDMPBI-HFA][I], ▼: [DBzDMPBI-HFA][BF_4], ●: [DBzDMPBI-HFA][Tf_2N]	66
Figure 4.12	Gas sorption isotherms of PBI-BuI and PIL at 35 ºC (a: PBI-BuI, b: [DBDMPBI-BuI][I], c: [DBDMPBI-BuI][BF_4], d: [DBDMPBI-BuI][Tf_2N], e: [DBDMPBI-BuI][HFB],f: [DBzDMPBI-BuI][I], g: [DBzDMPBI-BuI][BF_4], h:	67

	[DBzDMPBI-BuI][Tf_2N], i: [DBzDMPBI-BuI][HFB]).	
Figure 4.13	Gas sorption isotherm of PILs based on PBI-HFA at 35 ºC (a: PBI-HFA, b: [DBDMPBI-HFA][I], c: [DBDMPBI-HFA][BF_4], d: [DBDMPBI-HFA][Tf_2N], e: [DBDMPBI-HFA][HFB], f: [DBzDMPBI-HFA][I], g: [DBzDMPBI-HFA][BF_4], h: [DBzDMPBI-HFA][Tf_2N], i: [DBzDMPBI-HFA][HFB]).	68
Figure 4.14	CO_2 solubility coefficient of PBI-BuI based PIL at 35 ºC (■: [DBDMPBI-BuI][I],●: [DBDMPBI-BuI][BF_4], ▲: [DBDMPBI-BuI][Tf_2N], ▼: [DBDMPBI-BuI][HFB], □: [DBzDMPBI-BuI][I], ○: [DBzDMPBI-BuI][BF_4], △: [DBzDMPBI-BuI][Tf_2N], ▽: [DBzDMPBI-BuI][HFB]).	71
Figure 4.15	CO_2 solubility coefficient of PBI-HFA based PIL at 35 ºC (■: [DBDMPBI-HFA][I], ●: [DBDMPBI-HFA][BF_4], ▲: [DBDMPBI-HFA][Tf_2N], ▼: [DBDMPBI-HFA][HFB], □: [DBzDMPBI-HFA][I], ○: [DBzDMPBI-HFA][BF_4], △: [DBzDMPBI-HFA][Tf_2N], ▽: [DBzDMPBI-HFA][HFB]).	72
Figure 4.16	CO_2 solubility selectivity of PBI-BuI based PIL at 35 ºC (■: [DBDMPBI-BuI][I], ●: [DBDMPBI-BuI][BF_4], ▲: [DBDMPBI-BuI][Tf_2N], ▼: [DBDMPBI-BuI][HFB], □: [DBzDMPBI-BuI][I], ○: [DBzDMPBI-BuI][BF_4], △: [DBzDMPBI-BuI][Tf_2N], ▽: [DBzDMPBI-BuI][HFB]).	72
Figure 4.17	CO_2 solubility selectivity of PBI-HFA based PIL at 35 ºC (■: [DBDMPBI-HFA][I], ●: [DBDMPBI-HFA][BF_4], ▲: [DBDMPBI-HFA][Tf_2N], ▼: [DBDMPBI-HFA][HFB], □:[DBzDMPBI-HFA][I], ○: [DBzDMPBI-HFA][BF_4], △: [DBzDMPBI-HFA][Tf_2N], ▽: [DBzDMPBI-HFA][HFB]).	73
Figure 4.18	CO_2 permeability (Barrer) and permselectivity over N_2 of the present and methyl substituted PILs [Bhavsar (2014b)] based on PBI-BuI	76
Figure 4.19	CO_2 solubility expressed in mol% for (a) asymmetrically substituted PILs (■: [DBzDMPBI-BuI][I], ●: [DBzDMPBI-BuI][BF_4],▲: [DBzDMPBI-BuI][Tf_2N], ◆: [DBzDMPBI-HFA][HFB]), and (b) symmetrically substituted PILs (□: [TMPBI-BuI][I], ○:[TMPBI-BuI][BF_4], △: [TMPBI-BuI][Tf_2N], ◇: [TMPBI-HFA][HFB]).	78
Figure 4.20	Placement of present PILs on the Robeson's Upper bound, along with reported PILs (upstream pressure ○: 40 psi, ○: 2 atm ○: 10 atm, ●: present PILs (20 atm) and common	79

	polymers, viz., □: Matrimid, △:PSF, □: PC.	
Figure 4.21	PILs with upstream pressure 2 atm, ○: 10 atm, ●: present PILs (20 atm) and common polymers, viz., □: Matrimid, △: PSF	79
Figure 4.22	CO_2/H_2 permselectivity of PBI-BuI based PILs and other common polymers [Shao (2009)].	80
Figure 5.1	^{1}H-NMR spectra of pyrene and anthracene substituted polymeric ionic liquids (PILs).	84
Figure 5.2	FT-IR spectra of PILs based on PBI-BuI (a: PBI-BuI, b: [DPyDBzPBI-BuI][Br], c:[DPyDBzPBI-BuI][BF_4], d: [DPyDBzPBI-BuI][Tf_2N], e: [DAnDBzPBI-BuI][Br], f: [DAnDBzPBI-BuI][BF_4], g: [DAnDBzPBI-BuI][Tf_2N]).	85
Figure 5.3	XRD curves of PBI-BuI and PILs (a: PBI-BuI, b: [DPyDBzPBI-BuI][Br], c:[DPyDBzPBI-BuI][BF_4], d: [DPyDBzPBI-BuI][Tf_2N], e: [DAnDBzPBI-BuI][Br], f: [DAnDBzPBI-BuI][BF_4], g: [DAnDBzPBI-BuI][Tf_2N]).	88
Figure 5.4	TGA curves of PBI-BuI and PILs (a: PBI-BuI, b: [DPyDBzPBI-BuI][Br], c:[DPyDBzPBI-BuI][BF_4], d: [DPyDBzPBI-BuI][Tf_2N], e: [DAnDBzPBI-BuI][Br], f: [DAnDBzPBI-BuI][BF_4], g: [DAnDBzPBI-BuI][Tf_2N]).	89
Figure 5. 5	The tan δ curves from dynamic mechanical analysis (DMA) of PILs (■: [DPyDBzPBI-BuI][Tf_2N], ●: [DPyDBzPBI-BuI][BF_4], ▲: [DAnDBzPBI-BuI][Tf_2N]	90
Figure 5. 6a	Gas sorption isotherms for PILs based on PBI-BuI at 35 ºC (△: [DPyDBzPBI-BuI][Br], ○: [DPyPBI-BuI][BF_4], □: [DPyDBzPBI-BuI][Tf_2N], ▲: [DAnDBzPBI-BuI][Br], ●: [DAnDBzPBI-BuI][BF_4], ■: [DAnDBzPBI-BuI][TF_2N]).	91
Figure 5. 7a	Gas solubility in PILs as a function of critical temperature of gases (△: [DPyDBzPBI-BuI][Br], ○: [DPyPBI-BuI][BF_4], □: [DPyDBzPBI-BuI][Tf_2N], ▲: [DAnDBzPBI-BuI][Br], ●: [DAnDBzPBI-BuI][BF_4], ■: [DAnDBzPBI-BuI][TF_2N]).	93
Figure 5. 8a	Correlation of diffusion coefficient with kinetic diameter (Å) of gases in PILs at 35 °C (△: [DPyDBzPBI-BuI][Br], ○: [DPyPBI-BuI][BF_4], □: [DPyDBzPBI-BuI][Tf_2N], ▲: [DAnDBzPBI-BuI][Br], ●: [DAnDBzPBI-BuI][BF_4], ■: [DAnDBzPBI-BuI][TF_2N]).	95
Figure 5. 9a	Variation of diffusion coefficient with d_{sp} of PILs (■: H_2, ▼: N_2,	96

▲: CH_4, ●: CO_2)

Figure 5. 10a	CO_2 permeability and CO_2 based permselectivity of PILs	97
Figure 5. 11a	CO_2 permeability (▬) and CO_2 based permselectivity (▬ : P_{CO_2}/P_{N_2} , ▨: P_{CO_2}/P_{CH_4}) of some common glassy polymers and PBI based PILs.	98
Figure 5. 6b	UV-Visible spectra of a: PBI-BuI, b: [DPyDBzPBI-BuI][Br] and c: [DAnDBzPBI-BuI][Br].	100
Figure 5. 7b	Fluorescence emission of a: PBI-BuI, b: [DPyDBzPBI-BuI][Br] and c: [DAnDBzPBI-BuI][Br] in DMSO (λ_{ex} = 350 nm).	101
Figure 5. 8b	Fluorescence emission spectra of PILs A: [DPyDBzPBI-BuI][Br], B: [DAnDBzPBI-BuI][Br] in the presence of different concentrations of nitrobenzene in DMSO (λ_{ex} = 350 nm).	102
Figure 5. 9b	Fluorescence emission spectra of PILs A: [DPyDBzPBI-BuI][Br], B: [DAnDBzPBI-BuI][Br] in the presence of different concentrations of TNT in DMSO (λ_{ex} = 350 nm).	102
Figure 5. 10b	Fluorescence emission spectra of PILs A: [DPyDBzPBI-BuI][Br], B: [DAnDBzPBI-BuI][Br] in the presence of different concentrations of PA in DMSO (λ_{ex} = 350 nm).	103
Figure 5. 11b	Stern-Volmer plots for [DPyDBzPBI-BuI][Br] (●) and [DAnDBzPBI-BuI][Br] (●) using different NAC solutions; a: NB, b: TNT and c: PA; while d: percent quenching for [DPyDBzPBI-BuI][Br] (■) and [DAnDBzPBI-BuI][Br] (■) at 60 µM concentration of NACs.	104
Figure 5. 12b	Time dependent quenching of [DPyDBzPBI-BuI][Br] upon exposure to the saturated vapors of NACs and common interferents.	106
Figure 5. 13b	Time dependent quenching of [DAnDBzPBI-BuI][Br] upon exposure to the saturated vapors of NACs and common interferents.	106
Figure 5. 14b	Time dependent quenching of the PIL films ○: [DPyDBzPBI-BuI][Br] (12 µm), □: [DAnDBzPBI-BuI][Br] (12 µm) and ●: [DPyDBzPBI-BuI][Br] (40 µm) upon exposure to the saturated vapors of NB.	107

Figure 5. 15b	Regaining of quenching efficiency of PIL films; A: [DPyDBzPBI-BuI][Br], B: [DAnDBzPBI-BuI][Br] after exposure to saturated vapors of NB.	108
Figure 6. 1	IR spectra of PILs (a: [DBzDMPBI-BuI][$(CH_3)_3$C-Ph-BF_3],b: [DBzDMPBI-BuI][$(CF_3)_2$Ph-BF_3], c:[DBzDMPBI-BuI][Im_4B], d: [DBzDMPBI-BuI][Ph_4B], e: [DBzDMPBI-BuI][$(CF_3)_8Ph_4B$].	111
Figure 6. 2	WAXD spectra of PILs (a: [DBzDMPBI-BuI][I], b: [DBzDMPBI- BuI][$(CH_3)_3$C-Ph-BF_3],c: [DBzDMPBI-BuI][$(CF_3)_2$Ph-BF_3],d:[DBzDMPBI-BuI][Im_4B], e: [DBzDMPBI-BuI][Ph_4B] f: [DBzDMPBI-BuI][$(CF_3)_8Ph_4B$].	113
Figure 6. 3	TG curves of PILs (a: [DBzDMPBI-BuI][$(CH_3)_3$C-Ph-BF_3],b: [DBzDMPBI-BuI][$(CF_3)_2$Ph-BF_3],c:[DBzDMPBI-BuI][Im_4B], d: [DBzDMPBI-BuI][Ph_4B], e: [DBzDMPBI-BuI][$(CF_3)_8Ph_4B$].	114
Figure 6. 4	DMA curves (tan δ) of PILs as function of temperature (□: [DBzDMPBI-BuI][$(CH_3)_3$C-Ph-BF_3], △: [DBzDMPBI-BuI][Ph_4B], ■: [DBzDMPBI-BuI][$(CF_3)_8Ph_4B$].	115
Figure 6. 5	Gas sorption isotherms of PILs at 35 ºC (▲: [DBzDMPBI-BuI][I], +: [DBzDMPBI-BuI][BF_4] ■: [DBzDMPBI-BuI][$(CH_3)_3$C-Ph-BF_3], ●: [DBzDMPBI-BuI][$(CF_3)_2$Ph-BF_3], ▲: [DBzDMPBI-BuI][Im_4B], ■: [DBzDMPBI-BuI][Ph_4B], ●: [DBzDMPBI-BuI][$(CF_3)_8Ph_4B$].	116
Figure 6. 6	CO_2 permeability and permselectivities of PBI based reported and present PILs.	119
Figure 6. 7	Variation in CO_2 (■) and H_2 (●) permeability with d_{sp} of present PILs.	120
Figure 7. 1	Gas sorption isotherms of PIL at 35 ºC.	123
Figure 7. 2	Solubility coefficients of different gases in PIL [DBzDMPBI-BuI][BF_4] as a function of critical temperatures (T_c) of gases.	125
Figure 7. 3	Diffusivity of different gases in PIL as a function of critical volume (V_c) of gases.	125
Figure 7. 4	SEM images of TFC membranes a: PSF_{20}-$PIL_{4,}$ b: PSF_{20}-$PIL_{6,}$ c: PSF_{22}-$PIL_{4,}$ d: PSF_{22}-$PIL_{6.}$	127
Figure 7. 5	Permeance and permselectivity of different gases in TFC	129

membranes.

Figure 7. 6	Gas permeance of different gases in PIL as a function of kinetic diameters of gases.	129
Figure 7. 7	Comparison with common glassy polymers.	130

List of Tables

Figure No.	Description	Page No.
Table 1.1	Chemical structure of PILs demonstrated	31
Table 1.2	CO_2 permeation and selectivity of reported PILs	37
Table 4.1	Anion exchange (%) and solubility of PILs in organic solvents	61
Table 4.2	Physical properties of PILs	64
Table 4.3	Dual-mode sorption parameters[a] for PILs	69
Table 4.4	Solubility coefficient (S)[a] and solubility selectivity (S_A/S_B) of PILs	70
Table 4.5	Permeability coefficient (P)[a] and permselectivity (P_A/P_B) of PILs	74
Table 4.6	Diffusivity coefficient (D)[a] and diffusivity selectivity (D_A/D_B) of PBI based PILs	75
Table 5.1	Solubility of PILs in various solvents	86
Table 5.2	Physical properties of PILs	87
Table 5.3a	Dual-mode sorption parameters[a] obtained for PILs	92
Table 5.4a	Solubility coefficient (S^a) and solubility selectivity (S_A/S_B) of PILs at 20 atm	92
Table 5.5a	Permeability coefficient (P^a) and permselectivity (P_A/P_B) of PILs	95
Table 5.6a	Diffusivity coefficient (D^a) and diffusivity selectivity (D_A/D_B) of PILs estimated at 20 atm	96
Table 5.3b	Stern-Volmer constants (K_{sv}^a) of PILs	104
Table 6.1	Solubility of PILs in various solvents	112
Table 6.2	Physical properties of PILs	113
Table 6.3	Dual-mode sorption parameters[a] obtained during gas sorption in PILs	117
Table 6.4	Solubility coefficient (S)[a] and solubility selectivity (S_A/S_B) of	117

	PILs at 20 atm	
Table 6.5	Permeability coefficient (P)[a] and permselectivity (P_A/P_B) of PILs	118
Table 6.6	Diffusivity coefficient (D)[a] of gases in PILs and diffusivity selectivity (D_A/D_B) estimated at 20 atm.	120
Table 7.1	Dual-mode sorption parameters[a] for PILs	124
Table 7.2	Sorption, permeation, and diffusion properties of [DBzDMPBI-BuI][BF_4]	124
Table 7.3	Characteristics of UF membranes	126
Table 7.4	Permeance (P)[a] selectivity of TFC membranes (dip time = 30 sec) prepared with PSF based UF supports.	127
Table 7.5	Permselectivity of TFC membranes (dip time = 30 sec) prepared with PSF based UF supports	127
Table 7.8	Permselectivity of dense and TFC membranes	130

Chapter 1
Introduction and literature survey

Industrial scale gas separations rely mostly on cryogenic distillation, adsorption and membrane based processes. These separations include H_2 separation from hydro-processing purge systems, syngas, hydrocarbons, H_2 and N_2 separation in ammonia plant, separation of He from natural gas, spent gas; O_2 and N_2 enrichment of air, acid gas separations, natural gas upgradation, CO_2 separation in enhanced oil recovery, biogas processing, natural gas processing, flue gas, etc. [Abedini (2010)]. CO_2 separation has got niche importance due to its increasing amount in the earth's atmosphere that is causing global warming and related adverse environmental effects.

1.1. Need for CO_2 separation

Atmospheric concentration of various greenhouse gases has increased by about 25 percent since the industrial revolution has started in the mid 19^{th} century [Shekhavat (2003)]. In particular, anthropogenic CO_2 emissions have increased dramatically, due largely to the burning of fossil fuels, such as coal or natural gas for the production of electricity, and petroleum or diesel for transportation. Increasing concentrations of CO_2 are likely to accelerate the rate of climate change [Shekhawat (2003)]. As a result of human activity, approximately 11 Gt of carbon is emitted to the earth's atmosphere per year [Quere (2015)]. In addition to rising levels of atmospheric CO_2, the earth's temperature is increasing. In the absence of climate change policies, global temperatures are projected to rise between 1.4 - 5.8 °C by 2100 [Houghton (2001), Powel (2006)]. This increase in global temperatures is likely to cause a number of adverse effects; including rising sea levels, changes in ecosystems, loss of biodiversity and reduction in the crop yields [Powel (2006)]. Increased levels of CO_2 have also led to ocean acidification. Furthermore, as the temperature of the oceans increases, their ability to absorb heat and CO_2 from the atmosphere decreases.

Carbon capture and storage (CCS) from large point sources such as power plants is one of the options for reducing anthropogenic CO_2 emissions. It is estimated that CO_2

emissions to the atmosphere could be reduced by 80–90% by using power plant equipped with carbon capture and storage technology [Metz (2005), D'Alessandro (2010)]. In addition to CO_2 capture from the flue gas, CO_2 separation is necessary in various other applications such as natural gas purification, biogas upgradation, water gas shift reaction etc.

1.2 Established methods for CO_2 separation

1.2.1 Absorption

The process of CO_2 absorption by a liquid solvent or solid matrix is currently being explored for scrubbing CO_2 from the flue gas streams (Fig 1.1). In CO_2 absorption processes, a solvent is used that dissolves CO_2, but not oxygen and nitrogen [Aaron (2005)]. An effective, economical, and traditional solvent that can be used for CO_2 absorption is monoethanolamine (MEA), though several other amines have been widely evaluated. The flue gas from a fossil fuel power plant is passed through a column in which MEA preferentially absorbs CO_2 gas than other components of a flue gas stream. While absorption does have strong benefits, the total cost including addition of new solvent, operating and maintenance (O&M) costs is relatively high [Aaron (2005)]. It is estimated to be ~$40–70/ton of CO_2 separated. Though exact life of a batch of solvent was not reported for MEA or any other solvent, solvent generally degrades before it is replaced. In addition to high regeneration costs, sulfur compounds (SO_x gases) present in the flue gas degrade the solvents used for absorption. Approximately 3.5 lbm of solvent are lost per ton of CO_2 separated [Aaron (2005)].

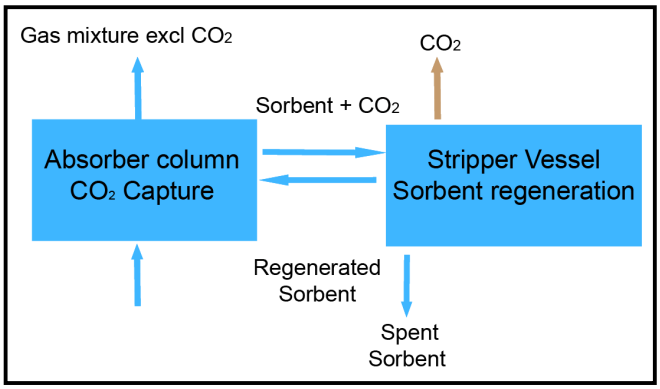

Fig 1.1. Solvent absorption of CO_2

1.2.2 Adsorption

Adsorption is another method that is used to separate CO_2 from flue gas. Adsorption process exhibit significant advantages for energy efficiency compared with chemical and physical absorption approaches [D'Alessandro 2010]. A key factor for physical adsorbents is balancing a strong affinity for removing the component with the energy consumption required for their regeneration. In addition, the selectivity is an important property for adsorptive gas separation. A variety of solid physical adsorbents have been evaluated for CO_2 capture. These include microporous and mesoporous materials (carbon-based sorbents such as activated carbon and carbon molecular sieves, zeolites, and chemically modified mesoporous materials), metal oxides, and hydrotalcite like compounds, amongst others [D'Alessandro 2010].

The two main methods for adsorption are pressure swing adsorption (PSA) and temperature swing adsorption (TSA). In either case, adsorption rates depend on temperature, partial pressures of CO_2, surface forces (interaction energy between sorbent and CO_2), and pore size or available surface area of the sorbent. It has been established that PSA is better than TSA due to its lower energy demand and higher regeneration rate [Aaron (2005)].

1.2.3 Cryogenic distillation

Cryogenic separation is a physical process that separates CO_2 under low temperature (critical temperature of CO_2 = 31.6 °C). It enables direct production of liquid CO_2 at a low pressure, so that the liquid CO_2 can be stored or sequestered instead of compression of gaseous CO_2 to a very high pressure, thereby saving on compression energy [Xu (2014)]. Cryogenic distillation has one advantage over other separation processes that its product is liquid CO_2, which is ready for transport *via* pipeline or tanker for the sequestration. In addition, the CO_2 recovery is very high and CO_2 purity after distillation can exceed 99.95%. The cryogenic process, however, is very energy intensive. The energy required to keep the system cool (often using liquid nitrogen) makes this process cost ineffective [Aaron (2005)].

1.2.4 Membrane based separation

Gas separation using polymeric membrane is becoming highly competitive over above conventional technologies owing to its several advantages. The installation costs for membrane systems are significantly low. The only equipment required for membrane separation is the membrane and fans. There are no moving parts, and the construction is practically simple (Fig. 1.2) [Aaron (2005)]. The only major cost is for gas compression and membrane replacement, which is significantly lower than the solvent replacement and energy costs associated with traditional technologies [Dortmundt (1999)]. Conversely, absorption /adsorption require regeneration of solvent/sorbents. These separation processes are carried out in cycles which involve complicated operations. This requires well trained manpower. The space efficiency in membrane based separation is especially important for offshore operations where energy and space management are important. The modular nature of membranes makes them simple to design and easy to be scaled up linearly [Li (2005)]. Membrane and pretreatment systems integrate various operations such as dehydration, CO_2 and H_2S removal, dew point control, etc. Generally, traditional CO_2 removal technologies require these operations as separate processes [Dortmundt (1999)].

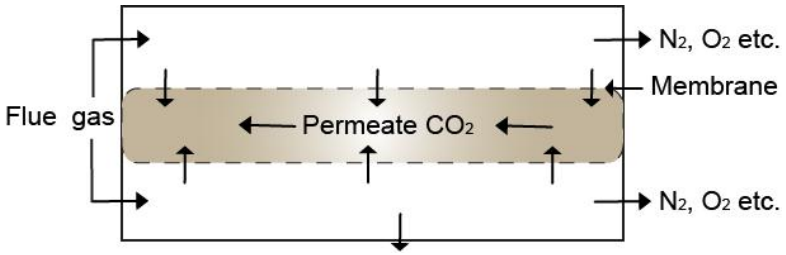

Fig. 1.2. Simple membrane separation tube

1.3 Gas transport through nonporous polymeric membranes

The practical applicability of polymeric membranes for gas separation relies on solution-diffusion mechanism through dense thin skin. Both the sorption and diffusion through the dense layer depend on properties of polymer as well as that of penetrant. The polymeric materials used for dense membrane preparation are either rubbery (operational

temperature higher than their glass transition temperature, T_g) or glassy (operational temperature lower than their T_g) in nature. It has been noted that the mode of gaseous transport is fairly different in the glassy state as compared to the rubbery state. The Henry's Law (Equation 1.1) applies to the gas sorption in rubbery state.

$$C = S \times P \tag{1.1}$$

where, C is the concentration of a gas in polymer matrix (cc(STP)/cc polymer), S is the Henry's solubility constant for a given gas-polymer pair (cc(STP)/(cc polymer cmHg) and P is the gas pressure in cmHg. Gas flux through the membrane normally follows Fick's first law.

$$Q = -D(dC/dx) \tag{1.2}$$

where, D is the diffusivity and C is the local concentration of a gas in the membrane. Integration over the membranes thickness, 'Q' yields

$$Q = D\frac{(C_1 - C_2)}{\ell} \tag{1.3}$$

where, C_1 and C_2 are the gas concentrations at the high and low pressure surfaces of the membrane, respectively, and *l* is the membrane thickness. Substituting Equation 1.1 into 1.3 yields:

$$Q = DS\frac{(P_1 - P_2)}{\ell} = P\frac{(P_1 - P_2)}{\ell} \tag{1.4}$$

where, P_1 and P_2 are the partial pressures of the gas on the high and low pressure side of the membrane, respectively, and P is the permeability, given by:

$$P = D \times S \tag{1.5}$$

In case of dense membranes, the permeability is usually expressed in the unit barrer (10^{-10} cm^3(STP)cm.$s^{-1}$$cm^{-2}$$cmHg^{-1}$); which is an intrinsic property of the material. The permeability can also be expressed in molar units (mol m s^{-1} m^{-2} Pa^{-1}). When the membrane is transformed into asymmetric or thin film composite form, the gas flux is expressed as permeance in GPU and is the property of formed membrane (1 GPU = 10^{-6} cm^3.(STP)cm^{-2} $s^{-1}$$cmHg^{-1}$).

The permeability can be determined by

a) Time-lag or variable pressure method

b) Variable volume method

In Time-lag or variable pressure method, both P and D can be obtained in a single experiment by measuring the "time lag" for the pressure increase on the low pressure side of the membrane. The time lag, θ, obtained by extrapolating the linear portion of the pressure versus time function back to the time axis (Figure 1.3) is given by:

$$\theta = \frac{\ell^2}{6D} \tag{1.6}$$

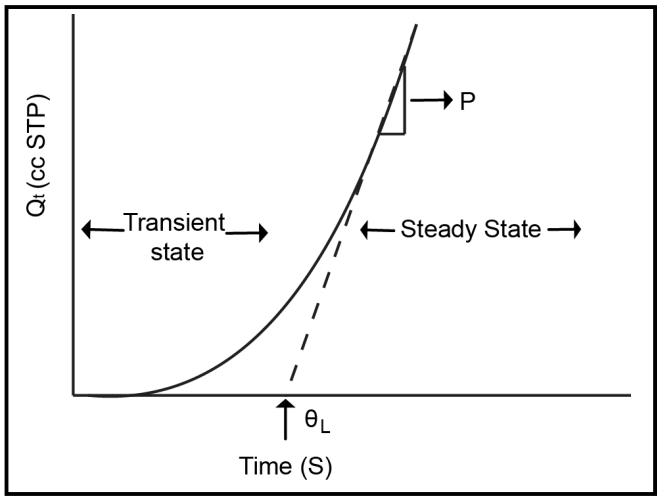

Fig. 1.3. Time-lag measurement of gas permeation

The permeability is given by the slope of the function and the solubility (S) can be calculated by equation 1.5. The permselectivity ($\alpha_{A/B}$) is the product of the diffusivity selectivity and sorption selectivity as given in Equation 1.7. This can be defined as follows:

$$\alpha_{A/B} = \frac{P_A}{P_B} = \left(\frac{D_A}{D_B}\right)\left(\frac{S_A}{S_B}\right) \tag{1.7}$$

where, $\alpha_{A/B}$ is the ratio of the permeability of gas A to gas B.

According to the variable volume method, a pressure is applied on one side of the membrane and the permeated gas is allowed to expand on the opposite side, which is maintained usually at atmospheric pressure. The change in the volume of the permeate is

then measured as a function of time by following, for example, the displacement of a short column of liquid in a capillary [Stern (1963)].

1.3.1. Transport in rubbery polymers

The sorption of low molecular weight penetrants in rubbery materials is generally described by Henry's law as below:

$$C = k_D P \tag{1.8}$$

where, C is the gas concentration, k_D is the Henry's law coefficient, and P is the penetrant pressure. The permeability coefficient, independent of feed pressure, is given by,

$$P = k_D D \tag{1.9}$$

However, deviations from Henry's law are observed for rubbery polymers in the presence of high activity gases or vapors. The Henry's law coefficient, k_D, appearing in Equations 1.8 and 1.9 is a is a constant that depends on the nature of gas, polymer and the temperature.

Diffusion coefficient for gases in rubbery polymers can be described by Equation 2.0,

$$D = D_0 . \exp(-E^* / RT) \tag{2.0}$$

The activation energy E^* is an energy that must be concentrated in the polymer adjacent to diffusing molecule to open a passage of enough free volume, to allow the penetrant to execute diffusional jump [Barrer (1939)]. The concept of "free-volume" or "empty" volume used to describe the transport of gases and liquids in polymers has been reviewed in the literature [Thran (1999), Stern (1994)].

1.3.2 Transport in glassy polymers

The membrane materials used in most of the separations are glassy in nature, which derive their selectivity primarily from their ability to separate gases based on differences in penetrant size. Transport is postulated to occur when there is the creation of a transient gap next to the penetrant molecule of sufficient size to accommodate the penetrant thereby permitting a diffusion step (Fig. 1.4) [Koros (2000)].

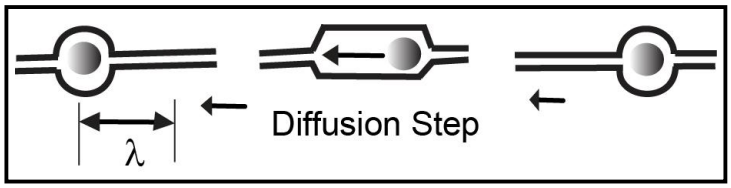

Fig.1.4. Schematic representation of gas diffusion through polymer matrix

The transient gaps form and fade throughout the polymer due to thermally induced segmental motions of the polymer. A number of statistical models have been developed to study the transport mechanism in glassy polymers and estimate the parameters P, D and S [(Stern (1994)]. One of the most popular theories is based on the available free-volume of the system [Stern (1994)]. This type of model suggests that gas permeability not only varies with the free volume, but also with its distribution in the polymer membrane.

The heterogeneity of glassy polymers results in deviations from Henry's Law with respect to linear dependence of concentration with applied pressure. Two types of sorption sites account for this non-linearity [Vieth (1976), Tsujita (2003)]. The first is known as 'Henry's site' and the second is called as 'Langmuir's site'. Henry sorption is the dominant mechanism of sorption into the matrix component and Langmuir sorption dominates in the microvoids region [Tsujita (2003)]. Molecules in Langmuir sites have lower mobility than the ones in Henry-type sites. Local equilibrium exists between molecules in Henry and Langmuir sites. The description of gas sorption and diffusion through glassy polymers utilizing two different sites is known as the 'dual-mode sorption theory' (Fig. 1.5).

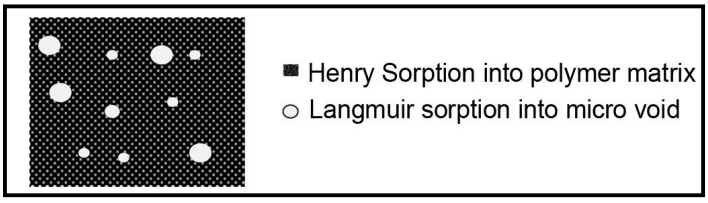

Fig.1.5. Schematic representation of polymeric glassy state depicting the matrix and the microvoids [Tsujita (2003)]

Dual-mode sorption is normally described by the sum of these two contributions as follows (Figure 1.6):

$$C = C_D + C_H = k_D p + \frac{C'_H bp}{1 + bp} \tag{1.8}$$

Where, C = total sorption amount in glassy polymeric membrane, C_D = Henry mode sorption, C_H = Langmuir sorption amount, P = applied gas pressure, k_D = Henry's solubility coefficient, C'_H = Langmuir saturation constant, b = Langmuir affinity constant.

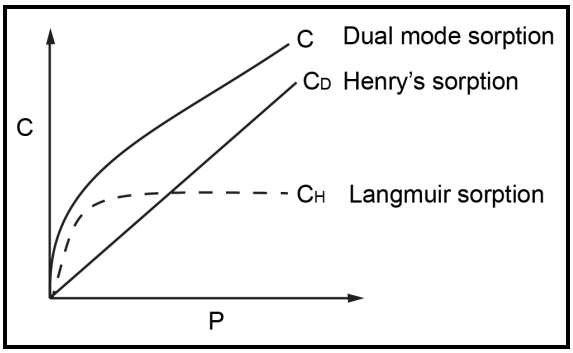

Fig.1.6. Schematic representations of dual-mode sorption [Tsujita (2003)]

The dual-mode sorption equation (1.8) provides a linear relationship with pressure in the high pressure region [Tsujita (2003)]. The linear slope in the high pressure region corresponds to the Henry's solubility coefficient and the intercept of the extrapolated line to the *C* axis represents the Langmuir saturation constant (Figure 1.2). Based on the gas sorption isotherm obtained experimentally, three dual-mode sorption parameters, k_D, C'_H, and b, can be determined by curve fitting using a nonlinear least squares method. C'_H is related to the unrelaxed volume (Equation 1.9), which is a measure of the departure from equilibrium or low energy in the glassy state, i.e. the difference between the specific volume of glassy state and liquid states ($V_g - V_l$).

$$C'_H = \left(\frac{V_g - V_l}{V_g} \right) \frac{22400}{V_p} \tag{1.9}$$

where, Vp = the molar volume of sorbant gas and C'_H is evaluated from the experimentally determined sorption isotherm. If a gas is polar in nature and condensable, gas sorption may exhibit an anomalous isotherm. For example, some glassy polymers can be plasticized to rubbery state by CO_2 gas owing to its interaction with them [Wang (1996)].

It is generally noted that polymers offering the best combinations of gas selectivity and permeability are generally glassy that exhibit poor chain packing. In essence, these polymers offer the size distribution of free volume elements required for approaching molecular sieving characteristics. Since transport in polymers occurs through a solution-diffusion mechanism, diffusivity of a penetrant can be tuned by modifying the polymer chain and subgroup flexibility, as well as free volume present in the polymer structure [Li (2013)]. Following section deals with properties of the glassy polymers that govern permeation properties.

1.4 Factors affecting gas permeation properties in glassy polymers

Gas permeation and permselectivity performance of polymer depends upon polymer as well as penetrant properties, as discussed in the following section.

1.4.1 Effect of polymer properties

1.4.1.1 Chain packing density

The penetrant diffusivity depends strongly on the polymer chain packing density. Both, *d*-spacing (dsp, average intersegmental distance) and fractional free volume (v_f or FFV) are used as indicators of the degree of openness of the polymer matrix. The parameter, v_f, is a fraction of total polymer volume that is not occupied by polymer chains. Fractional free volume (v_f) can be estimated by the following equation:

$$v_f = \frac{V - V_W}{V} \tag{1.10}$$

where, V (= M/ρ) is the molar volume of the structural repeat unit (of molecular weight M) and (ρ) is the measured density. The term, V_w is the van der Waals volume usually calculated by the group contribution method [Bondi (1964)].

Within a given family of glassy polymers, gas solubility increases with increasing polymer free volume. Solubility is usually a much weaker function of the free volume than that of diffusivity, as shown in Fig. 1.7. The gas diffusion coefficient is typically related to the free volume by following expression [Ghosal (1996)].

$$D = D_0 \exp\left[-\frac{B}{FFV}\right] \qquad (1.11)$$

where, D_o and B are constants characteristic of the polymer-penetrant system.

The commonly used methods to determine the free volume is based on semi-empirical calculation. The method uses experimentally determined density of the polymer and V_w by group contribution method. The positron annihilation lifetime spectroscopy and photochromic and fluorescence technique are also used for determining the v_f [Victor (1987)].

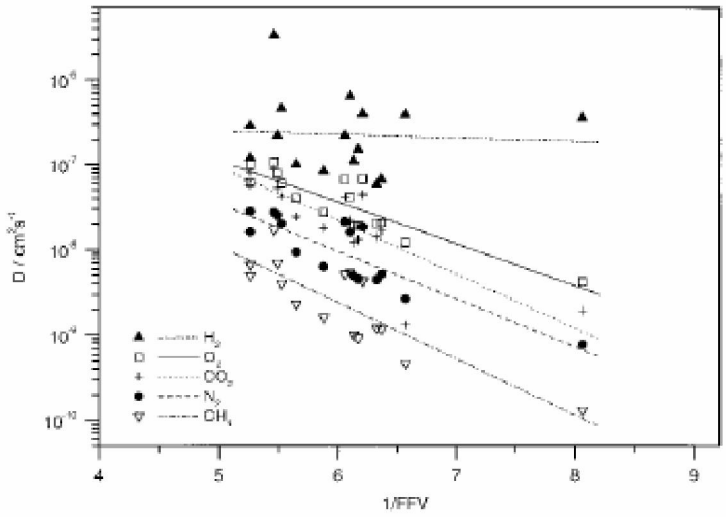

Fig.1.7. Plot of log *D* versus 1/FFV for diffusion of He, H_2 O_2, N_2, CO_2, and CH_4, in various polymers [Thran (1999)].

1.4.1.2 Chain and subgroup mobility

Chain mobility in the polymer matrix is expressed by various transition temperatures and has direct relationship with the penetrant permeability and inverse relationship with the selectivity. An emphasis in new material development for the gas separation is on improving the selectivity with marginal effects on permeability. Simultaneously inhibiting chain packing and the torsional mobility around flexible linkages in the polymer backbone increase both, the permeability and permselectivity or a significant increase in permeability with negligible loss in permselectivity [Koros (1989)].

Rigid groups which are polar in nature act to increase interchain cohesive energy density (in addition to increasing intramolecular barriers to segmental motion). This leads to the decrease in penetrant diffusion coefficients. Inhibition of the segmental and sub-segmental mobility can be judged by increase in glass transition (Tg) or sub-T_g temperatures [Koros (1992)]. In addition to usual methods of determining Tg, dynamic mechanical analysis and dielectric properties help in gathering an understanding towards sub-t_g transitions of a glassy polymer.

1.4.1.3 Polarity

Polarity is related to the unevenness of the distribution of electrons about atoms, functional groups or molecules. The cohesive energy density is a measure of expressing the polarity in the polymer. Interchain attractions induced by polar groups can be used to inhibit motion, thereby adding another means of tailoring membrane material properties. In addition to interchain attractions, the solubility of a polar penetrant such as CO_2 within a polymer is important in determining permeation properties. This can promote plasticization at high pressure [Koros (1985)].

1.4.1.4 Crosslinking

The chemistries of membrane materials, cross-linking agents, and their interactions have a large impact on the cross-linked structure, degree of cross-linking and the gas transport properties. Experimental results suggested that polymer cross-linking imparted resulting membranes with anti-plasticization, good chemical resistance and even long-term performance ability [Liu (2001)]. The crosslinking reduces the polymer segmental mobility and thus the diffusion coefficients of gases in membrane typically decrease [Liu (1999)].

1.4.1.5 Crystallinity

Impermeable crystallites increase the tortuous path for the penetrant molecules through the membrane matrix [Ghosal (1994)]. They also restrict segmental mobility in the non-crystalline regions of the polymer. Both these effects reduce the gas diffusivity. Since crystalline regions reduce both the penetrant solubility and diffusivity, the overall

permeability is reduced. The gas permselectivity is relatively unaffected or may increase slightly with the increase in crystallinity. Various techniques have been employed to evaluate the relative and absolute degree of crystallinity, including X-ray diffraction, density methods, thermal analysis, nuclear magnetic resonance (NMR) and infrared (IR) spectroscopy [He (2000)]. Each technique has its own advantages and disadvantages in terms of crystallinity determination.

1.4.2 Effect of penetrant properties on permeability and permselectivity

1.4.2.1 Condensability of gas molecules

Gas solubility in the polymer matrix normally increases with increase in the gas condensability [Ghosal (1994)]. Gas critical temperature, T_c, normal boiling point, T_b or Lennard-Jones force constant (ε/κ) represent the condensability of a gas and correlate well with the solubility coefficients of the penetrants in a polymer [Ghosal (1994)]. For example, in most of the polymers, CO_2 (T_c = 31°C) is more soluble than CH_4 (T_c = -82.1°C) and O_2 (T_c = -118.4°C) than N_2 (T_c = - 147°C).

1.4.2.2 Size and shape of gas molecules

The diffusion coefficient of a penetrant depends on its size, as characterized by the Van der Waals volume or kinetic diameter. Generally, the diffusion coefficient decreases with increase in penetrant size. The diffusion coefficient in polymers is also dependent on shape of the penetrant [Ghosal (1994)]. The van der Waals volume can be calculated by geometrical method, provided, the covalent radius and the van der Waals radius of each atom in the molecule are known [Bondi (1964)]. Nevertheless, the van der Waals volume does not account for the shape of the penetrant. The diffusivity of linear or dumbbell shaped penetrant molecules such as CO_2 is higher than the diffusivities of spherical molecules of equivalent molecular volume. The Van der Waals volumes of CO_2 and CH_4 are predicted to be 17.5 and 17.2 cm^3/mol. These molecular volumes give almost equivalent spherical diameters of 3.33 and 3.31Å for CO_2 and CH_4, respectively. Thus, the kinetic diameter is frequently used to characterize the penetrant size [Ghosal (1994)]. The effect of penetrant characteristics in governing permeability is given in Fig. 1.8 [Koros (1992)].

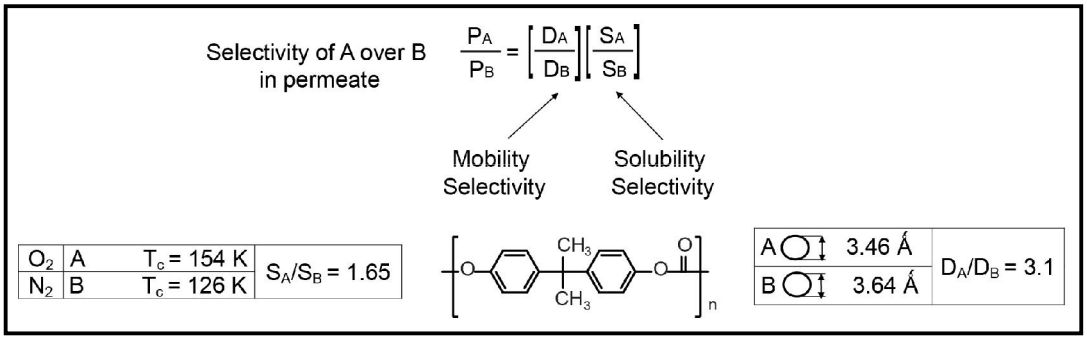

Fig. 1.8. Effect of penetrant characteristics on diffusion and solubility selectivities [Koros (1992)]

1.4.3 Effects of operational conditions

a) Temperature

The gas diffusivity increases significantly at elevated temperatures. For small gas molecules, such as H_2, N_2, O_2, CH_4; diffusivity is more temperature sensitive than the solubility. For example, the solubilities of H_2, CH_4 and CO_2 in natural rubber vary less than 30% as temperature increases from 25 to 50 °C [Ghosal (1994)]. Over temperature ranges in which no significant polymer phase thermal transitions occur, gas permeability of a membrane, can be expressed by an Arrhenius-type equation. The temperature dependence of gas permeation in various glassy polymers is well known in the literature [Kim (1989), Costello (1994), Gülmüs (2007), de Sales (2008)], where increase in permeability with increase in temperature was reported. The solubility coefficient for a given penetrant generally decreases with temperature. Nevertheless, this decrease is overcome by the substantial increase in the diffusion coefficients producing a net increase in the permeability coefficient. The decrease in diffusivity selectivity at higher temperature leads to decrease in overall permselectivity.

b) Pressure

The diffusivity, solubility and, in turn, permeability may vary considerably as the pressure of the penetrant in contact with the polymer changes [Ghosal (1994)]. Low sorbing penetrants such as H_2, He, N_2, O_2 show negligible pressure dependence on permeability of rubbery or glassy polymers. In case of condensable gases, permeability decrease monotonically with increasing pressure as explained by the dual mode model. This behavior is typically observed in case of more soluble penetrants such as CO_2 in

glassy polymers. The permeability of a rubbery polymer to an organic vapor often show monotonic increase in permeability which is associated with an increase in penetrant solubility and diffusivity with increasing pressure. The permeability of a glassy polymer to a plasticizing penetrant such as an organic vapor or CO_2 exhibit dual mode behavior at low pressures and penetrant induced plasticization at high pressures.

1.4.4 Effects of membrane preparation parameters

There is enough literature indicating effects of preparation parameters on the separation performance of dense homogenous membranes. Majority of the dense membranes used for evaluation of gas permeation properties are prepared by solution casting method and the solvent used for making polymer solution may affect the permeation properties. Khulbe et al. [1997] used various solvents for preparing PPO membranes. Author observed that the permeability increased and the selectivity (O_2/N_2 and CO_2/CH_4) decreased with the increase in the boiling points of the solvents. The membrane morphology and the separation performance depends upon properties of the solvents used in preparing polymer solutions, solution concentration, surface (glass, steel, teflon, etc.) on which the membrane is cast, casting techniques such as drop casting, blade casting etc., casting temperature and annealing temperature [Hacarlioglu (2003)]. Small amount of solvent in glassy polymer can act as the plasticizer to increase the chain mobility. It was observed that the permeability of PTMSP to helium may vary almost five fold, depending on the solvent used to cast the membrane. In another example, a melt-extruded polysulfone film was approximately 20% less permeable to CO_2, than the solvent-cast film [Ghosal (1994)]. Previous exposure of a glassy polymer to highly soluble gases such as CO_2 expands the non-equilibrium excess volume resulting in enhanced solubility [Wonders (1979)]. Polycarbonate exposed to high pressure CO_2 and liquid N_2, led to increase in microvoid content and hence the sorption. Tsujita et al. (2003) observed that the dual-mode sorption parameter (C'H); as well as the CO_2 permeability coefficient of polyamic acid (a precursor of polyimide), partially imidized polyimide, polyimide, poly(2,6-dimethyl phenylene oxide) (PPO), and polycarbonate increased remarkably by thermal quenching and CO_2 pressure conditioning. The effect of film casting temperature (from 25-65 °C) was demonstrated for PPO using, 1,2-

trichloroethylene as the solvent [Khulbe (2004)]. The membrane surface morphology and the gas permeation through the membrane were influenced by evaporation temperature as well. It was reported that permeability increased and the selectivity (O_2/N_2 and CO_2/CH_4) decreased with an increase in the boiling point of the solvent used for casting [Khulbe (1997)].

The effect of film thickness of poly(vinyltrimethyl silane) (PVTMS) and poly(trimethylsilyl norbornene) (PTMSNB) cast from hydrocarbon solutions on permeation properties was observed [Shishatskii (1996)]. For all the gases, diffusion coefficients decreased with the lowering in film thickness and increase in film density. Recently, Huang et al. [2007] correlated the effect of film thickness on aging time and consequently gas permeation properties of polysulfone, PPO and Matrimid. The rate of the aging effect was higher in the thinner films.

A sub-T_g thermal annealing can be used to reduce microvoids of glassy polymers, which decreases gas solubility, diffusivity and, in turn, permeability. The annealing temperature and duration of the annealing step controls the amount of excess volume relaxation and, in turn, decreases the gas solubility and diffusivity [Ghosal (1994)].

1.5 Selected commercially relevant polymers for CO_2 separation

The fundamental polymeric materials for gas separation are typically classified as: inorganic (ceramic, metal oxide, metallic, molecular sieves, thin layer of Pd on ceramic or porous alumina cylinder as support, metal–organic frameworks, etc.) or organic (cellulose acetate, polymers such as polysulfone, polyamide, polyimide, cross-linked poly(2,6 dimethylphenyleneoxide), etc. The preferred membrane configuration is hollow fibers (rather than spiral modules based on flat sheet) with high surface area to volume ratios of 1500-2000 m^2m^{-3}) [D'Alessandro (2010)]. For a membrane to be useful for CO_2 separation, it should possess high permeability, higher CO_2 selectivity over other gases, thermal and chemical robustness, resistant to plasticization and aging, cost effectiveness and be able to be cheaply manufactured into different membrane forms such as flat sheet or hollow fibers [Powel (2006), Brunetti (2010)]. The development in polymeric membranes for this purpose have been extensively reviewed [Sridhar (2007), Schole (2008), Bernardo (2009, 2013), Sanders (2013)]. The following section will highlight

commercially relevant polymers such as polysulfone (PSF), cellulose acetate (CA), poly(phenylene oxide) (PPO) and polyimide (PI) widely investigated for gas permeation properties.

1.5.1 Polysulfones

Polysulfones are an important commercial membrane material for gas separations due to their excellent mechanical properties, a wide operating temperature range, fairly good chemical resistance, and easy fabrication of membranes in a wide variety of configurations and modules [Guo (2002)]. The first large-scale membrane separation process, developed by Monsanto Co. in the late 1970s, utilized asymmetric hollow fiber membranes of bisphenol-A polysulfone coated with a thin layer of silicone rubber [Henis (1977)]. Structural variations in polysulfone are well reported. The gas transport properties of commercial PSF and PSF variants, particularly the influence of various bridging moieties between the phenyl rings and the groups substituted on the phenyl rings have been extensively studied extensively [Aitken (1992), Ghoshal (1993), Ghosal (1996), McHattie (1990), McHattie (1992), Julion (2012), Sanders (2013)]. Symmetric bulky substitutions (e.g., methyl groups) on the phenyl rings significantly increase the gas permeability, while it is decreased with asymmetric substitution of the same groups [McHattie (1992)]. Replacing the isopropylidene bridging moiety with bulkier groups, like hexafluoro isopropylidene (–$(CF_3)_2$–), makes the polymers much more permeable, mainly due to the enhanced free volume.

1.5.2 Cellulose acetates

Cellulose acetate (CA) and its derivatives were among the first generation of commercial membranes used for natural gas separation. In addition to desirable transport properties, the development of the asymmetric membrane concept by Loeb and Sourirajan greatly reduced the surface area necessary to achieve high gas productivity [Sanders (2013)]. CA continues to be used in gas separations for removal of acid gases (CO_2 and H_2S) from natural gas as well as the separation of CO_2 from mixtures with hydrocarbons in enhanced oil recovery operations. The permeability value of CA is a function of the degree of acetylation in these polymers, and varying the degree of

acetylation from 1.75 to 2.85 increased CO_2 permeability from 1.84 to 6.56 Barrer [Puleo (1989), Sanders (2013)]. This increase is due to the replacement of polar hydroxyl groups with bulky acetate groups, which decreases polymer density and creates a higher free volume in the polymer matrix [Puleo (1989)].

1.5.3 PPO

Poly(2,6-dimethyl-1,4-phenylene oxide) (PPO) is a high-performance engineering thermoplastic with good mechanical properties and thermo-oxidative stability because of a low barrier to rotation and resonance stabilization of the aromatic ether bond (Ar–O–Ar) [Sanders (2013)]. The material was discovered by Hay [Hay (1959)] over 50 years ago and was commercialized by General Electric [Hay (1967)] (now SABIC Plastics) and AKZO [Hein (1968)]. Currently most of the research on PPO is focused on its chemical modification to elevate its CO_2 based permselectivity [Sanders (2013)]. Monsanto developed a cross-linked PPO membrane by bromination [Zampini (1983)]. The transport properties of PPO can be manipulated by altering the bromine content and degree of substitution [Chern (1987)]. PPO has also been modified in various other ways to enhance gas transport properties [Bhole (2006)]. It is often blended with polystyrene for commercial use [Hamad (2002), CIZEK (1965)]. In all cases, the membrane properties strongly depend on the extent of chemical modification and the location of substitution, i.e., on the ring or on the methyl groups. Although the properties can be improved *via* chemical modification, there is still a need to develop an economic and efficient way to conduct such modifications in a controllable manner.

1.5.4 Polyimides

Of the emerging polymers listed in this section, polyimides are among the most studied materials for gas separation polymers. Although aromatic polyimides are used as gas separation membrane materials today, the polyimide family encompasses a large number of structural variants, and many studies on polyimide gas separation membranes indicate that the separation properties can be tailored by using different dianhydride and diamine monomers. Structure/property studies in the late 1980s showed that restricting both chain mobility and chain packing can simultaneously increase permeability and

selectivity in polyimides [Kim (1988), Stern (1989)]. In particular, polyimides with a hexafluoro substituted carbon (e.g., – $(CF_3)_2$–) in the polyimide backbone have been the object of much research, as they tend to be considerably more gas-selective, particularly toward CO_2 relative to CH_4, than other glassy polymers with comparable permeabilities. The hexafluoro group in the dianhydride moieties (e.g., hexafluoro isopropylidene diphthalic anhydride (6FDA)) increases the stiffness of the polymer chain, and it frustrates chain packing due to the steric hindrance from the CF_3 groups, which serve as molecular spacers and chain stiffeners in the polymer [Xiao (2009a)]. These initial 6FDA-based polymers are labeled as "*First Generation Polyimides*" As of 2002, polyimides were reportedly used by Air Liquide, Praxair, Parker-Hannifin, and Ube for various gas separation applications. However the major drawback of these 6FDA-based polyimides is their relatively higher cost. The molecular design of polyimides can be broadly classified into two categories. The first encompasses purely polyimide system whereby the chemical constituents and configurations of the dianhydrides and/or diamines used for polyimide synthesis are varied in a systematic manner. The other category is the chemical fusion (copolymerization) of polyimides with polymers from other classes [Xiao (2009a)].

The performance of the polymer membranes described above is limited by several factors such as plasticization, physical aging, permeability/selectivity tradeoff which is elaborated below.

1.6 Challenges in polymeric membrane materials for gas separation

1.6.1 Plasticization

As the concentration of interacting gas (such as CO_2, H_2S, water vapor, NH_3, etc) inside the polymer matrix increases, the polymer swells, which increases its chain mobility. This, in turn, increases the gas diffusion coefficients and decreases diffusion selectivity [Sanders (2013)]. This phenomenon is typically known as plasticization and is explained in Fig. 1.9.

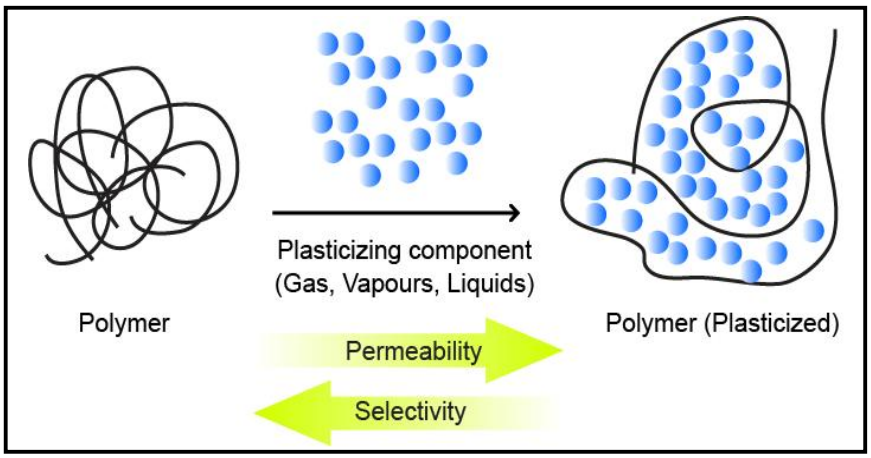

Fig. 1.9. Plasticization induced swelling of polymer chains

Plasticization results into higher gas permeability but lower selectivity, particularly at high pressures. Among gases of importance in gas separation applications, CO_2 and water vapors are widely known to plasticize polymer matrix.

1.6.2 Physical aging

Physical aging affects of membrane's industrial viability [Sanders (2013)]. Many polymers used in gas separations are glassy in nature. They exhibit non-equilibrium or excess free volume due to kinetic constraints on the polymer segmental motions that prevent the close polymer chain packing. In the kinetically constrained glassy state, polymers undergo local scale segmental motions. These motions act to gradually increase the density of the polymer (therefore, reduce its free volume), while approaching toward the thermodynamic equilibrium state. The reduction in free volume in turn, reduces gas permeability. The observed decrease in permeability is generally accompanied by an increase in selectivity. It is reported that physical aging also depends on the thickness of the membrane under study, particularly when the thickness becomes of the order of less than 1 micron [Sanders (2013)].

1.6.3 Permeability/selectivity tradeoff (the upper bound)

For a polymer to be applicable as a gas separation membrane material, both high permeability and selectivity are desirable. Higher permeability decreases the amount of membrane area required to treat a given amount of gas, in turn, decreasing capital cost of

the membrane unit. Higher selectivity gives higher purity of gas. Over the past 25 years, the gas separation properties of many polymers have been studied, and a substantial effort in industrial and academic research laboratories has resulted in polymers that are both more permeable and more selective. A tradeoff has been recognized between permeability and selectivity; i.e., polymers that are more permeable are generally less selective and vice versa. On the basis of an exhaustive literature survey, Robeson summarized this concept by graphically illustrating available data as shown in Fig. 1.10, which presents the hydrogen permeability coefficients and H_2/N_2 separation factors for various polymers [Robeson (1991)]. The upper bound correlation follows the relationship $P_i = k\alpha^n_{ij}$, where P_i is the permeability of the fast gas, $\alpha_{ij}(P_i/P_j)$ is the separation factor, *k* is referred to as the "front factor" and *n* is the slope of the log–log plot of the noted relationship. Below this line on a plot of log αij versus log P_i, virtually all the experimental data points exist. Thus, a hypothetical line, which defines the limits of intrinsic permeability and selectivity of polymeric materials, is drawn. This line defines the so-called "Upper Bound" combination of permeability and selectivity of known polymer membrane materials for various gas pairs. Materials with high permeability as well as high selectivity would be in the upper right corner of this figure. However, such materials with permeability/ selectivity combinations are exceptionally rare. The upper bound was further modified by Robeson in 2008 [Robeson (2008)]. The results show only modest shifts from the 1991 upper bound correlation for various gas pairs, e.g., O_2/N_2, H_2/N_2, H_2/CH_4, CO_2/CH_4 and He/N_2. From the 1994 correlations of H_2/CO_2 and He/CO_2, H_2/CO_2 shows only a minor change. Significant shifts in the position of the upper bound line were observed for He/CH_4, He/CO_2 and He/H_2. The shifts in the upper bound for He/CO_2, He/CO_2 and He/H_2 were due to aliphatic fluorocarbon polymers for which very limited data existed in 1991. The fluorinated polymers noted are commercial systems including Nafion®, Hyflon®, Viton®, Cytop™ and Teflon® AF variants. These polymers exhibit an uncharacteristic higher He permeability relative to the other gas components of the pairs noted. Two new upper bound correlations, CO_2/N_2 and N_2/CH_4 were introduced and the N_2/CH_4 upper bound data points were comprised of the perfluorinated polymers noted above were added in 2008 upperbound.

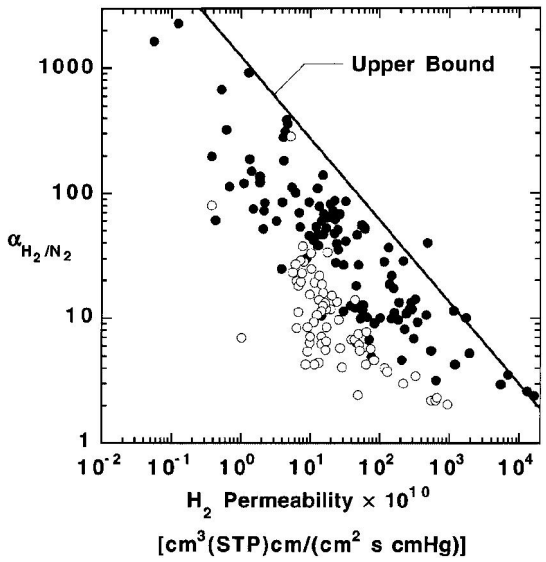

Fig. 1.10. Relationship between hydrogen permeability and H_2/N_2 selectivity for rubbery (o) and glassy (●) polymers and the empirical upper bound relation [Robeson (1991)]

1.7 Emerging membrane materials

In recent years, new classes of membrane materials are being developed due to increasing demands of process economics in terms of not only the enhanced intrinsic permeability and selectivity; but also better physical properties. Efforts are on to overcome the challenges as mentioned above. The new classes of materials include thermally rearranged (TR) polymers, polymers of intrinsic microporosity (PIMs), perfluoropolymers, etc. Ethylene oxide (EO) containing polymers/block copolymers or, more generally, polyethers have been identified as outstanding CO_2- selective materials [Yave (2010), Car (2008)]. Their high performance has been attributed to the interaction between the EO unit and the CO_2 molecule [Yave (2010)]. Facilitated transport of CO_2 from CO_2/CH_4, CO_2/N_2 and CO_2/C_2H_6 mixtures using various carrier species such as monoethanol amine, diethanolamine [Terrence (1980), Masaaki (1996)], alkyl diamine [Yamaguchi (1996)], and carbonate/bicarbonate solutions [Chen (1999)] have also been investigated. The performance of these membranes can be limited by the saturation limit of carrier species, their long term stability and regeneration.

Among the CO_2 selective materials interestingly, ionic liquids (ILs) broadly known as "green solvents" have recently been noticed for their outstanding physicochemical properties and applications specifically in CO_2 capture and separation. It

is worth mentioning here that ILs possess significant CO_2 solubility and selectivity over other gases. It would be worth to look at their various peculiarities, which would be useful in new material design.

1.7.1 Ionic Liquids (ILs) for CO_2 separation

Ionic liquids (ILs) are salts composed of ions and generally are liquids below 100 °C [Petkovic (2011), Mecerreyes (2011), Yaun (2013)]. If melting point is below room temperature, the IL is called as room-temperature ionic liquid (RTIL) [Thomas (1999)]. Ionic liquids, which have been widely promoted as "green solvents", are attracting much attention for applications in many fields of chemistry and industry due to their chemical stability, thermal stability, low vapor pressure, high ionic conductivity, etc. [Petkovic (2011), MacFarlane (2014), Lu (2009)]. Their potential is further emphasized by the fact that their physical and chemical properties may be fine tuned by varying both, the cation and the anion. ILs have been proposed as an alternative to the volatile, corrosive, and degradation sensitive amine-solvents for CO_2 capture. Blanchard et al. were the first to observe that significant amounts of CO_2 could be dissolved in imidazolium-based ionic liquids [Blanchard (1999)]. This study initiated an explosion of scientific research on CO_2 absorption with ionic liquids, leading to a rapid growth of the literature on this specific topic. CO_2 capture using ionic liquids is gaining interest due to their unique characteristics, i.e., wide liquid range, thermal stability, negligible vapor pressure, tunable physicochemical character and high CO_2 solubility. By choosing an appropriate combination of cation and anion, the viscosity of ILs can be adjusted over an acceptable range of <50 cP to >10,000 cP. Among the various paths followed in the research, work are on the use of ionic liquids for CO_2 capture involving room temperature ionic liquids (RTILs), task-specific ionic liquids (TSILs) or supported ionic-liquid membranes (SILMs).

1.7.2 CO_2 capture by room-temperature ionic liquids (RTILs)

The number structural variations in ILs are very large. A few examples of commonly used cations and anions of ILs are shown in Figure 1.11. Considerable

research work is being done showing high CO_2 solubility in certain RTILs, especially in those possessing imidazolium-based cations [Rahaman (2010)].

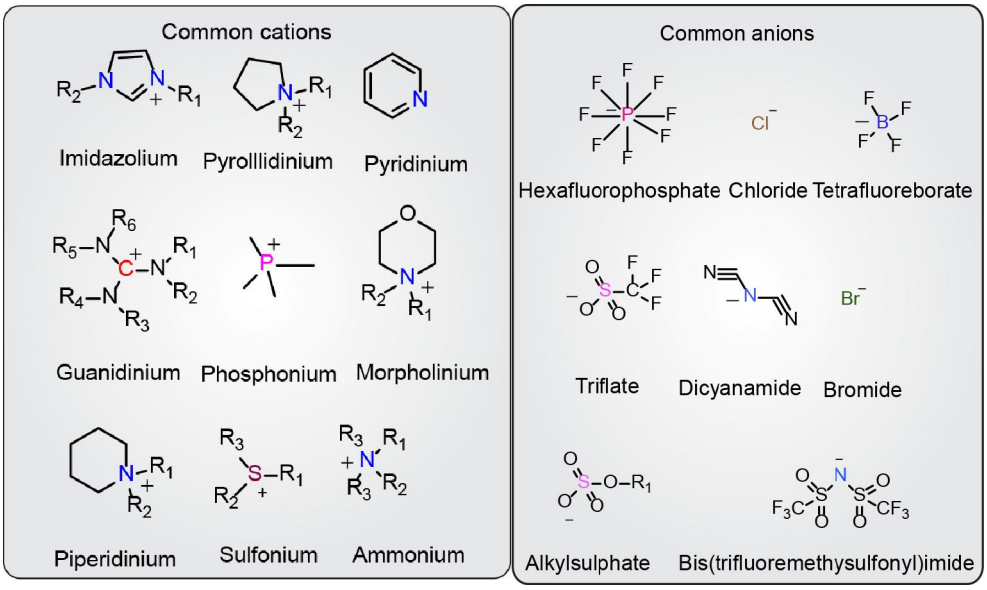

Figure 1.11. Commonly used anions and cations of ionic liquids.

A number of factors like free volume, size of the counter ions and strength of the cation–anion interactions within the ionic liquid structure appear to govern the CO_2 solubility in RTILs. The anion is believed to play a key role in the dissolution of CO_2, whereas the cation is supposed to have a secondary role [Aki (2004)]. This finding is supported by molecular simulation studies and experimental data [Cadena (2004)]. Aki et al. (2004), found that CO_2 solubility in *1*-*n*-butyl-*3*-methylimidazolium, [BMIM]+ based ILs increased with following order of anion variation; $[NO_3] < [DCA] < [BF_4] < [PF_6] < [TfO] < [Tf_2N] <$ [methide].

1.7.3 CO_2 capture by task-specific ionic liquids (TSILs)

It is said that large scale application of ILs for CO_2 capture from flue-gas is mainly hindered by the low CO_2 absorption capacity at post-combustion conditions [Ramdin (2012)]. To overcome this problem, researchers appealed to the amine chemistry by arguing that including an amine moiety to conventional ILs (amine-functionalized TSILs) could greatly improve CO_2 absorption capacity [Bates (2001), Gurkan (2010a)].

The CO_2 absorption ability of TSILs can reach up to threefold of the corresponding RTILs. Gurkan et al. used ab initio calculations to investigate the relationship between the position of the amine functional group and the reaction stoichiometry of IL and CO_2 [Gurkan (2010a)]. They showed that tethering the amine to the cation favored the formation of the carbamate leading to 1:2 stoichiometry, while tethering the amine to the anion favored 1:1 reaction stoichiometry. In spite of the tunable approach towards TSILs, these functionalized ILs posses much higher viscosities as compared to the corresponding RTILs or other commercially available CO_2 scrubbing solutions, rendering serious complications on their applicability for industrial scale. The problem can be avoided by using mixtures of TSILs and RTILs or TSILs adsorbed onto porous membrane support.

Carboxylate functionalized anions, such as acetate, also justify special interest. Chinn et al. investigated that [bmim][acetate] diluted in a 14 wt % water solution exhibits an absorption behavior, which is typical for a chemical complexation process [Chinn (2009), Ramdin (2012)]. An economic evaluation of the process using [bmim][acetate] for CO_2 capture carried out by Shiflett et al. showed that the IL-process could reduce the energy losses by 16% compared to the MEA process Furthermore, they estimated 11% reduction in the investment for the IL-process and 12% lowering in equipment footprint relative to the MEA process [Shiflett (2010)].

Recently, Gurkan et al. used a computational approach to design a new class of ILs, namely aprotic heterocyclic anions (AHAs) [Gurkan (2010b)]. The authors computed the structure and energetics of pyrrolidine, an AHA, and CO_2 reaction product using molecular electronic structure calculations. The pyrrolide was observed to directly combine with CO_2 to form a carbamate with a computed enthalpy of reaction of −109 kJ/mol. Furthermore, they showed that the reaction enthalpy could be tuned depending on the position of substitution on the pyrrolidine ring.

1.7.4 Supported ionic-liquid membranes (SILMs) for CO_2 separation

A number of studies have been performed to investigate the prospects of supported ionic-liquid membranes involving RTILs for CO_2 separation. To take advantage of high CO_2 solubility, low volatility of ILs and to deal with limitations of ILs due to viscosity, supported ionic liquids (SILMs) may prove a better choice in CO_2

separation from flue gases [Rahaman (2010)]. SILMs also increase the contact area between gas and ionic liquid. RTIL, [bmim][Tf_2N], supported on porous alumina membrane revealed very promising results in favor of CO_2 capture ability [Baltus (2005)]. The SILM with [bmim][Tf_2N] showed higher selectivity of 127 (CO_2/N_2) than 72 with [C_8F_{13}mim][Tf_2N].

Nevertheless, industrial application of these SILMs is still limited, majorly due to concerns about SILM stability and their long-term performance [Bara (2008a), Bara (2008b)]. Typically, SILMs reported in the literature are quite thick (~150 μm or more). Industrial applications will require selective layers of less than 1 μm [Bara (2009a)]. One more drawback of SILMs is that the liquid component is observed to leach out through the pores of the support when the trans-membrane pressure across the membrane exceeds the capillary forces stabilizing the liquid within the matrix [Bara (2010)]. Thus, the trans-membrane pressure differential that can be applied is limited to perhaps only a few atmospheres. Natural gas processing with membranes is performed at high pressures (30-60 bar) [Bara (2009a)]. The current SILM configurations are certainly incapable of withstanding with such high pressures. CO_2 capture from flue gas occurs at atmospheric pressure and is perhaps a more realistic target separation for SILMs. These limitations about SILMs urge to polymerize IL monomers and constitute a new family of functional polymers, generally known as polymeric ionic liquids or poly(ionic liquid)s (PILs) possessing unique characteristics of ILs and a macromolecular framework. The major advantages of using a PIL instead of an IL proposed are enhanced mechanical stability, improved processability, durability, and spatial controllability over the IL species [Yuan (2011)].

1.8 Polymeric ionic liquids (PILs)

Polymeric ionic liquids (PILs) refer to a special type of polyelectrolytes which carry an ionic group on their repeating unit. It is worth noting that although ILs are in a liquid state near room temperature, PILs are solids in most of the cases, except a couple of exceptions [Yuan (2011), Mecerreyes (2011)].

1.8.1 Synthesis of PILs

PIL can be synthesized *via* two basic methodologies: (1) direct polymerization of IL monomers, (2) chemical modification of existing polymers. In each of them, a couple of polymerization techniques are involved, such as conventional and controlled radical polymerizations, ring opening metathesis polymerization, step-growth polymerization, and many more [Yuan (2011)]. From a synthetic perspective, each of these strategies as well as the polymerization techniques governs different structural parameters of PILs that demonstrates distinct advantages as well as limitations with respect to the macromolecular design.

1.8.1.1 Polymerization of IL monomers

An IL monomer is an IL in which one or more polymerizable units are incorporated. The polymerization of IL monomers is a conceptually simple, intuitive, straightforward, and widely adopted strategy to prepare PILs in many research groups [Yuan (2011)]. In an IL monomer, a polymerizable unit can be located either on the cation or anion, depending on the desired polymeric architecture. Copolymer with both cationic and anionic backbone can be obtained when cationic monomers such as imidazolium functional acrylate are copolymerized with anionic monomers such as sulphonate functional acrylate. The other type of copolymers involves the copolymerization of similar cationic monomers (or anionic) which posses the same polymerizable ionic moieties but different counter-ions [Mecerreyes (2011)].

1.8.1.2 Chemical modification of existing polymers

PILs can be synthesized *via* chemical post modification of polymers in order to obtain the PIL. The attractiveness of this strategy is that the formed PIL will naturally adopt the degree of polymerization, architecture and monomer composition that is present in the original polymer or copolymer chains [Yuan (2011)]. This way, PILs with unique architectures and composition that are difficult to be synthesized by direct polymerization of IL monomers can be prepared by modifying a carefully chosen precursor polymer of well-defined structure, mass, and architecture. In the case of imidazolium-based PILs, two major paths demonstrated to perform the modification are: (1) grafting N-alkyl

imidazole or its derivatives onto the halo-alkyl function present in each repeating unit of polymers and (2) reacting halo-alkane with polymers containing imidazole.

1.9 Applications of PILs

There are several emerging technological applications of polymeric ionic liquids such as polymer electrolytes in electrochemical devices, building blocks in materials science, nanocomposites, gas separation membranes, innovative anion sensitive materials, smart surfaces, and a countless set of applications in different fields such as energy, environment, optoelectronics, analytical chemistry, biotechnology or catalysis [Green (2009), Mecerreyes (2011), Yaun (2011, 2013)].

1.10 CO_2 separation performance

In order to overcome drawbacks associated with SILMs, incorporating the IL character in the polymer chains offering 'polymeric ionic liquid' (PIL) is a potential option. Pioneering works by Tang et al. showed that PILs exhibit higher CO_2 absorption capacity than the corresponding ILs [Tang (2005a-e), Bara (2007a,b)]. Most importantly, CO_2 absorption and desorption of PILs were faster and are completely reversible as compared to that in ionic liquids. Similar comparison was demonstrated for PILs and their monomeric ILs [Supasitmongkol (2010), Mecerreyes (2011), Xiong (2012), Yaun (2013), Privalova (2013)]. It observed that effects of the anion, cation and backbone of a PIL on its CO_2 sorption capacity were much different than those of RTILs. Tang et al. (2009) investigated that CO_2 sorption capacities of the PILs decreased in the order of cation variation as ammonium > pyridinium > phosphonium > imidazolium. Similarly, the effect of anion on CO_2 sorption was also demonstrated. PILs with mostly investigated anions CO_2 sorption decreased in the order: BF_4^- > PF_6^- > Tf_2N^- [Tang (2009)]. A tetraalkylammonium-based PIL could absorb up to 77 wt% of CO_2 with high CO_2/N_2 selectivity (70) [Supasitmongkol (2010)]. A series of polymeric ionic liquids (PILs) based on poly(diallyldimethylammonium chloride), P[DADMA][Cl] as a precursor was investigated by Bhavsar *et al.* with variation of anions categorized into carboxylates, sulphonates and inorganic type. The work showed the potential of acetate anion for CO_2 sorption and its selectivity over other gases. The sorption capacity of these anions was

correlated with the pKa of conjugate acid of these anions [Bhavsar (2012)]. The major problem of the demonstrated PILs was their brittle nature and thus could not be used at higher pressure [Tang (2005e), Hu (2006), Bara (2007b, Bara (2008a)].

To mitigate this issue, many attempts were made in order to understand and improve the mechanical strength of PIL membranes and their permeability, while maintaining their superior CO_2 based selectivity. The alternative methodologies for making membrane involved copolymerization [Hu (2006), Li (2010, 2013), Chi (2013)], crosslinking [Bara (2007b, 2008a, 2008b, 2010), Li (2011, 2012), Carlisle (2012)] or polymerization on porous polymer support [Bara (2007b, 2008a, 2008b, 2010), Hudiono (2011), Carlisle (2012)] for their effective testing in a flat film form. The gas permeation of these PILs at higher pressure yielded only little success. Hu et al. (2006) developed a mechanically stable membrane by grafting polyethylene glycol (PEG) on to PILs. Higher amount of PEG was required for formation of a mechanically strong film, which limits the RTIL concentration in the copolymer. Nobel's group developed styrene and acrylate containing imidazolium-based PILs with varying *N*-alkyl substituents by polymerization of IL monomer in presence of crosslinker on porous polymer support [Bara (2007b)]. They noted that the gas permeability (CO_2, N_2 and CH_4) of PILs was increased with increasing length of the *N*-alkyl substituent [Bara (2007b)]. In further study, they developed PILs based on cross-linked Gemini room temperature ionic liquid monomer on porous polymer support. It was observed that diffusion of gases through these highly cross-linked poly(RTIL) membranes is quite restricted and hence these membranes exhibited low gas permeability [Bara (2008a)]. They also demonstrated that PILs containing oligo(ethylene glycol) or nitrile-terminated alkyl polar substituents have excellent CO_2/N_2 separation and surpass the Robeson upper bound [Bara (2008b)]. The main-chain imidazolium polymer membranes possessing two different anions (Br^- and Tf_2N^-) were developed wherein, the PIL containing bulky anion (Tf_2N^-) exhibited higher gas permeability than the other one [Carlisle (2010)]. Li et al. (2011), have developed a vinyl imidazolium based PIL by adding crosslinker, which possessed high CO_2 permeability of 101.4 Barrer. The gas permeation of this PIL membrane could be analyzed at 10 atm upstream pressure, indicating good mechanical stability. The same group reported gas permeability of imidazolium based PILs by following same strategy

as used earlier, with increasing side alkyl chain length and dicyanamide as an anion [Li (2011), Li (2012)]. Carlisle et al. (2013) have investigated several vinyl imidazolium based PIL membranes by UV polymerization on porous polymer support and their gas permeation was reported at 2 atm. The CO_2 permeability of these PILs was up to 130 Barrer, with the loss of CO_2/N_2 and CO_2/CH_4 selectivity (14 and 8.7, respectively). The gas permeation of a free standing PIL, P[DADMA][Tf_2N] was reported at 1 atm [Tome (2013b)], which did not use crosslinker, copolymerization or polymer support. The IL based copolyimides were also reported with the different proportion of IL monomer [Li (2010, 2013)]. The gas permeation of these copolyimide (IL content upto 25 mol%) was recorded at 10 atm upstream pressure, while the polyimide with 100 % IL monomer was unable to form film. Authors noted that increasing IL content in the copolyimide exhibited gradual decrease in gas permeability, solubility as well as diffusivity. The reduction in free volume was said to be responsible for this decrease in gas permeation properties. The PVC-grafted PIL was also investigated and the gas permeation was reported with maximum 65 wt % of IL moiety [Chi (2013)]. The advantage PVC-g-PIL graft copolymer system was said to be good mechanical properties than reported earlier. The structures of these reported PILs, their CO_2 permeability and selectivity over N_2 and CH_4 of reported PILs is summarized in the Tables 1.1 and 1.2. For improvement in CO_2 permeation of PILs, the composite membranes of IL and PILs were investigated by several researchers [Bara (2008c, 2008d, 2009b, 2010), Hudino (2011), Li (2011, 2012), Carlisle (2010, 2012, 2013)]. These composite membranes combined the better mechanical properties of polymeric materials and the good CO_2 sorption properties of ionic liquids [Li (2011)] and showed enhanced CO_2 separation properties.

PILs possessing aromatic backbone obtained by an altogether different methodology of post modification of polybenzimidazole (PBI-BuI) were investigated by Bhavsar *et al*. [Kumbharkar (2014), Bhavsar (2014a,b)]. This new methodology offered PILs possessing excellent film formation ability and the permeation properties were recorded at 20 atm applied pressure. Salient features of this methodology included wide structural tunability *via* structural variations in monomers of PBI, alkyl/aryl group used for *N*-substitution and anion diversity. The most significant outcome of the work was the validation on proposition that the fully aromatic backbone is necessary in obtaining film

forming PILs that would withstand high pressures. This suggested that considerable research is still required for a complete understanding of the relationship between molecular composition, macromolecular structure and the gas permeation properties. The knowledge gained from these studies, particularly with regard to structure–property relationships is a necessary step for developing improved PIL based membranes.

Table 1.1 Chemical structure of PILs demonstrated

Chemical structure of PILs or ILs	**Ref.**
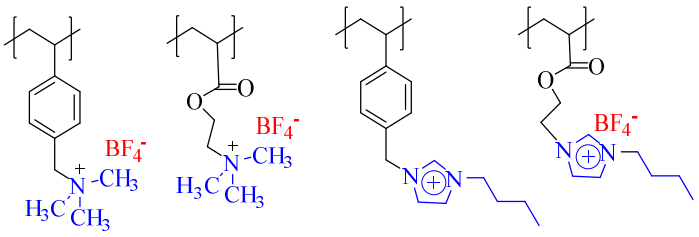 a: P[VBTMA][BF_4] a: P[MATMA][BF_4] c: BF_4^- P[VBBI][BF_4] e: P[MABI][BF_4] d: Tf_2N^- P[VBBI][BF_4]	Tang (2005a), (2005c)
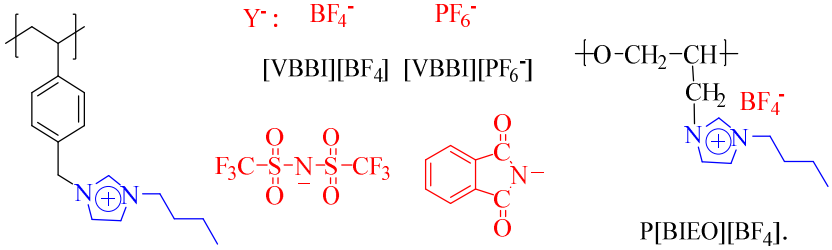 Y^- : BF_4^- PF_6^- [VBBI][BF_4] [VBBI][PF_6^-] P[BIEO][BF_4]. [VBBI][Tf_2N] [VBBI][Sac]	Tang (2005b)
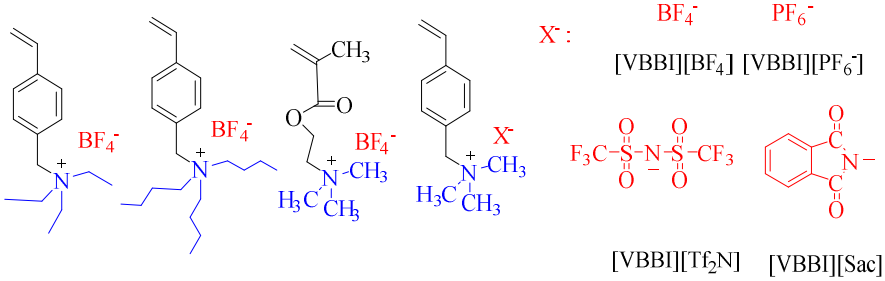 X^- : BF_4^- PF_6^- [VBBI][BF_4] [VBBI][PF_6^-] [VBBI][Tf_2N] [VBBI][Sac]	Tang (2005d)

Chemical structure of PILs or ILs	**Ref.**
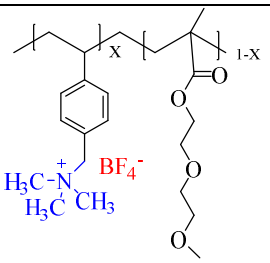 P[VBTMA][BF_4]-g-PEG 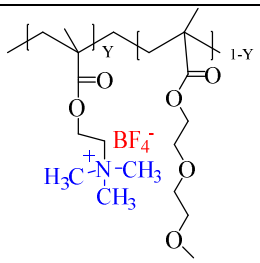 P[MTMA][BF_4]-g-PEG	Hu (2006)
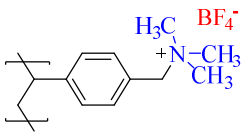 P[VBTMA][BF_4] 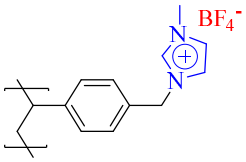 P[VBBI][BF_4] 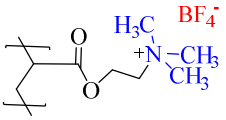 [MATMA][BF_4]	Blasig (2007a, 2007b)
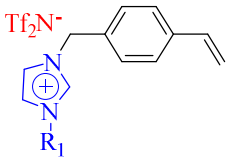 Where, R_1=Me, *n*-Bu, *n*-Hex 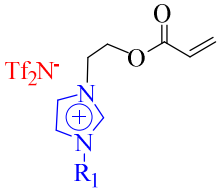 Where, R_1=Me, *n*-Bu RTIL monomers	Bara (2007b)
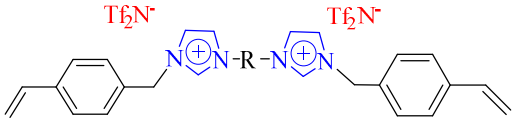 where, R= -$(CH_2)_6$- -$(CH_2)_2O(CH_2)_2$- -$((CH_2)_2O)_2(CH_2)_2$- GRTIL crosslinkable monomers	Bara (2008a)

Chemical structure of PILs or ILs (Continued)	**Ref.**
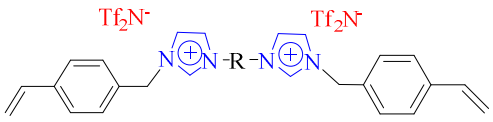 where, R= -$(CH_2)_6$- -$(CH_2)_2O(CH_2)_2$- -$((CH_2)_2O)_2(CH_2)_2$- GRTIL crosslinkable monomers	Bara (2008a)
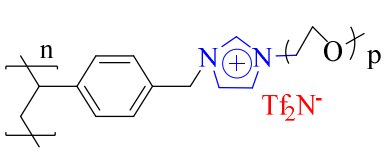 where, p=1,2 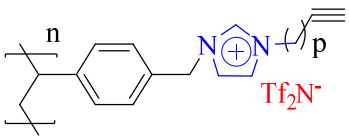 where, p=3,5	Bara (2008b)
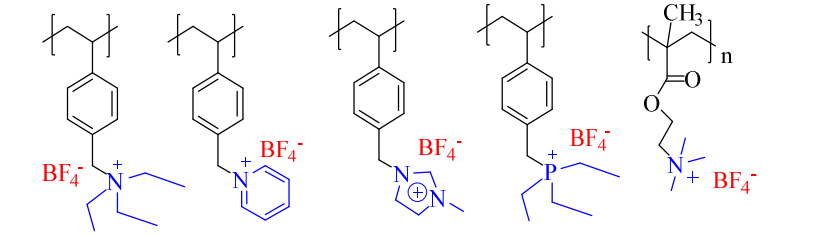 P[VBTMA][BF_4] P[VBP][BF_4] P[VBMI][BF_4] P[VBTEP][BF_4] P[MATMA][BF_4] 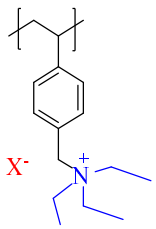 Where, x= BF_4^- PF_6^- $F_3C\text{-}S(=O)_2\text{-}N^-\text{-}S(=O)_2\text{-}CF_3$ P[VBTMA][BF_4] P[VBTMA][PF_6] P[VBTMA][Tf_2N]	Tang (2009), Supasitmongkol (2010)
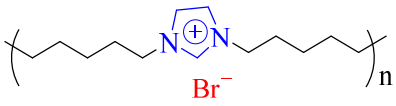 poly(imidazolium)-1 poly(imidazolium)-2	Carlisle (2010)

Chemical structure of PILs or ILs (Continued)	Ref.
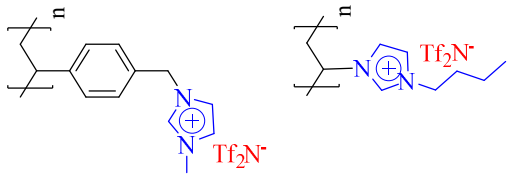 Stryrene based PIL Vinyl based PIL	Hudino (2011)
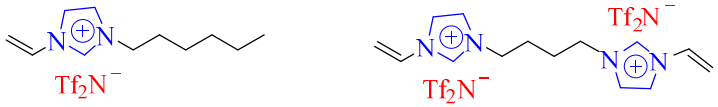 [vbim][Tf_2N] (RTIL monomer) [C_4(dvim)$_2$][Tf_2N] (RTIL based crosslinker)	Li (2011a)
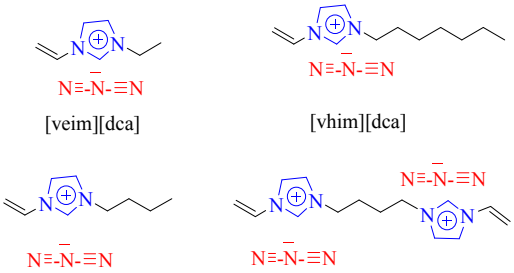 [veim][dca] [vhim][dca] [vbim][dca] crosslinker	Li (2012)
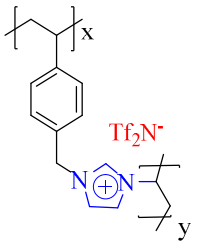 [3-(4-vinylbenzyl)-1-vinylimidazolium)[Tf_2N]	Wilke (2012)
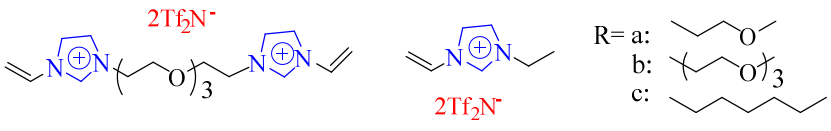 Crosslinking monomer 1 monomer 1	Carlisle (2012)

Chemical structure of PILs or ILs (Continued)	**Ref.**
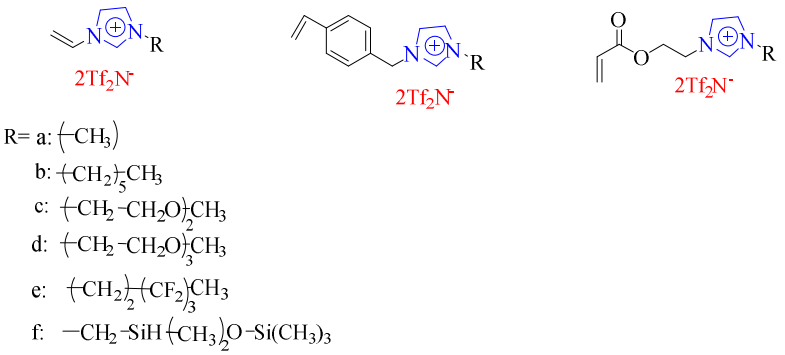	Carlisle (2013)
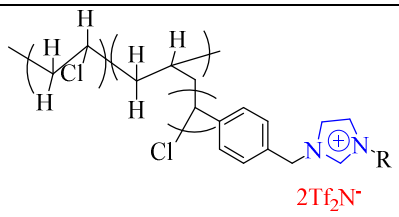 PVC-g-PIL	Chi (2013)
Cation Anions 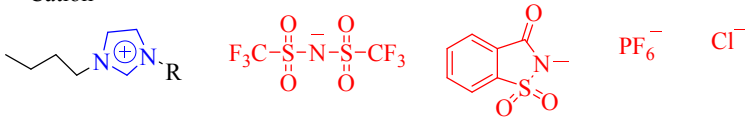	Fang (2013)
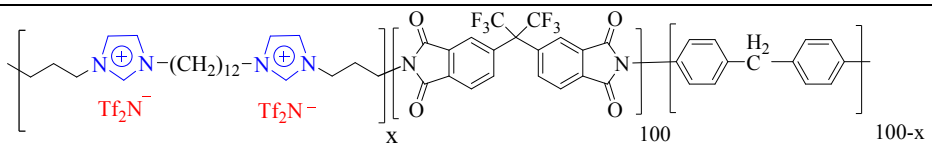 (6FDA-(MDA/RTIL-(6FDA-RTIL) backbone	Li (2013)
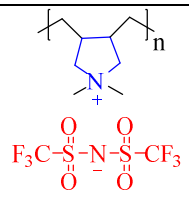 Poly([pyr11][NTf2]	Tome (2013b)

Chemical structure of PILs or ILs (Continued)	**Ref.**
Cation 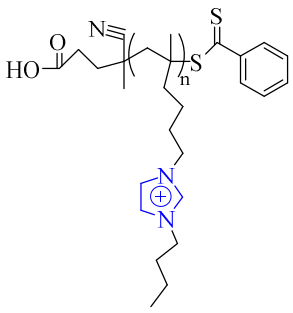 P[BIEMA] Anions [Br] [BF_4] [PF_6] 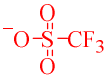 [OTf] [acetate] 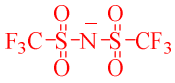 [Tf_2N]	Privalo-va (2013)

Table 1.2. CO_2 permeation and selectivity of reported PILs.

PILs	T_g (°C)	Temp. (°C)	Pressure (atm)	P_{CO_2}	P_{CO_2} / P_{N_2}	P_{CO_2} / P_{CH_4}	Ref
P[VBTMA][BF_4]-g-PEG2000	158	35	2.81	17	60	22	Hu (2006)
P[VBTMA][BF_4]-g-PEG475	156	35	2.81	6	—	—	
P[MTMA][BF_4]-g-PEG2000	NA	35	2.81	38	70	31	
P[MTMA][BF_4]-g-PEG475	NA	35	2.81	3	—	—	
Styrene-Based Poly(RTILS)-methyl	NA	20	2	9.2	32	39	Bara (2007b)
Styrene-Based Poly(RTILS)-butyl	NA	20	2	20	30	22	
Styrene-Based Poly(RTILS)-hexyl	NA	20	2	32	28	17	
Acrylate-Based Poly(RTILS)-methyl	NA	20	2	7	31	37	
Acrylate-Based Poly(RTILS)-butyl	NA	20	2	22	30	22	
Poly(GRTIL) -$(CH_2)_6$-spacer	NA	20	2	4.4	22	27	Bara (2008a)
Poly(GRTIL) -$(CH_2)_2O(CH_2)_2$-spacer	NA	20	2	4	28	32	
Poly(GRTIL) -$(CH_2)_2O)_2(CH_2)_2$-spacer	NA	20	2	3.8	23	28	Bara (2008a)
Poly(RTIL) OEG_1 substituents	NA	22	2	16	41	33	Bara (2008b)
Poly(RTIL) OEG_2 substituents	NA	22	2	22	44	29	
Poly(RTIL) C_3CN substituents	NA	22	2	4.1	37	37	
Poly(RTIL) C_5CN substituents	NA	22	2	8.2	40	30	
poly(imidazolium) membranes	NA	RT	2	0.13	-	-	Carlisle (2010)
poly(imidazolium) membranes	NA	RT	2	5.2	24	20	
6.5% block [DAPIM][NTf_2]$_2$ copolyimide	286	35	10	14.4	23.2	46.7	Li (2010)
14.8% block [DAPIM][NTf_2]$_2$ copolyimide	281	35	10	11.7	24.9	55.6	
25.8% [$DAPIM_2$][NTf_2]$_2$ copolyimide	276	35	10	9.2	22.2	61.5	
8% [C_{12}(DAPIM)$_2$] [NTf_2]$_2$ copolyimide	276	35	10	7.4	23.5	46.4	
Styrene based PIL	NA	23	1-1.5	9.2	32	39	Hudino (2011)
Vinyl based PIL	NA	23	1-1.5	67.3	14.5	10.6	
P[vbim][Tf_2N]	-39	35	10	101.4	22.3	—	Li (2011a)

PILs	T_g (°C)	Temp. (°C)	Pressure (atm)	P_{CO_2}	P_{CO_2} / P_{N_2}	P_{CO_2} / P_{CH_4}	Ref
Poly([veim][dca]	29	35	10	0.09	—	—	Li (2012)
Poly([vbim][dca]	-27	35	1	4.24	26.5	—	
Poly([vhim][dca]	-37	35	1	33.5	20.9	—	
P(vbim)Tf_2N	-60	35	3.5	101	20.6	12.9	Hao (2013)
8 mol% block $[C_{12}(DAPIM)_2][NTf_2]_2$ copolyimides	276	35	10	7.4	23.5	46.4	Li (2013)
10 mol% random $[C_{12}(DAPIM)_2][NTf_2]_2$ copolyimides	257	35	10	7.5	25.8	44.2	
20 mol% random $[C_{12}(DAPIM)_2][NTf_2]_2$ copolyimides	239	35	10	3.5	29.3	46	
Poly[pyr_{11}][NTf_2]	NA	21	1	5.09	22.2	28.6	Tome (2013b)
poly(1a)	48	RT	2	4.8	29	40	Carlisle (2013)
poly(1b)	40	RT	2	69	17	9.9	
poly(1c)	-10	RT	2	14	32	32	
poly(1d)	-15	RT	2	26	34	25	
poly(1e)	52	RT	2	69	11	14	
poly(1f)	-10	RT	2	130	14	8.7	
poly(2a)	NA	RT	2	9.2	32	39	
poly(2b)	NA	RT	2	32	28	17	
poly(2c)	NA	RT	2	22	44	29	
poly(3a)	NA	RT	2	7	31	37	
poly(3b)	NA	RT	2	22	30	22	
PVC-g-PIL 33 wt%	50-90	35	2	7.5	25	—	Chi(2013)
PVC-g-PIL 65 wt%	50-90	35	2	17.9	24.7	—	Chi (2013)

NA: Not available

Chapter 2
Scope and Objectives

The area of strong film forming polybenzimidazole (PBI) based polymeric ionic liquids (PILs) was pioneered by our group. These PILs showed promising results in terms of gas permeation characteristics, especially for CO_2. Chosen structural variations on PBI backbone included variations through tetramine and aliphatic/aromatic dicarboxylic acid monomers, *N*-substitution of resulting PBI by various alkyl groups with aliphatic/aromatic functionality, etc.

There are several reports which describe impact of the cation asymmetry on physical properties of the ionic liquids (ILs). The low viscosity ILs possessing cation asymmetry were demonstrated to improve the CO_2 absorption. Asymmetric substitution in ionic liquids is anticipated to exhibit high structural heterogeneities and loose molecular packing, as compared to the symmetric ILs. Inspired by these observations, we anticipated that this peculiarity can be conveniently used to tailor structural aspects of PILs based on polybenzimidazoles (PBIs) while performing alkyl group substitution on their imidazole group. Such structural tuning is anticipated to disturb chain packing of PILs in order to improve CO_2 sorption and permeation characteristics.

Based on the above rationale, the objective of present work converged as:

a) Modification of polybenzimidazole by 'Asymmetric' *N*-substitution

Investigation of effects of 'substitution asymmetry' on imidazole moiety of two structurally different polybenzimidazoles (PBI-BuI and PBI-HFA) became the first aspect to study. PBI-BuI and PBI-HFA were chosen owing to their better gas permeation properties as compared to their structural analogues with different dicarboxylic acid monomers. The *N*-substitution was carried out with suitable alkyl group (either long alkyl or bulkier in nature, viz., *n*-butyl or *4-tert*-butylbenzyl); while, *N*-quaternization was performed with the methyl group. The halide exchange of obtained PILs was also performed using selected anions (Tf_2N^-, BF_4^- and HFB^-) in order to explore effects of nature of anion on permeation properties. The PILs were evaluated for their physical

properties such as IR, NMR, TGA, DSC, DMA, XRD, density etc. The gas sorption and permeation properties were investigated with He, H_2, N_2 and CO_2.

b) Modification of polybenzimidazole by 'rigid polyaromatic' *N*-substituents

The objective of this part of the work was to investigate effects of incorporation of rigid and bulky polyaromatic hydrocarbons, viz., pyrene and anthracene on physical and gas permeation properties of formed PILs. The pyrene and anthracene substituted PILs, intentionally synthesized for elevating gas permeation properties were also investigated for the detection of nitro-explosive owing to fluorescent nature of them.

c) Investigation of effects of bulky anions

The objective of this part of the work was to gain insight towards effects of bulk of the anion on physical and gas permeation properties of resulting PILs. Five different bulky anions that are alkyl substituted analogues of BF_4^- anion were chosen. The results are correlated to the bulk and CO_2 specificity of the anion.

d) Investigation of separation performance of PILs for olefin/paraffin mixtures

This study aims at investigating gas permeation properties PIL membranes for olefin/paraffin. The separation performance of ethane-ethylene and propane-propylene was evaluated with dense and Thin Film Composite (TFC) membranes using [DBzDMPBI-BuI][BF_4] as a chosen PIL, based on above work. The TFC membranes were prepared using PSF based UF membrane as a structural support and polymeric ionic liquid (PIL) as a selective layer. The main objective of TFC membrane preparation was to study the separation performance of this PIL for light hydrocarbons such as ethane, ethylene, propane, propylene. The permeability of these gases in dense membrane form was very low. Some of them were beyond detection limit of the permeation equipment. Among PILs studied above, [DBzDMPBI-BuI][BF_4] was selected to prepare TFC membranes based on its better permeation properties.

Organization of thesis

The work carried out towards defined objectives is presented in 8 chapters.

Chapter 1: A review is presented on the gas separation requirements and the need of CO_2 separation in current environmental scenario. Current technologies used for CO_2 separations followed by advantages of the membrane based separation over the conventional processes are described. Theoretical aspects of gas permeation and factors affecting gas permeation properties in polymeric membranes are briefly described. The positioning of IL and PILs as membrane materials for CO_2 separation is highlighted.

Chapter 2: The chapter describes scope, aims and objectives of the present work. This chapter ends with organization of the thesis.

Chapter 3: Experimental procedures for synthesis, polymer characterization, sorption and gas permeation analysis are detailed in this chapter. The synthesis of PBI based PILs with substitution asymmetry is described. The experimental protocol for the preparation of *N*-substituted PBIs with different substituents and subsequent exchange of halide anion is given. Dense membrane preparation, methods used for characterization of physical properties, gas sorption and permeation properties is presented. TFC membrane preparation using PSF based UF membrane as a structural support and polymeric ionic liquid (PIL) as a selective layer is described in detail.

Results obtained during this study are grouped into 4 chapters as follows.

Chapter 4: The approach of obtaining asymmetrically substituted PILs for improving CO_2 sorption and permeation properties is evaluated by performing primary structural variations in PIL. Imidazole groups of two different PBI backbones (PBI-BuI and PBI-HFA) were substituted using different alkyl groups to offer PILs with asymmetric substitution. One of the substituent was maintained as methyl, while other was long alkyl or bulkier in nature (*n*-butyl or *4-tert*-butylbenzyl). These substitutions were anticipated to inhibit chain packing. The halide exchange of obtained PILs was also performed using selected anions (Tf_2N^-, BF_4^- and HFB^-) in order to understand effects of nature of anion on permeation properties. Thus obtained 'asymmetric PILs' were evaluated for physical and permeation properties.

Chapter 5: This chapter presents effects of incorporation of rigid polyaromatic hydrocarbons, viz., pyrene and anthracene in PBI-BuI on gas permeation properties. The pyrene and anthracene groups were first used for the *N*-substitution. Further, the *N*-quaternization was performed using bulky *4-tert* butylbenzyl (Bz) group, in order to obtain PILs that are anticipated to possess elevated gas permeation properties. PILs with halide anions were further anion exchanged with two chosen anions, viz., Tf_2N^- and BF_4^-. Obtained PILs were characterized by requisite physical properties, pure gas sorption and permeability. The present PILs were also evaluated for the nitro-explosive vapor detection by fluorescence quenching.

Chapter 6: In the present work, five different bulky anions which are alkyl substituted analogues of BF_4^- anion in were chosen for the halide exchange of a PIL. The I^- anion of a PIL, [DBzDMPBI-BuI][I] was exchanged with selected bulky anions. The obtained PILs were characterized by their physical and gas permeation properties.

Chapter 7: In this chapter, investigations towards permeation properties of olefin/paraffin of a chosen PIL are presented. The separation performance of these gases was evaluated with dense and Thin Film Composite Membranes (TFC) membranes. The potential of PBI based PIL as gas separation membrane materials was well discussed in previous chapters. However, their separation performance could not be studied for hydrocarbons such as ethane, ethylene, propane, propylene due to their low permeability. To circumvent this, the TFC membranes were prepared using PSF based UF membrane as a structural support and polymeric ionic liquid (PIL) as a selective layer. Among studied PILs, [DBzDMPBI-BuI][BF_4] was selected to prepare TFC membranes due to its better intrinsic permeation properties. Effects of concentration of dope solution used to cast porous PSF support and concentration of the coating solution were evaluated by analyzing pure as well as mixed gas permeance and selectivity of the formed TFC membranes.

Chapter 8: The results obtained and conclusions drawn are summarized in this chapter.

Chapter 3

Experimental

3.1. Monomers and materials

3,3′-Diaminobenzidine (DAB), 4,4′-hexafluoroisopropylidene)bis(benzoic acid) (HFA), 5-*tert*-butylisophthalic acid (BuI), sodium hydride (60% dispersion in mineral oil), 4-*tert*-butylbenzyl bromide (BzBr), *n*-butyl iodide (BI), 9-(chloromomethyl)anthracene (AnCl), *1*-(bromomethyl)pyrene (PyBr), sodium tetrafluoroborate ($NaBF_4$), lithium bis(trifluoromethane) sulfonimide (Li-Tf_2N), silver heptaflurobutyrate (C_3F_7COOAg, Ag-HFB), potassium (4-(*tert*-butyl)phenyl) trifluoroborate [$(CH_3)_3Ph\text{-}BF_3$], potassium (3,5 bis(trifluoromethyl) phenyl) trifluoroborate [$(CF_3)_2Ph\text{-}BF_3$], sodium tetrakis (1-imidazolyl)borate [Im_4B], potassium tetraphenylborate [Ph_4B], potassium(2,4-bis(trifluoromethyl)phenyl)tris(3,5-bis (trifluoromethyl)phenyl)borate [$(CF_3)_8Ph_4B$], *N*,*N*-dimethylacetamide (DMAc), *N*-methyl-pyrrolidinone (NMP) and dry dimethyl sulfoxide (DMSO, 0.01% H_2O) were procured from Aldrich Chemicals (Germany). Polyphosphoric acid (PPA, 85% P_2O_5) was procured from Alfa Aesar (UK), while conc. H_2SO_4 and *N,N*-dimethylformamide (DMF) were procured from Merck (India). Chloroform, methanol, toluene, acetone and acetonitrile were obtained from S.D. Fine Chemicals (India). Pure gases, viz., He, H_2 and N_2 (minimum purity 99.9%) were procured from Vadilal Chemicals Ltd. (India), while CH_4 and CO_2 (99.995%) were procured from Air Liquide (USA).

3.2. Synthesis

3.2.1 PBI Synthesis

Polybenzimidazoles based on DAB and suitably chosen aromatic dicarboxylic acids were synthesized by solution polycondensation method in PPA, which acts as a solvent as well as condensation agent [Iwakura (1964c), Saegusa (1997)]. The reaction pathway is represented in Scheme 3.1. In a typical procedure, a three-necked flask equipped with a mechanical stirrer, N_2 inlet and a $CaCl_2$ drying tube was charged with 2400 g of PPA, 80 g (0.3738 mol) of DAB and temperature was raised to 120 ºC. After

complete dissolution of DAB, 0.3738 mol of respective dicarboxylic acid (BuI/HFA) was added; temperature was slowly raised to 170 ºC and maintained at that temperature for 5 h under constant flow of nitrogen. The temperature was further raised to 200 ºC and maintained for certain duration, depending upon the dicarboxylic acid used. After completion of the reaction, temperature was lowered and the highly viscous reaction mixture was poured in to the stirred water. The precipitated polymer was crushed and thoroughly washed with water till it was neutral to pH. The polymer was then kept overnight in 10% aqueous Na_2CO_3 solution, washed with water until neutral to pH and soaked in acetone for 16 h to remove water. The dried polymer (100 ºC, 3 days) was further purified by precipitation. It was dissolved in DMAc, undissolved particles were removed, if any, by centrifugation at 3000 rpm for 1 h and reprecipitation in to the stirred water. The polymer was finally dried at 60 °C for 24 h and then in vacuum oven at 100 °C for 3 days. Structures of obtained polymers along with their abbreviations used are given in Scheme 3.1.

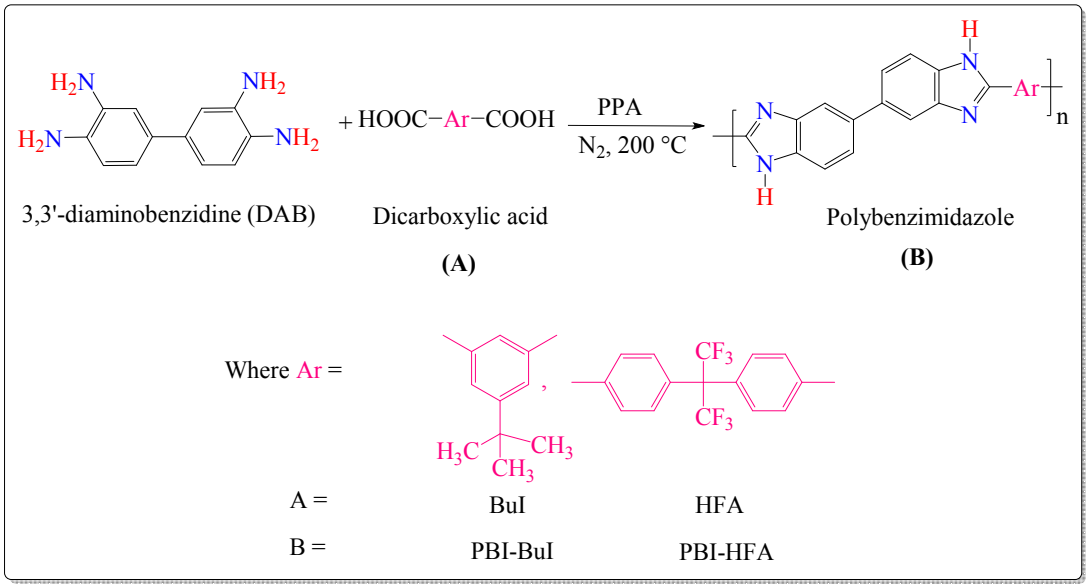

Scheme 3.1. Synthesis of PBI by condensation of DAB with aromatic dicarboxylic acids

3.2.2 *N*-Substitution of PBIs

The *N*-Substitution of PBI was carried out in dry DMSO by preparing its sodium salt, followed by addition of an alkyl halide. Typically, a three-necked round bottom flask

equipped with N_2 balloon was charged with 300 mL of dry DMSO, 10 g of PBI, 2.1 equivalents of NaH and stirred at ambient temperature for 24 h. The reaction mixture was then heated at 80 ºC for 3 h. A deep blood red color developed after the dissolution of PBI. The solution was allowed to cool to the ambient and 2.1 molar equivalents of alkyl halide [*4-tert*-butylbenzyl bromide, *n*-butyl iodide, *9*-(chloromethyl)anthracene or *2*-(bromomethyl)pyrene)] dissolved in 10 mL of dry DMSO was added in a drop wise manner over a period of 15 minutes. The reaction mixture was precipitated indicating formation of the *N*-substituted PBI, which was stirred further for 12 h in order to achieve completion of the reaction. It was slowly poured on to the stirred water. The precipitated polymer was washed several times with water and dried in a vacuum oven at 100 °C for a week. Synthesized polymers were purified by dissolution in DMAc and reprecipitation in water.

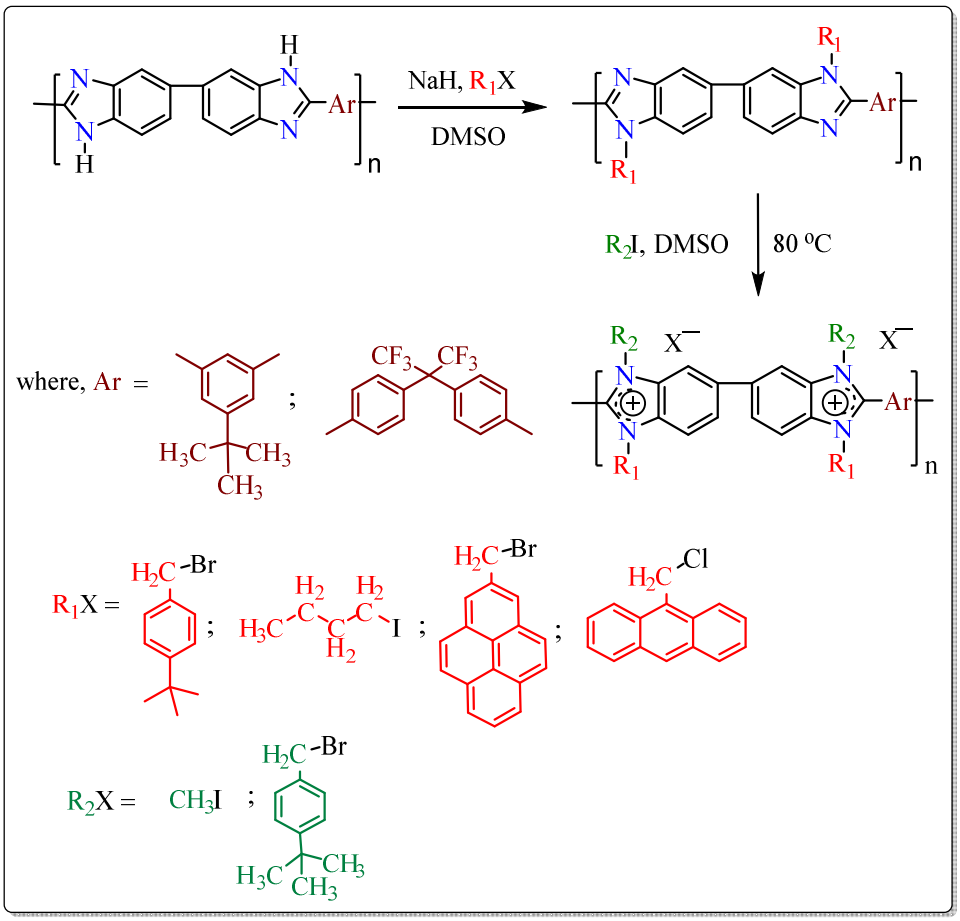

Scheme 3.2. Synthesis of PILs with different substituents

3.2.3 *N*-Quaternization of *N*-substituted PBIs

The *N*-quaternization of *N*-substituted PBIs as obtained above was carried out using either methyl iodide or *4-tert*-butylbenzyl bromide as shown in Scheme 3.2. Typically, a 3-necked round bottom flask was charged with 300 mL of dry DMSO, 10 g of *N*-substituted PBI, 2.5 equivalents of alkyl halide and stirred under N_2 atmosphere at the ambient temperature for 12 h. After this, reaction mixture was further heated at 80 ºC for 12 h in order to achieve quantitative anion exchange. After 12 h, reaction mixture was allowed to cool down to the ambient temperature and then precipitated in a mixture of toluene and acetone (1:1v/v). The obtained golden yellow fibrous polymer was dried at 80 ºC for 24 h. Obtained polymer was further purified by dissolution in DMF and reprecipitation in the toluene: acetone (1:1v/v) mixture. Polymer was finally dried in the vacuum oven at 100 ˚C for a week to ensure complete removal of water.

3.2.4. Anion exchange of *N*-Quaternized PILs

An exchange of halide anion of a quaternized PBI was done in DMF as the solvent. A conical flask equipped with a $CaCl_2$ drying tube, was charged with 150 ml of DMF and 5 g of quaternized PBI (PIL with halide as the counter ion), as shown in Scheme 3.3 and 3.4. After complete dissolution of polymer while stirring, 2.1 molar equivalents of Na/K/Li salt of an anion (except for HFB^-) were added. The reaction mixture was further stirred at the ambient for 24 h in order to ensure maximum possible replacement of the anion. The reaction mixture was precipitated in deionized water, filtered, repeated washed with water and dried at 80 ºC for 24 h. The obtained polymer was further purified by dissolving in DMF (7% w/w), precipitating in water and drying at 60 ºC in vacuum oven for 3 days.

An exchange of iodide anion of a quaternized PBI with heptafluorobutyrate (HFB^-) was done using Ag-HFB. Visual observations based on immediate formation of AgI precipitate after the Ag-HFB addition provided an indication for the exchange. The reaction mixture was further stirred for 24 h in order to ensure maximum possible exchange. The solution was centrifuged, precipitated in water, filtered and dried at 80 ºC. The polymer was further purified by dissolution in DMF (7% w/w), precipitation in water and drying at 60 ºC in vacuum oven for 3 days. The obtained polymer was stored in

desiccator until use. The degree of quaternization was obtained by estimating halide content in the formed PIL by Volhard's method [Vogel (1989)]. A 0.1 g of PIL powder was stirred in 20 ml of 0.01M $AgNO_3$ solution for 24 h. Excess of unreacted $AgNO_3$ was titrated against 0.01 M KSCN, from which, halide content and thus the extent of halide exchanged was estimated. An exchange of halide by a desired anion was estimated by titrating formed metal halide salt (M^+X^-) with 0.01 M $AgNO_3$ by Volhard's method.

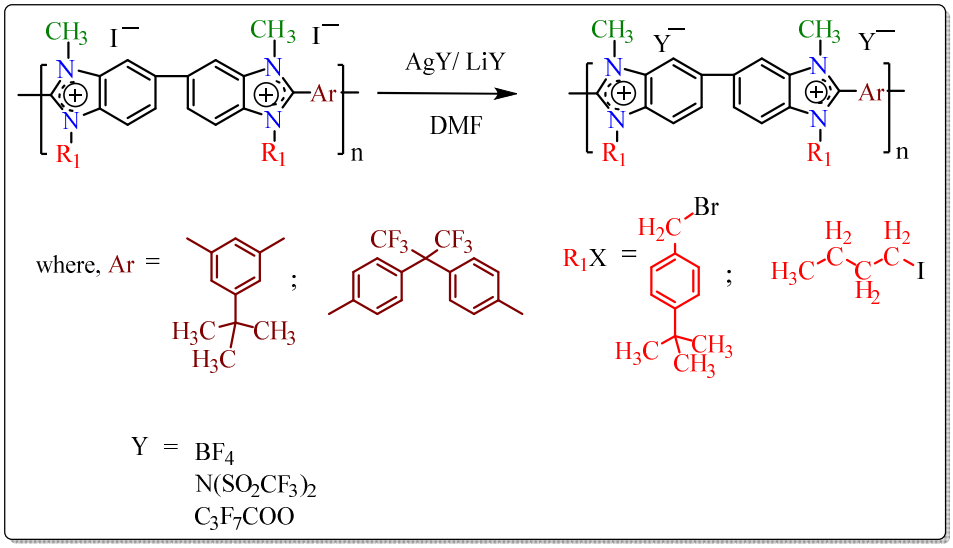

Scheme 3.3. Anion exchange of PILs based on PBI-BuI and PBI-HFA

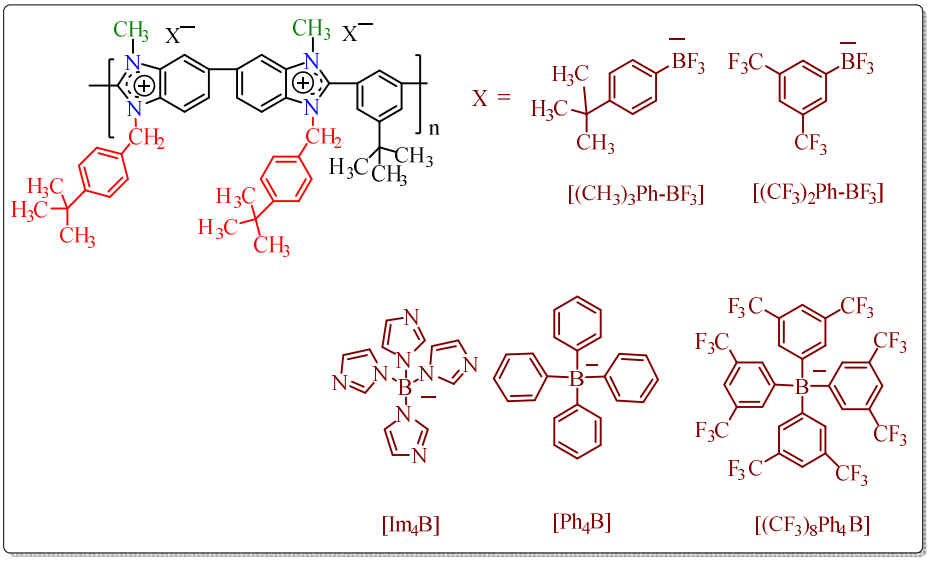

Scheme 3.4. Anion exchange of PILs based on PBI-BuI with bulky anions

3.3. Polymer characterizations

3.3.1 Solvent solubility, WAXD analysis and density

The solubility of PILs in common organic solvents was determined by adding 0.1 g of PIL in a 10 mL of a solvent while stirring at the ambient for 24 h. In case of insolubility, heating at 80 °C (or near boiling point, in case of the low boiling solvents) was employed. Inherent viscosity (η_{inh}) of PBI-BuI was determined using Ubbelohde viscometer with 0.2 $g.dL^{-1}$ polymer concentration in 98% H_2SO_4 at 35 °C. Wide angle X-Ray diffraction (WAXD) analysis of membranes in film form (3 samples prepared under identical conditions) was carried on a Phillips Analytical diffractometer in reflection mode using CuKα radiation (λ = 1.54 Å). The 2θ range from 5° to 40° was scanned with a scan rate of 2.5° min^{-1}. The average intersegmental d_{sp} was calculated from the amorphous peak position (reproducibility: ±0.05 Å). The density (ρ) of membranes was measured at 35 °C by using specific gravity bottle and decalin as the solvent that exhibited < 1.2 % sorption in PILs. The density measurement was repeated with three samples and the deviation from the average value was < 0.01 $g.cm^{-3}$.

3.3.2 Spectral Characterizations

FT-IR spectra of polymers in a thin film (~10 μm) form were recorded at the ambient temperature on Perkin Elmer Spectrum GX spectrophotometer. ^{1}H-NMR spectra were recorded on Bruker AC-200 using DMSO-d_6 as the solvent. UV spectra of PBI-BuI and PIL solutions prepared in DMSO (conc. = $3x10^{-5}$ $M.L^{-1}$) were recorded on a Jasco V-570 UV-visible spectrometer. Fluorescence measurements were carried out using a Cary eclipse fluorescence spectrophotometer at the ambient temperature in DMSO. Spectrosil quartz cuvettes having a path length of 1 cm were used to measure fluorescence of solution samples. For quenching of florescence by nitroaromatics in solid state, the film (~ 12 μm) was introduced in a desiccator saturated with NB vapors for varying duration. For other TNT and PA, the solid state analysis was carried out in a small glass vial saturated with explosive vapors.

3.3.3 Thermal Characterizations

Thermogravimetric analysis (TGA) of polymers was performed after vacuum drying treatment at 100 °C for a week. TGA was carried out in the temperature range of 50–900 °C using TGA-7 at a heating rate of 10 °C min^{-1} under N_2 atmosphere. Dynamic mechanical analysis (DMA, Rheometric Scientific, USA) of present PILs (in film form of 0.045x8x10 mm^3 size) was employed to determine the glass transition temperature (T_g) of PILs. The scans were recorded in the dynamic temperature ramp test mode at a frequency of 1 Hz. The testing temperature ranged from 50 to 280 °C and the heating rate was 10 ° min^{-1}.

3.4. Membrane preparation

3.4.1 Dense membrane preparation

Dense membranes were prepared by the solution casting method using 3% (w/v) polymer solution in appropriate solvent; prepared while stirring at 80 °C for 14-18 h under dry atmosphere. Formed membrane (~ 45 μm thick) was peeled off. Such membranes were finally dried in vacuum oven at 100 °C for a week and used for subsequent analyses.

3.4.2 Ultrafiltration (UF) membrane preparation

The support used for TFC membrane preparation, a PSF based UF membrane was prepared by phase inversion process using pilot scale membrane casting facility. The solutions were prepared by dissolving (i) 200 g of PSF in 1000 g of DMF (20%) and (ii) 220 g of PSF in 1000 g of DMF (22%) while stirring at ambient for 48 hr. The degassed solution was cast on to a running nonwoven polyester fabric (Hollytex – 3329) with air-dry time of 8 sec, before it entered into the gelation bath containing water as the nonsolvent at 27 °C. Formed UF membrane of ~ 250 μm thickness was left in running water for 16 hr to ensure complete removal of the solvent and then stored at 4 °C. The membranes were designated as PSF_{20} and PSF_{22}, where the suffix denotes the concentration of polymer in the dope solution. Molecular weight cut off (MWCO, which implies a molecular weight of the solute that is 90% retained by the membrane) of the UF membranes was determined using polyethylene glycols (PEGs) of increasing

molecular weight as solutes. Water flux of membranes was measured using a stirred cell in dead-end mode at 2 bar pressure. Initially, 50 mL of distilled water was allowed to permeate through the membrane to remove formalin, and then the water flux was measured. The measurements were repeated at least for 4 coupons and the variation was found to be ± 10%.

3.4.3 TFC membranes preparation

UF membranes of 15x8 cm^2 size were used as the support for the preparation of TFC membrane by dip coating method. The support UF membrane was mounted on a glass plate with all four sides taped with a scotch tape. This way, only the top side of the support UF membrane was allowed to expose to the coating solution. This plate was then dipped into a tray of 18x10x4 cm^3 size, filled with the PIL solution made in acetonitrile for 30 to 45 sec. After dip coating, the formed TFC membranes were air dried for 5 min and then in an oven at 60 °C for 45 min. Minimum six TFC membranes were prepared under identical set of conditions and analyzed for the gas permeance by a variable volume method at upstream pressure of 50 to 60 psi, while keeping permeate side at the ambient pressure.

3.5. Gas permeation analysis

3.5.1 Gas sorption

The pure gas sorption isotherms (H_2, N_2, CH_4 , CO_2 , C_2H_4, C_2H_6, C_3H_6 and C_3H_8) were obtained at 35 °C using equipment that consisted of the dual-volume, single-transducer set up based on the pressure decay method [Koros (1976), Karadkar (2007)]. The schematic of sorption equipment is given in Figure 3.1, while the photograph is given in Figure 3.2. The polymer sample in film form (~ 12 μm) was placed in the sorption cell, evacuated and flushed with gas several times. The system was then evacuated to 0.00001 mbar using oil diffusion pump. The gas was introduced rapidly and initial pressure was recorded. As the sorption proceeds, the pressure starts decreasing and ultimately remains constant after the equilibrium is established. Incremental raise in pressure of the equilibrated system until about 20 atm was attained. The amount of gas

sorbed in the polymer sample at each equilibrium pressure was determined from the initial and final pressure. The estimated experimental uncertainty was up to ± 1.7 %, as calculated based on the uncertainty principle.

The gas sorption in glassy polymers is described by Eq. 1 [Koros (1976), Karadkar (2007)]

$$S_A = \frac{C}{p} = K_D + \frac{C'_H b}{(1+bp)} \qquad (1)$$

where, C is the gas concentration in the polymer, p is the applied gas pressure, k_D is the Henry's solubility coefficient, C'_H is the Langmuir saturation constant and b is the Langmuir affinity constant. These constants were obtained by the nonlinear regression analysis of experimentally determined gas sorption by genetic algorithm, an optimization technique capable of searching global optima [Goldberg (1989), Kumbharkar (2006)].

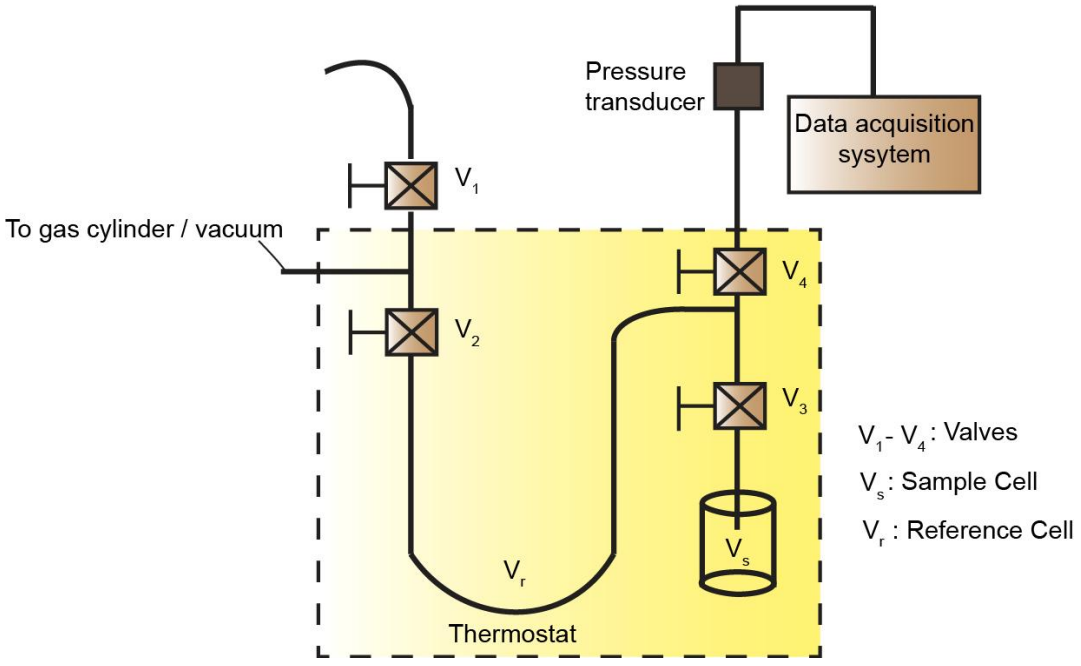

Fig. 3.1. Schematic of gas sorption equipment

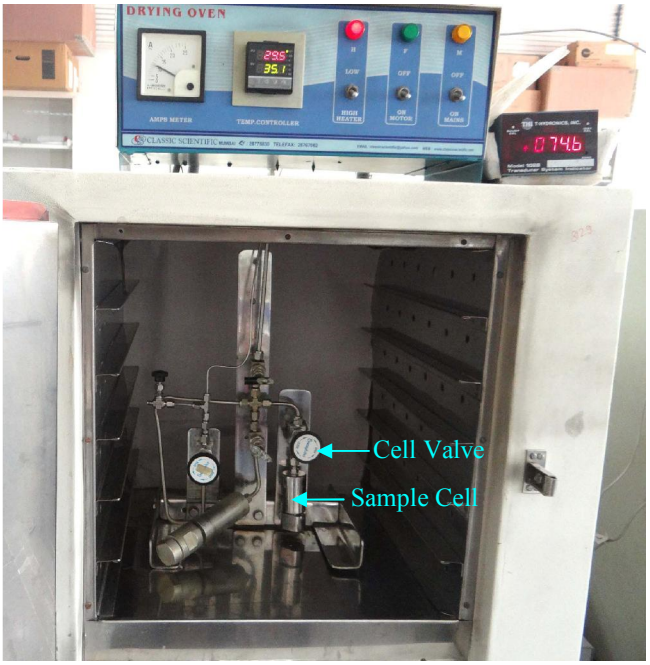

Fig. 3.2. Photograph of gas sorption equipment

3.5.2 Permeation analysis

The permeability measurement using pure gases (He, H_2, N_2, CH_4 , CO_2 , C_2H_4, C_2H_6, C_3H_6 and C_3H_8) was carried out by standard variable volume method at upstream gas pressure of 20 atm and at 35 °C; while maintaining the permeate side at the atmospheric pressure [Kumbharkar (2006)]. The schematic of permeation equipment is given in Figure 3.3, while the photograph is given in Figure 3.4. One end of the feed side of the cell was connected through valve V1 to the feed gas cylinder outlet and a pressure gauge (0-550 psi range). The valve V2 (vent) was used to control the feed pressure. On the permeate side of the cell, a calibrated borosilicate glass capillary (I.D. = either 1.0 or 1.5 mm) containing a small mercury slug (~ 4-6 mm in length) was connected. The membrane cell assembly was kept in a thermostat. Displacement of the mercury slug was monitored against time.

Membrane samples (5 cm in diameter) after removing from the vacuum oven were immediately mounted in the permeation cell. The gas permeability was calculated using following equation:

$$P = \frac{N \cdot l}{(p_1 - p_2)} \qquad (2)$$

where, 'P', the permeability coefficient expressed in Barrer, 'N' is the steady-state penetrant flux ($cm^3.cm^{-2}.sec$), 'p_1' and 'p_2' are the feed and permeate side pressures (cm Hg), while 'l' is the membrane thickness (cm). The permeability measurements were repeated with at least 3 different membrane samples prepared under identical conditions and the data was averaged. Variations in the permeability from average data collected for 3 samples prepared under identical conditions was 5-13% depending upon the gases analyzed.

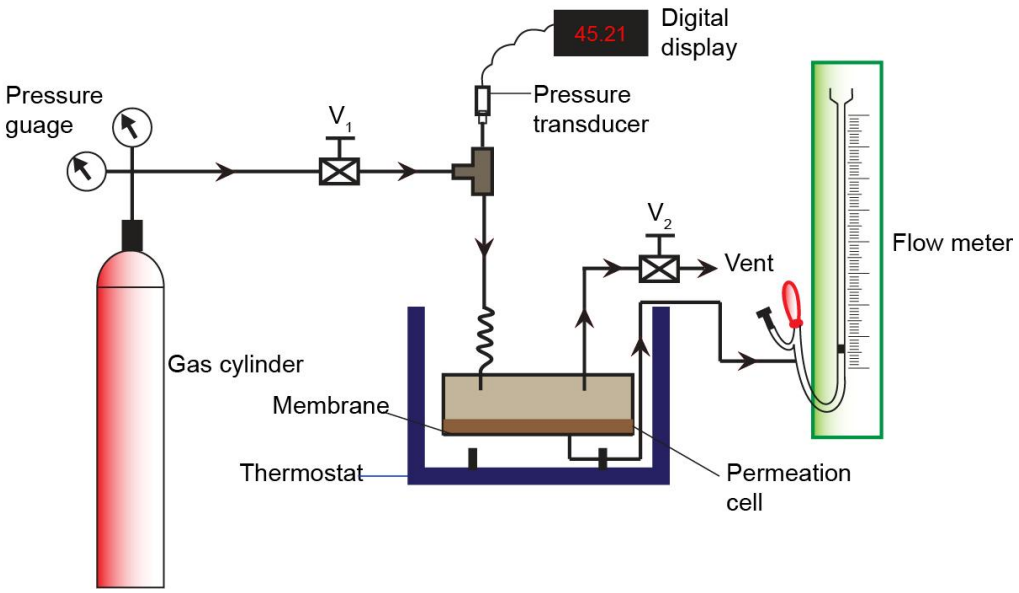

Fig. 3.3. Schematic of gas permeation equipment

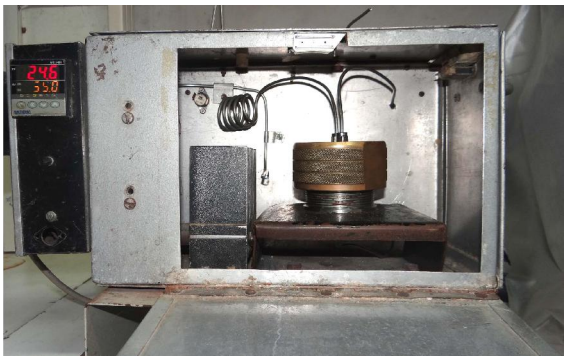

Fig. 3.4. Photograph of gas permeation equipment

3.5.3 Estimation of diffusivity coefficient

The permeability coefficient for a particular gas along with its solubility coefficient at 20 atm was used to estimate the diffusivity coefficient using Eq. (3).

$$P_A = D_A S_A \quad (3)$$

where, P_A is an intrinsic permeability, D_A the average effective diffusivity and S_A is the gas solubility coefficient of a gas A.

3.6 Mixed gas permeation

The mixed gas permeation system was similar to the Wicke-Kallenbach technique [Huang (2012)]. The mixed gas was fed to the membrane mounted in the cell. The sufficiently large feed volume (530 mL) was taken to avoid any significant change in the feed composition by membrane permeation. On the permeate side of membrane, the pure nitrogen was swept continuously in order to avoid the concentration polarization. The permeated gases swept out with nitrogen were analyzed with gas chromatograph (GC) to determine their quantity and ratio.

The Haysep-Q packed column of 3 meter length was used for the hydrocarbon analysis. First, the different known amounts of pure gases were injected into the GC and their corresponding peak area was determined to construct the calibration plots. Now in the further experiments, the unknown gas samples were quantified by determining their peak area and placing that on the calibration plot.

The mixed gas selectivity is calculated from the mole fraction ratio of gas 'a' and gas 'b' in the downstream to the upstream as expressed by the following equation:

$$\alpha_{a/b} = \frac{Pa}{Pb} = \left(\frac{Y_a / Y_b}{X_a / X_b} \right) \quad (4)$$

where P_a and P_b represent the permeability of gas 'a' and gas 'b', respectively. The '*X*' and '*Y*' refer to the volume fractions of the indicated gas in the feed and permeate, respectively.

Chapter 4

Variations in '*N*-substituent' of PILs in an asymmetric manner: Investigations on physical and gas permeation properties

4.1 Introduction

The effects of substitution of alkyl groups on imidazole ring of low molecular weight ionic liquids (ILs) in an asymmetric manner on properties such as melting point, density, viscosity, crystallinity, etc. have been documented in the literature [Yu (2009), Payagala (2007), Rocha (2013)]. The lower viscosity of 'asymmetrically substituted ILs' was demonstrated to improve the CO_2 absorption [Xiao (2009b)]. Asymmetrically substituted imidazolium-based ILs exhibited higher structural heterogeneities and lower molecular packing compared to their symmetric counterparts. This peculiarity can be conveniently exploited to tailor structural aspects of PBI based PILs while performing alkyl group substitution on their imidazole moities. Such structural tuning is anticipated to disturb chain packing in PILs and favourably influence CO_2 permeation characteristics.

The present work evaluates the approach of obtaining asymmetrically substituted PILs for improved CO_2 sorption / permeability characteristics. In order to do so, imidazole groups of two different PBI backbones *viz*. PBI-BuI and PBI-HFA were substituted using different alkyl groups to obtain PILs with asymmetric substitution. One of the substituent was maintained as methyl, while other was bulky or long alkyl chain in nature viz. 4-*tert*-butyl benzyl or *n*-butyl, so as to result into inhibition of chain packing. The halide exchange of obtained PILs was performed using selected anions, viz., Tf_2N^-, BF_4^- and HFB^-. These anions were selected based on their capability to offer elevated CO_2 sorption properties in ILs and PILs [Bhavsar (2014b)]. Thus obtained PILs were investigated for their physical and gas permeation properties.

4.2. Synthesis of PILs and their characterization by spectroscopic techniques

The *N*-substitution of PBI-BuI and PBI-HFA was carried out in dry DMSO by preparing their sodium salt, followed by reaction with *n*-butyl (B) or 4-*tert*-butylbenzyl

(Bz) *via* formation of Na-salt of a PBI, as detailed in Chapter 3. The *N*-substituted polymers were isolated, purified and the degree of substitution was assessed by ^{1}H NMR spectroscopy (Fig. 4.1 and Fig. 4.2). In both the cases, high degree of substitution (90-95%) was obtained. The purified *N*-substituted polymer was then alkylated by methyl iodide (M) in the next step in order to obtain PILs with asymmetric *N*-substitution. They were further purified and characterized by ^{1}H NMR and IR spectroscopy.

In ^{1}H-NMR spectra of PILs (Fig 4.3 and 4.4), a peak in the range of δ 13-14, attributable to the 'imidazole' N-H protons of PBI-HFA / PBI-BuI were completely disappeared. This was a primary indication of almost quantitative nature of the substitution reaction. An assessment of degree of quaternization was done by comparing integration of protons belonging to the methyl group (appearing in the range δ 4.0-4.5) with that of aromatic protons of the precursor PBI appearing in the range of δ 7.5-9.5. For PILs, viz., [DBzDMPBI-BuI][I], [DBDMPBI-BuI][I], [DBzDMPBI-HFA][I] and [DBDMPBI-HFA][I]; the degree of quaternization obtained was 93, 92, 87 and 91%, respectively. The degree of quaternization was also determined by Volhard's method [Jeffery (1989)] and was found to be 93, 87, 90 and 89%, respectively, for these PILs. A good agreement was found between the degree of quaternization obtained by both the methods (^{1}H-NMR and Volhard's).

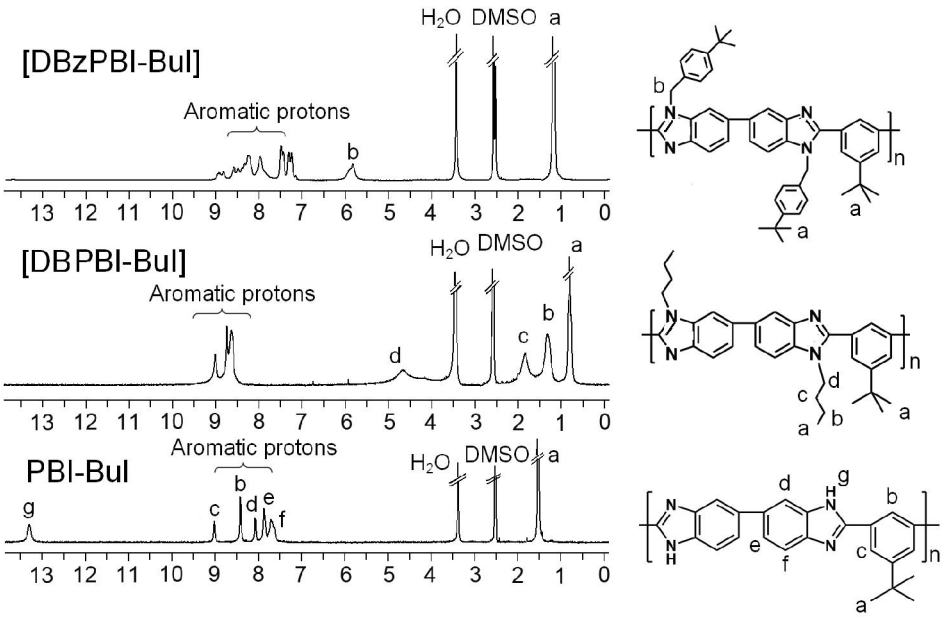

Fig. 4.1. ^{1}H NMR spectra of *N*-substituted PBI-BuI.

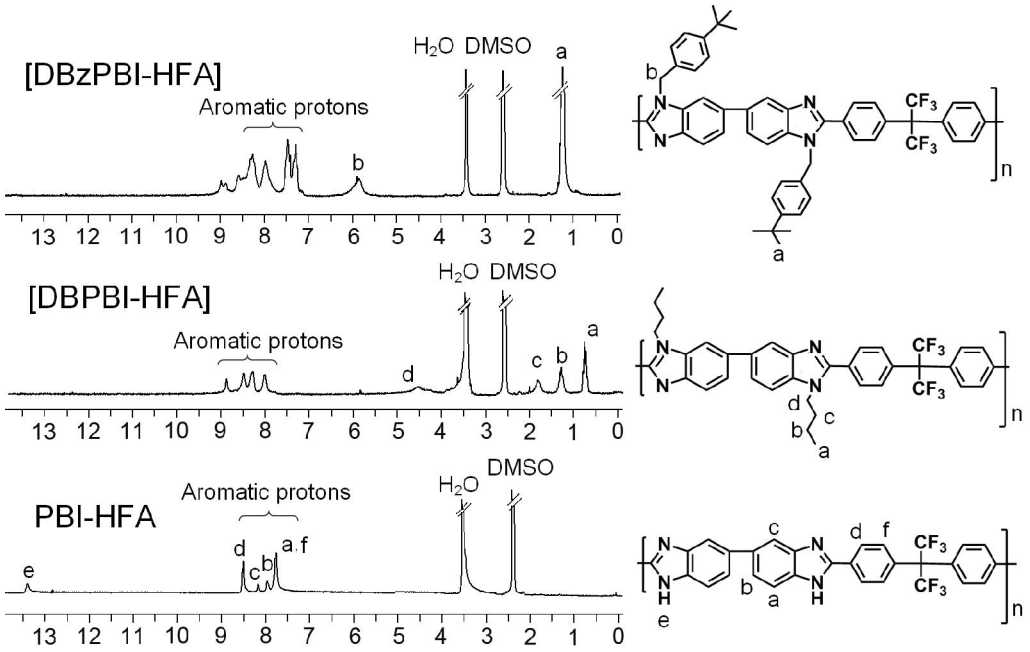

Fig. 4.2. ^{1}H NMR spectra of *N*-substituted PBI-HFA.

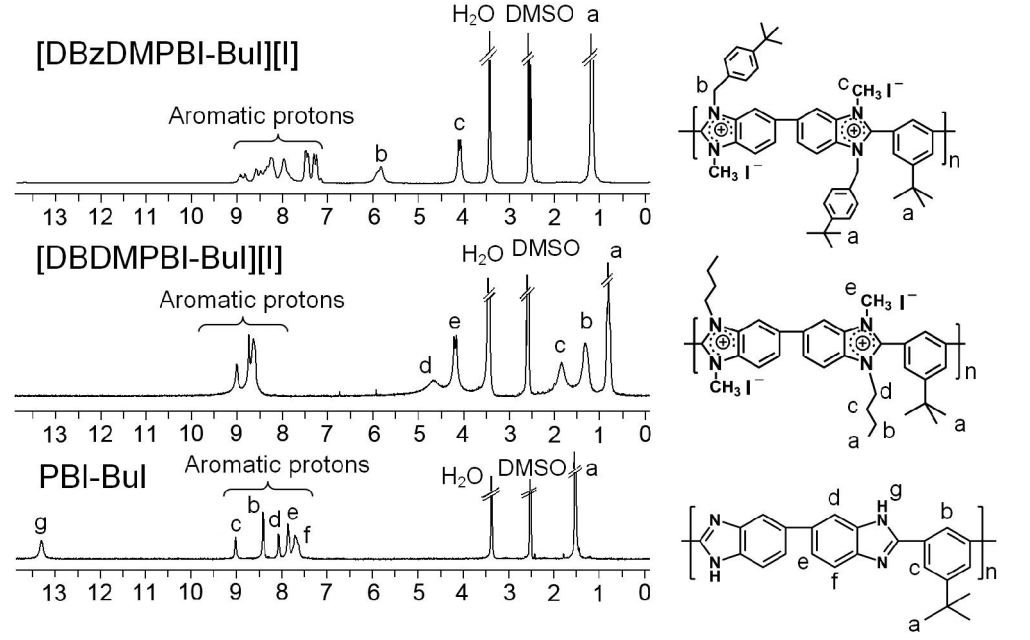

Fig. 4.3. ^{1}H NMR spectra of asymmetrically substituted PILs based on PBI-BuI.

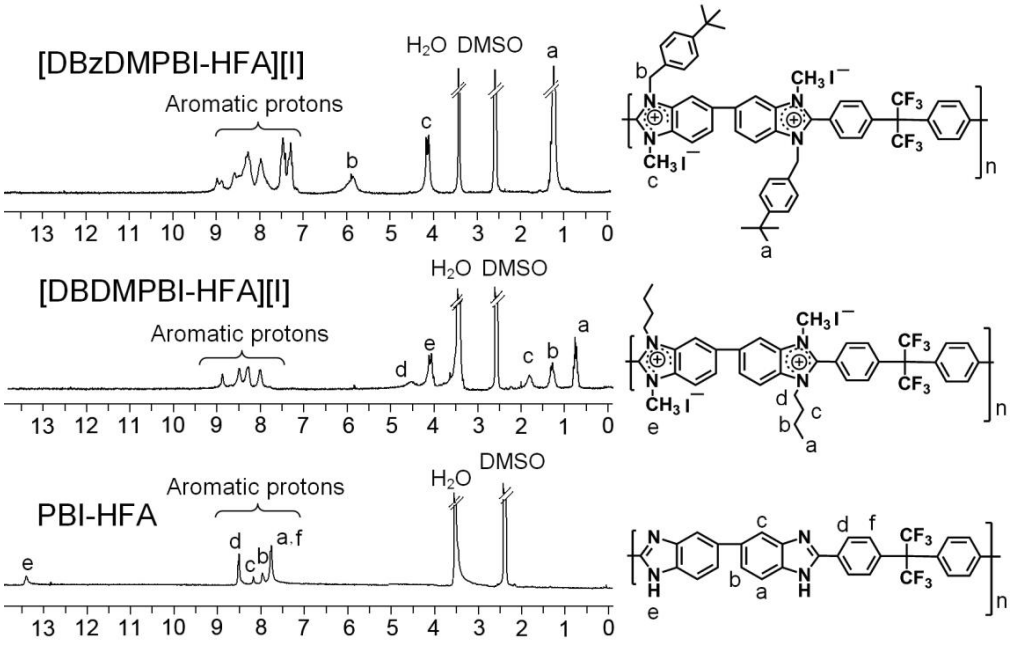

Fig. 4.4. ^{1}H NMR spectra of asymmetrically substituted PILs based on PBI-HFA.

An exchange of iodide anion from above PILs was performed using sodium tetrafluoroborate (BF_4), lithium trifluoromethane sulphonimide (Tf_2N) and silver heptafluorobutyrate (HFB) in DMF. This solvent was chosen owing to good solubility of the parent PILs as well as chosen salts in it. In the cases of exchange by BF_4^- and Tf_2N^- anions, formed byproduct (LiI or NaI) was separated from the polymer by precipitating the reaction mixture in water followed by repeated water wash to remove the salt completely. This made separation of the byproduct, NaI or LiI, an easy task. On the other hand, in case of exchange of iodide by $C_3F_7COO^-$ (HFB), the byproduct (AgI) was formed as a fine suspension that could be separated by the centrifugation. Analysis of iodide (if remained unexchanged) in these 'anion exchanged' PILs was done by Volhard's method. The extent of iodide exchanged as given in Table 4.1 was appreciable. Extent of iodide exchange by HFB^- anion was found to be higher than that by Tf_2N^- and BF_4^-anions. This could be attributed to the use of silver salt of anion in earlier case; while in the latter, alkali metal salt of an anion was used. In case of use of silver salt, anion exchange reaction leads to the precipitation of AgI salt and thus the reaction becomes irreversible in nature.

In the case of exchange of iodide by Tf_2N^- and BF_4^- anions, the use of Li and Na salt, respectively, may not offer such irreversible nature of exchange, since the salt remains soluble in the reaction mixture. For all PILs, FTIR spectra were scanned at the ambient temperature showed a broad band at ~3610 cm^{-1} (Fig 4.5 and 4.6). This is attributable to the sorbed moisture, as was observed for PBIs and PILs based on them [Bhavsar (2014a), Kumbharkar (2009)]. The characteristic bands for benzimidazole at ~1500-1650 cm^{-1} are attributable to C=C/C=N ring vibration [Musto (1993)].

FTIR analysis supported the exchange of iodide by a particular anion. Fig. 4.5 and 4.6 show appearance of new bands attributable to the respective anion. In PILs possessing BF_4^- anion, a band at ~1080 cm^{-1} is attributable to the B-F stretching vibrations [Suarez (1996)]. In the spectra of PILs with HFB^- as anion, the C=O stretching was observed between ~1690 cm^{-1} to 1720 cm^{-1}. Bands in the range of 1100-1230 cm^{-1} are attributable to C-F stretching of Tf_2N and HFB^- anion [Silverstein (1981)].

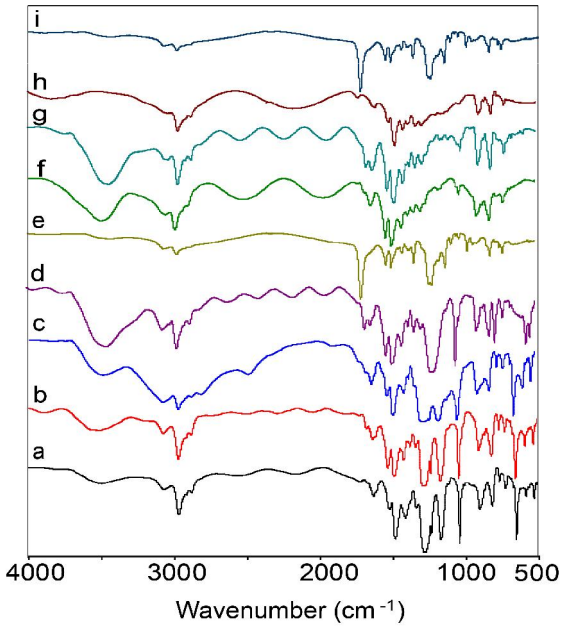

Fig. 4.5. FT-IR spectra of PILs based on PBI-BuI (a: PBI-BuI, b: [DBDMPBI-BuI][I], c: [DBDMPBI-BuI][BF_4], d: [DBDMPBI-BuI][Tf_2N], e: [DBDMPBI-BuI][HFB], f: [DBzDMPBI-BuI][I], g: [DBzDMPBI-BuI][BF_4], h: [DBzDMPBI-BuI][Tf_2N], i: [DBzDMPBI-BuI][HFB]).

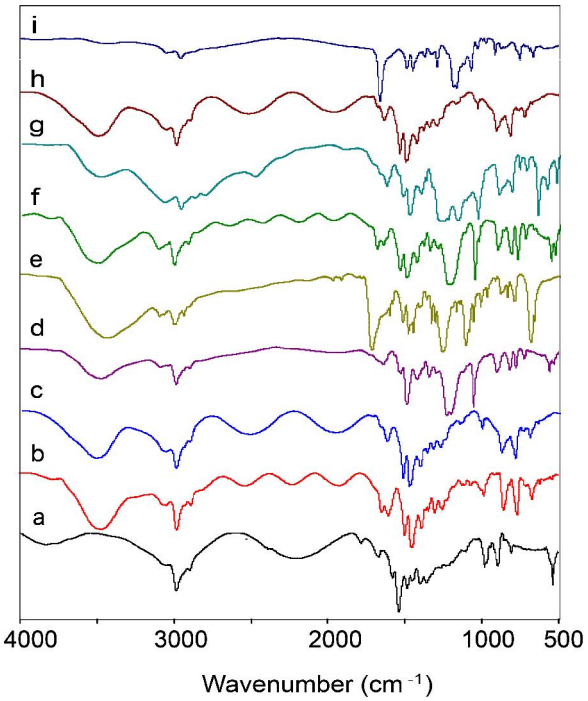

Fig. 4.6. FT-IR spectra of PILs based on PBI-HFA (a: PBI-HFA, b: [DBDMPBI-HFA][I], c: [DBDMPBI-HFA][BF_4], d: [DBDMPBI-HFA][Tf_2N], e: [DBDMPBI-HFA][HFB], f: [DBzDMPBI-HFA][I], g: [DBzDMPBI-HFA][BF_4], h: [DBzDMPBI-HFA][Tf_2N], i: [DBzDMPBI-HFA][HFB]).

4.3. Physical properties

4.3.1 Solvent solubility, WAXD analysis and density

PILs based on all three anions exhibited good solvent solubility (Table 4.1) and thus easy processability, offering excellent films. The PILs with iodide anion were soluble in acetonitrile, in addition to the high boiling solvents (DMF and NMP). The solubility of PILs was further enhanced when the iodide was exchanged by another anion. For example, some of the PILs with Tf_2N^-, BF_4^- and HFB^- as anions became soluble even in acetone and methanol at the ambient temperature, which are usually non-solvents for many of the aromatic polymers. Above results indicated that the solvent solubility of PBI, which is known to be soluble only in high boiling solvents [Bhavsar (2014a)], is now improved to a great extent after its conversion to the PIL. Such improvement in the solubility of polybenzimidazole based PILs can be attributed to the presence of ionic character as well as the *N*-substituents used.

Table 4.1. Anion exchange (%) and solubility of PILs in organic solvents

PILs	Iodide exchange [a] (mol %)	DMF	DMSO	NMP	Acetone	CH_3CN	MeOH
PBI-BuI based PILs							
[DBDMPBI-BuI][I]	0	++	++	++	—	+	—
[DBDMPBI-BuI][BF_4]	85	++	++	++	—	++	—
[DBDMPBI-BuI][Tf_2N]	86	++	++	++	++	++	++
[DBDMPBI-BuI][HFB]	93	++	++	++	—	++	+
[DBzDMPBI-BuI][I]	0	++	++	++	—	+	—
[DBzDMPBI-BuI][BF_4]	84	++	++	++	—	—	—
[DBzDMPBI-BuI][Tf_2N]	84	++	++	++	++	++	++
[DBzDMPBI-BuI][HFB]	87	++	++	++	++	++	—
PBI-BuI[b]	—	++	++	++	—	—	—
PBI-HFA based PILs							
[DBDMPBI-HFA][I]	0	++	++	++	—	+	—
[DBDMPBI-HFA][BF_4]	86	++	++	++	—	++	++
[DBDMPBI-HFA][Tf_2N]	83	++	++	++	++	++	++
[DBDMPBI-HFA][HFB]	88	++	++	++	++	++	+
[DBzDMPBI-HFA][I]	0	++	++	++	—	+	—
[DBzDMPBI-HFA][BF_4]	83	++	++	++	—	++	++
[DBzDMPBI-HFA][Tf_2N]	82	++	++	++	++	++	++
[DBzDMPBI-HFA][HFB]	91	++	++	++	++	++	++
PBI-HFA[b]	—	++	++	++	—	—	—

[a]: Determined by Volhard's method, ++: soluble at ambient temperature, +: soluble after heating at 80 ºC (reflux in case of low boiling solvents), —: insoluble, [b]: data taken from Ref. [Kumbharkar (2006)].

WAXD patterns of these PILs indicated their amorphous nature (Fig. 4.7 and 4.8). An average intersegmental *d*-spacing (d_{sp}) of PILs as obtained from the amorphous peak maxima are given in Table 4.2. The d_{sp} of PILs possessing 4-*tert*-butylbenzyl group were slightly higher than for those possessing *n*-butyl group. It may be possible that 4-*tert*-butylbenzyl group being bulkier in nature than *n*-butyl, it would inhibit closer chain packing. Moreover, flexible *n*-butyl chain may get accommodated in the initially available free space and may not be effective enough in loosening the chain packing as that of 4-*tert*-butylbenzyl group. For PILs based on either PBI-BuI or PBI-HFA as the backbone and for a given substituent, d_{sp} increased in the order of anion variation as I^- <

BF_4^- < Tf_2N^- ≤ HFB^-. This shows that bulk of the anion would also contribute in governing the chain packing in PIL matrix.

Density values of PILs are given in Table 4.2. The nature of *N*-substituent as well as an anion hold by the PIL seems to govern its density. In case of PILs based on either PBI-BuI or PBI-HFA backbone, the density was lower for those with 4-*tert*-butylbenzyl group as the substituent, than with *n*-butyl group. This is attributable to the bulkier nature of 4-*tert*-butylbenzyl group that inhibits close chain packing, as supported by the WAXD analysis. The density within a series of PIL (based on a particular PBI and *N*-substituent) increased in the order of anion variation as: BF_4^- < HFB^- ≤ Tf_2N^- ≈ I^- (Table 4.2).

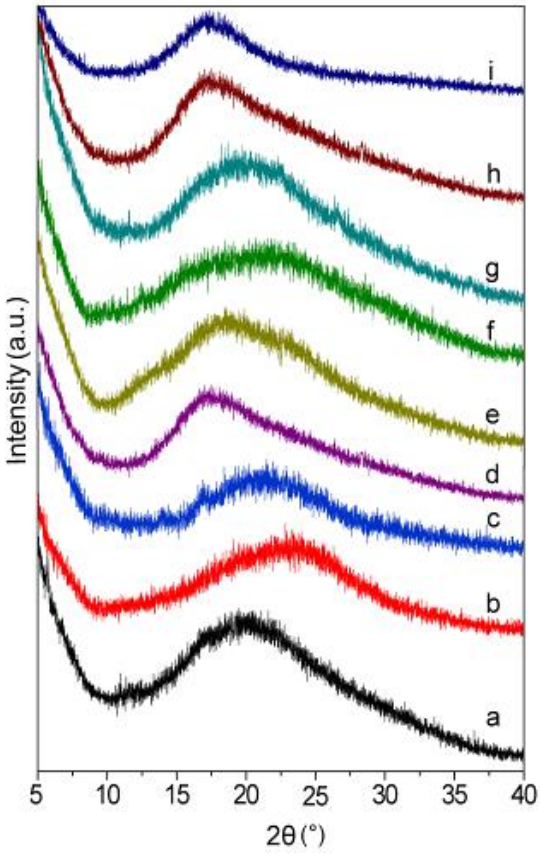

Fig. 4.7. WAXD pattern ofPILs based on PBI-BuI (a: PBI-BuI, b: [DBDMPBI-BuI][I], c: [DBDMPBI-BuI][BF_4], d: [DBDMPBI-BuI][Tf_2N], e: [DBDMPBI-BuI][HFB], f: [DBzDMPBI-BuI][I], g: [DBzDMPBI-BuI][BF_4], h: [DBzDMPBI-BuI][Tf_2N], i: [DBzDMPBI-BuI][HFB]).

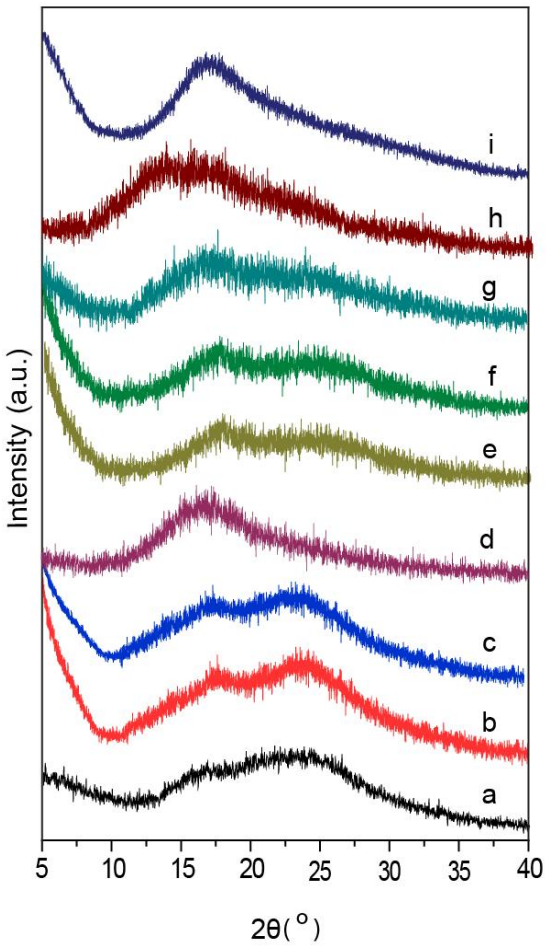

Fig. 4.8. WAXD pattern of PILs based on PBI-HFA (a: PBI-HFA, b: [DBDMPBI-HFA][I],c: [DBDMPBI-HFA][BF_4], d: [DBDMPBI-HFA][Tf_2N], e: [DBDMPBI-HFA][HFB],f: [DBzDMPBI-HFA][I], g: [DBzDMPBI-HFA][BF_4], h: [DBzDMPBI-HFA][Tf_2N],i: [DBzDMPBI-HFA][HFB]).

It may be noted that present PILs showed lower density as compared to the 'symmetric' methyl-substituted PILs based on PBI as reported earlier [Bhavsar (2014b)]. The lowering in density is better obeyed by PILs with 4-*tert*-butylbenzyl group as a substituent than those with *n*-butyl group, which supports the speculation of *n*-butyl group getting accommodated in the available free space, as discussed above during WAXD interpretation. This behavior may be attributed to its straight chain nature of *n*-butyl group bearing flexibility. These analyses indicated role of both the substituent and the anion in governing chain packing in PILs.

Table 4.2. Physical properties of PILs

PILs	d_{sp}[a] (Å)	ρ[b] (g/cm^3)	TG analysis		T_g[e]
			IDT[c](ºC)	W_{900}[d](%)	
PBI-BuI based PILs					
[DBDMPBI-BuI][I]	3.80	1.480	217	32	ND
[DBDMPBI-BuI][BF_4]	4.22	1.358	227	25	ND
[DBDMPBI-BuI][Tf_2N]	4.40	1.399	273	24	272
[DBDMPBI-BuI][HFB]	4.66	1.385	165	31	ND
[DBzDMPBI-BuI][I]	5.04	1.199	205	35	ND
[DBzDMPBI-BuI][BF_4]	5.06	1.087	221	37	ND
[DBzDMPBI-BuI][Tf_2N]	5.24	1.138	239	33	238
[DBzDMPBI-BuI][HFB]	5.25	1.252	159	20	ND
PBI-BuI[f]	4.04, 4.69	1.193	525	65	ND
PBI-HFA based PILs					
[DBDMPBI-HFA][I]	3.74, 5.00	1.371	165	31	ND
[DBDMPBI-HFA][BF_4]	3.73, 5.06	1.119	223	42	213
[DBDMPBI-HFA][Tf_2N]	5.09	1.360	273	33	271
[DBDMPBI-HFA][HFB]	3.57, 4.94	1.239	165	35	ND
[DBzDMPBI-HFA][I]	3.60, 5.05	1.360	252	40	194
[DBzDMPBI-HFA][BF_4]	5.14	1.107	178	22	169
[DBzDMPBI-HFA][Tf_2N]	5.34	1.280	223	33	180
[DBzDMPBI-HFA][HFB]	5.26	1.262	177	37	ND
PBI-HFA[f]	4.05, 5.37	1.368	535	61	330

[a]: d-spacing obtained from wide angle X-ray diffraction spectra, [b]: density measured at 35 ºC, [c]: initial decomposition temperature, [d]: char yield at 900 °C, [e]: Glass transition temperature obtained by DMA, ND: Not detected, [f]: Data taken from Ref. [Kumbharkar (2006)].

4.3.2. Thermal stability of PILs

Initial degradation temperature (IDT) of present PILs is given in Table 4.2 and thermogravimetric curves are shown in Fig. 4.9 (for PBI-BuI based PILs) and Fig. 4.10 (for PBI-HFA based PILs). In case of PILs with common anion and a backbone PBI (either PBI-BuI or PBI-HFA), those possessing *n*-butyl substituents showed higher thermal stability than those possessing 4-*tert*-butylbenzyl as a substituent. The decrease in thermal stability of 4-*tert*-butylbenzyl could be attributed to the presence of aralkyl group that is susceptible for the degradation. The reduction in IDT of aromatic polymers by substitution of alkyl group that is susceptible for degradation is known in the literature [Chen (2006)].

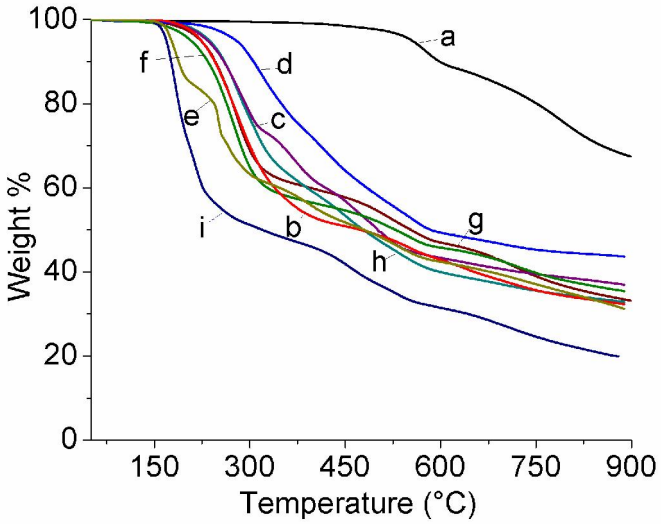

Fig. 4.9. TG curves of PILs based on PBI-BuI (a: PBI-BuI, b: [DBDMPBI-BuI][I], c: [DBDMPBI-BuI][BF_4], d: [DBDMPBI-BuI][Tf_2N], e: [DBDMPBI-BuI][HFB], f: [DBzDMPBI-BuI][I], g: [DBzDMPBI-BuI][BF_4], h: [DBzDMPBI-BuI][Tf_2N], i: [DBzDMPBI-BuI][HFB]).

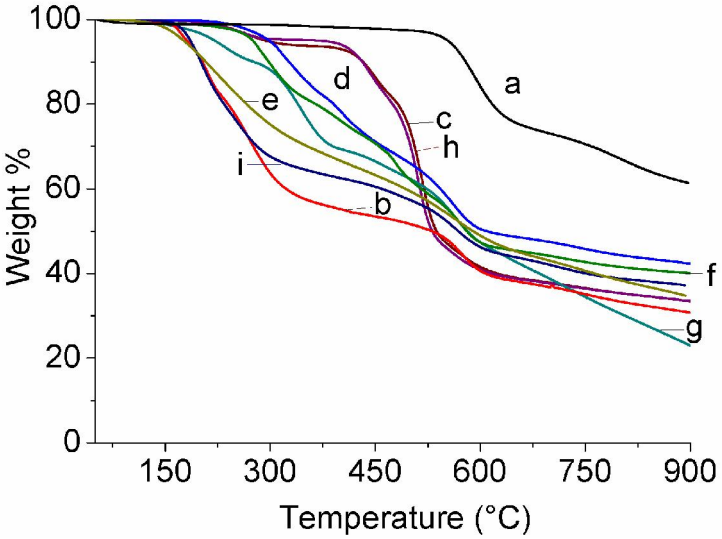

Fig. 4.10. TG curves of PILs based on PBI-HFA (a: PBI-HFA, b: [DBDMPBI-HFA][I], c: [DBDMPBI-HFA][BF_4], d: [DBDMPBI-HFA][Tf_2N], e: [DBDMPBI-HFA][HFB], f: [DBzDMPBI-HFA][I], g: [DBzDMPBI-HFA][BF_4], h: [DBzDMPBI-HFA][Tf_2N], i: [DBzDMPBI-HFA][HFB]).

In case of PILs bearing a particular substituent but with varying anion, thermal stability was increased with the order of anions as $HFB^- < I^- \leq BF_4^- < Tf_2N^-$. The effect

of anion on the degradation behaviour was also seen in case of PILs with either aromatic (PBI based) or aliphatic backbone [Bhavsar (2014b), Bhavsar (2012)]. The pKa of conjugate acid of anions is: [Tf_2N] = −4.0, [BF_4] = −0.44, [HFB] = 0.4 [MacFarlane (2006), Cabusas (2013)]. Thermal stability of ionic liquids is known to increase with decreasing basicity of anion [Wang (2011)]. This indicated that both, the nature of substituents as well as an anion play a profound role in governing the thermal stability of PILs. In case of PILs with HFB^- anion, lowest thermal stability (IDT ~ 150 °C) could be attributed to higher basic nature and thermal instability of the carboxylate group.

Glass transition temperature (T_g) of present PILs could not be detected in the DSC thermogram, even after repeated cycles of heating and cooling; except for [DBzDMPBI-BuI][Tf_2N], wherein the T_g was observed to be 235°C. Therefore, dynamic mechanical analysis (DMA) was further performed and some of the PILs exhibited tan δ transition, as shown in Fig. 4.11. , This transition is usually ascribed to the chain segmental motions, i.e. T_g. High T_g values of these PILs established their glassy nature. For some of the PILs, tanδ could not be observed. It may be concluded that their Tg is beyond their degradation temperature. Although, these PILs can be assumed to be glassy polymers since they possess similar aromatic rigid PBI backbone and similar substituents.

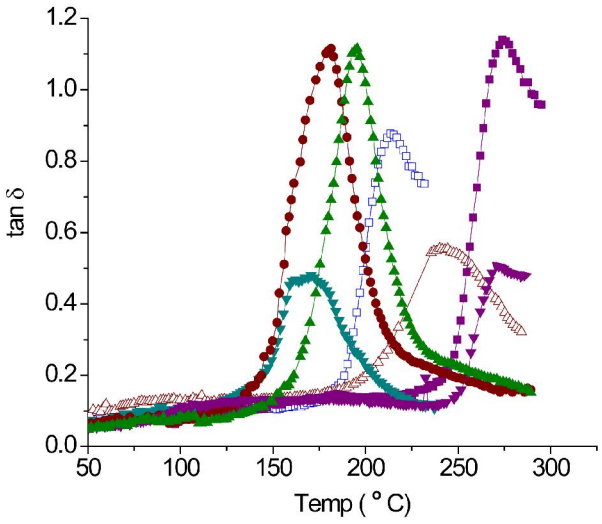

Fig. 4.11. DMA curves (tan δ) of PILs as function of temperature (■ : [DBDMPBI-BuI][Tf_2N], △: [DBzDMPBI-BuI][Tf_2N], □: [DBDMPBI-HFA][BF_4], ▼: [DBDMPBI-HFA][Tf_2N], ▲: [DBzDMPBI-HFA][I], ▼: [DBzDMPBI-HFA][BF_4], ●: [DBzDMPBI-HFA][Tf_2N]

4.4 Gas sorption properties

4.4.1 Sorption parameters

Equilibrium sorption isotherms of H_2, N_2 and CO_2 in present PILs exhibited typical dual-mode nature (Fig. 4.12 and 4.13), as usually observed for glassy polymers [Bhavsar (2014b), Kumbharkar (2006), Koros (1976)]. The gas sorption parameters (k_D, b and C'_H) are given in Table 4.3. It could be seen that Henry's solubility coefficient, k_D (ascribed to the gas dissolution in rubbery state) for all gases was considerably lower than C'_H. This behavior is attributable to the glassy nature of PILs.

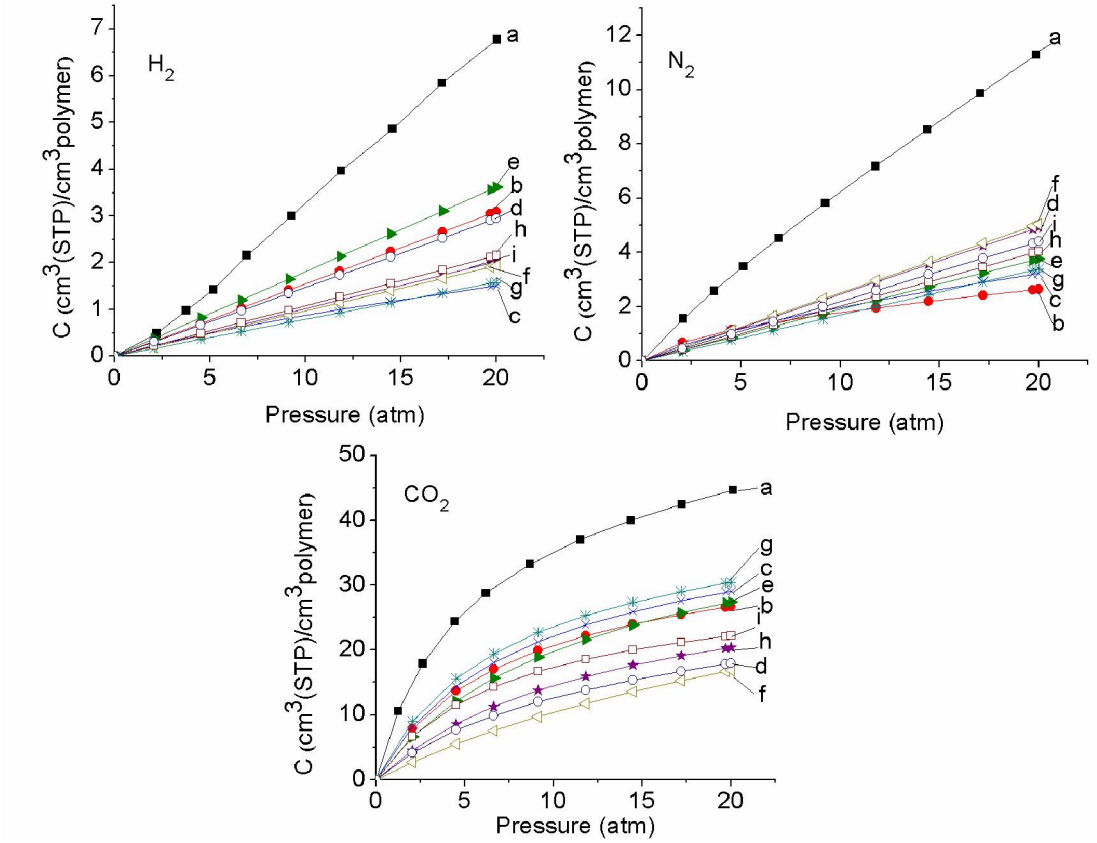

Fig. 4.12. Gas sorption isotherms of PBI-BuI and PIL at 35 ºC (a: PBI-BuI, b: [DBDMPBI-BuI][I], c: [DBDMPBI-BuI][BF_4], d: [DBDMPBI-BuI][Tf_2N], e: [DBDMPBI-BuI][HFB],f: [DBzDMPBI-BuI][I], g: [DBzDMPBI-BuI][BF_4], h: [DBzDMPBI-BuI][Tf_2N], i: [DBzDMPBI-BuI][HFB]).

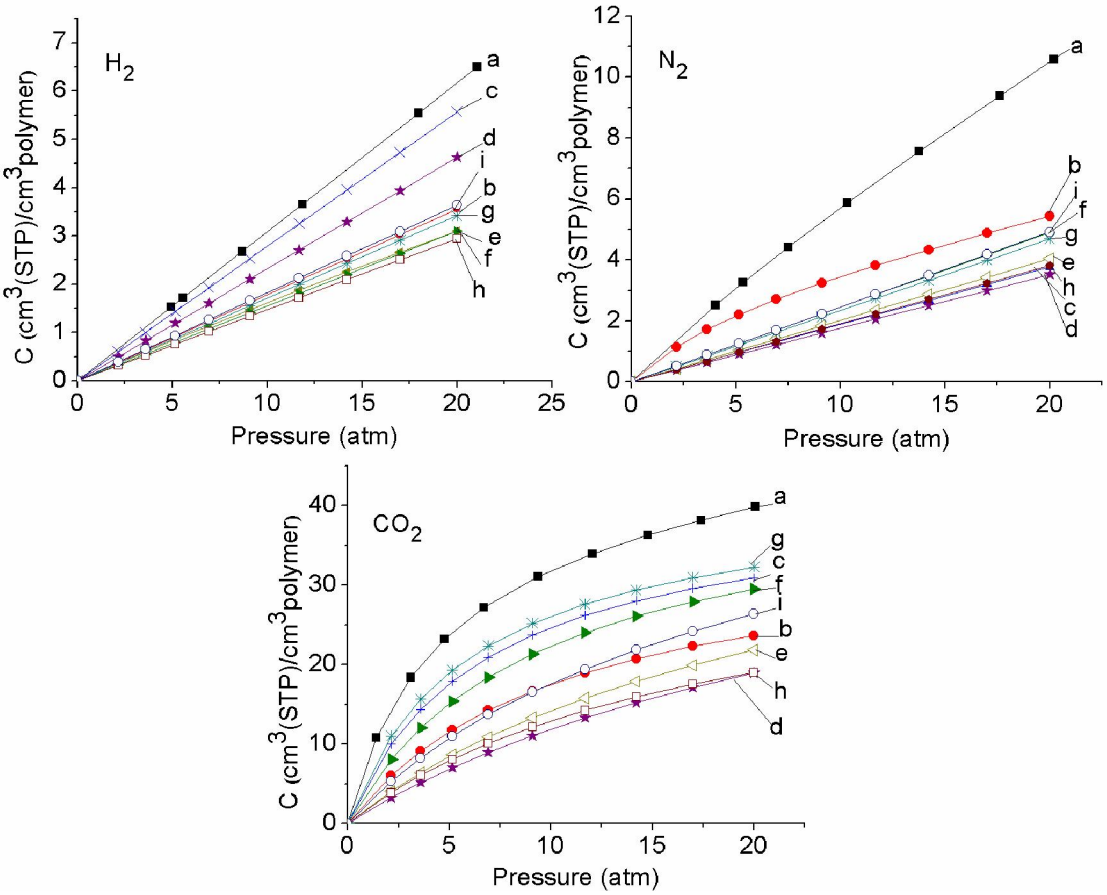

Fig. 4.13. Gas sorption isotherm of PILs based on PBI-HFA at 35 ºC (a: PBI-HFA, b: [DBDMPBI-HFA][I], c: [DBDMPBI-HFA][BF_4], d: [DBDMPBI-HFA][Tf_2N], e: [DBDMPBI-HFA][HFB], f: [DBzDMPBI-HFA][I], g: [DBzDMPBI-HFA][BF_4], h: [DBzDMPBI-HFA][Tf_2N], i: [DBzDMPBI-HFA][HFB]).

The C'_H is considered as the hole-filling constant in the glassy state, which represents maximum amount of the penetrant sorbed into 'microvoids' or the unrelaxed volume of the polymer matrix [Kanehashi (2005), McHattie (1992)]. For all PILs, C'_H was higher for CO_2 than that of other gases. This is in accordance with the gas sorption behavior observed for most of the common glassy polymers, including PILs [Bhavasar (2014b), Kumbharkar (2006), Kanehashi (2005), Barbari (1988), Barbari (1989)], possessing higher C'_H for CO_2 than for other gases owing to higher condensability of this gas [McHattie (1992)]. The affinity constant 'b' is the ratio of rate constants of sorption and desorption processes and characterizes the sorption affinity of a particular gas-polymer system [McHattie (1992)]. This parameter was negligible for H_2 and N_2, but was

considerably higher in the case of CO_2. The C'_H values of present PILs (especially those containing BF_4^- anion) are higher than for conventional glassy polymers. For example, [DBDMPBI-HFA][BF_4] exhibited C'_H of 41.3; while, that for bisphenol-A based polymers, it was considerably lower (polysulphone: 16.63, polyhydroxyether: 8.89, polyetherimide: 23.38 and polyarylate: 20.54 Barbari (1989)]. Similar lower values are reported for polycarbonate, polysulfone and polyetherimide by Hu et al [Hu (2003)].

Table 4.3. Dual-mode sorption parameters[a] for PILs

PILs	H_2			N_2			CO_2		
	k_D	C'_H	B	k_D	C'_H	b	k_D	C'_H	b
PBI-BuI based PILs									
[DBDMPBI-BuI][I]	0.15	1.74	$4.2x10^{-4}$	0.07	1.54	0.27	0.05	34.90	0.14
[DBDMPBI-BuI][BF_4]	0.05	0.73	$9.0 x10^{-2}$	0.10	1.55	0.16	0.12	36.15	0.14
[DBDMPBI-BuI][Tf_2N]	0.10	0.72	$3.0x10^{-6}$	0.25	2.84	0.13	0.07	33.74	0.07
[DBDMPBI-BuI][HFB]	0.09	0.94	$6.1x10^{-6}$	0.15	0.65	$7.4x10^{-5}$	0.25	23.38	0.05
[DBzDMPBI-BuI][I]	0.18	1.80	$5.0x10^{-4}$	0.17	1.90	0.01	0.14	36.90	0.10
[DBzDMPBI-BuI][BF_4]	0.08	1.63	$3.5x10^{-5}$	0.17	3.99	$2.7x10^{-5}$	0.10	38.29	0.15
[DBzDMPBI-BuI][Tf_2N]	0.10	1.03	$1.0x10^{-5}$	0.20	0.18	$6.4x10^{-5}$	0.06	28.15	0.15
[DBzDMPBI-BuI][HFB]	0.15	1.35	$1.4x10^{-5}$	0.22	0.70	$4.6x10^{-4}$	0.19	20.43	0.11
PBI-BuI[b]	0.33	0.40	$2.0 x10^{-4}$	0.46	2.80	0.13	0.44	43.70	0.24
PBI-HFA based PILs									
[DBDMPBI-HFA][I]	0.18	3.90	$1.5x10^{-5}$	0.16	2.93	0.18	$6x10^{-5}$	36.44	0.09
[DBDMPBI-HFA][BF_4]	0.28	2.56	$1.4x10^{-5}$	0.19	3.59	$1.6x10^{-5}$	$2x10^{-6}$	41.34	0.15
[DBDMPBI-HFA][Tf_2N]	0.23	0.67	$1.1x10^{-4}$	0.17	0.96	$2.6x10^{-4}$	0.16	33.81	0.04
[DBDMPBI-HFA][HFB]	0.10	5.00	0.01	0.20	2.49	$9.4x10^{-5}$	0.11	39.01	0.05
[DBzDMPBI-HFA][I]	0.15	1.36	$7.0x10^{-5}$	0.24	0.56	$1.5x10^{-4}$	0.02	42.71	0.11
[DBzDMPBI-HFA][BF_4]	0.17	1.61	$1.7x10^{-5}$	0.23	5.57	$3.9x10^{-5}$	0.02	41.32	0.17
[DBzDMPBI-HFA][Tf_2N]	0.14	0.01	$5.9x10^{-4}$	0.18	2.77	$4.1x10^{-4}$	0.03	34.01	0.06
[DBzDMPBI-HFA][HFB]	0.18	0.20	$9.2x10^{-4}$	0.24	0.03	$4.3x10^{-3}$	0.20	39.06	0.07
PBI-HFA[b]	0.31	0.43	$1.0 x10^{-3}$	0.50	3.36	0.13	0.53	34.40	0.31

[a:] k_D is expressed in $cm^3(STP).cm^{-3}$polymer.atm, C'_H is expressed in $cm^3(STP).cm^{-3}$ polymer, while b is expressed in atm^{-1}, [b]: Data taken from Ref. [Kumbharkar (2006)].

It is noteworthy that PILs containing BF_4^- anion exhibited higher 'b' than that of PILs with other anions, indicating favored CO_2 interactions in BF_4^- containing PILs. The high CO_2 solubility coefficient in PILs containing BF_4^- anion was observed in case of methyl substituted PBI-based PILs [Bhavsar (2014b)] as well as P[DADMA] based PILs

[Bhavsar (2012)], conveying significant role of this anion in elevating CO_2 sorption in PILs.

4.4.2 Sorption coefficients

Table 4.4 presents the solubility coefficient (S) and solubility selectivity (S_A/S_B) for different PILs at 20 atm.

Table 4.4. Solubility coefficient (S)[a] and solubility selectivity (S_A/S_B) of PILs

PILs	S_{H_2}	S_{N_2}	S_{CO_2}	S_{H_2}/S_{N_2}	S_{CO_2}/S_{H_2}	S_{CO_2}/S_{N_2}
PBI-BuI based PILs						
[DBDMPBI-BuI][I]	0.15	0.13	1.33	1.2	8.6	10.1
[DBDMPBI-BuI][BF_4]	0.08	0.16	1.45	0.5	19.3	9.0
[DBDMPBI-BuI][Tf_2N]	0.10	0.25	1.02	0.4	10.1	4.1
[DBDMPBI-BuI][HFB]	0.15	0.25	0.84	0.6	5.7	3.3
[DBzDMPBI-BuI][I]	0.18	0.19	1.37	1.0	9.6	7.2
[DBzDMPBI-BuI][BF_4]	0.08	0.17	1.52	0.5	19.2	9.0
[DBzDMPBI-BuI][Tf_2N]	0.11	0.20	1.11	0.5	10.3	5.5
[DBzDMPBI-BuI][HFB]	0.15	0.22	0.90	0.7	6.1	4.0
PBI-BuI[b]	0.33	0.57	2.24	0.5	6.8	3.9
PBI-HFA based PILs						
[DBDMPBI-HFA][I]	0.18	0.27	1.18	0.7	6.6	4.4
[DBDMPBI-HFA][BF_4]	0.28	0.19	1.54	1.5	5.5	8.2
[DBDMPBI-HFA][Tf_2N]	0.23	0.18	0.95	1.3	4.1	5.3
[DBDMPBI-HFA][HFB]	0.15	0.20	1.09	0.8	7.0	5.4
[DBzDMPBI-HFA][I]	0.15	0.25	1.48	0.6	9.5	6.0
[DBzDMPBI-HFA][BF_4]	0.17	0.23	1.59	0.7	9.3	6.8
[DBzDMPBI-HFA][Tf_2N]	0.15	0.19	0.94	0.8	6.4	5.0
[DBzDMPBI-HFA][HFB]	0.18	0.25	1.32	0.7	7.2	5.4
PBI-HFA[b]	0.31	0.62	2.00	0.5	6.7	3.2

[a] Expressed in $cm^3(STP).cm^{-3}$ polymer.atm, [b]: Data taken from Ref. [Kumbharkar (2006)].

The solubility coefficient for different gases in all PILs at 20 atm increased in the order: $H_2 < N_2 < CO_2$; which followed the order of increasing inherent condensability of these gases [Bhavsar (2014b), Li (2009)]. This behavior holds true irrespective of the backbone (PBI-BuI or PBI-HFA) or the *N*-substituent (*n*-butyl or 4-*tert*-butylbenzyl) of a PIL. In case of PILs with the 4-*tert*-butylbenzyl as substituent, CO_2 solubility coefficient was slightly higher than those bearing *n*-butyl substituent. This could be correlated to the

comparatively looser chain packing in earlier case of PILs, leading to higher free volume, as discussed in Section 4.2. As could be seen from data in Table 4.4, variation in an anion has more pronounced effect in governing the gas solubility coefficient, than the bulk of the substituent. It was observed that for a particular PBI backbone (PBI-BuI or PBI-HFA) and a substituent (*n*-butyl or 4-*tert*-butylbenzyl), CO_2 sorption coefficient generally increased in the order of anion variation as $HFB^- \leq Tf_2N^- < I^- < BF_4^-$. This led to enhanced S_{CO_2}/S_{H_2} and S_{CO_2}/S_{N_2} sorption selectivity in cases of PILs possessing BF_4^- anion. It may be recalled that PILs with BF_4^- anion also exhibited higher C'_H than for those PILs with other anions. This indicated that BF_4^- is a better anion for obtaining preferential CO_2 sorption in PILs. It was also observed that present PILs exhibited higher CO_2 based sorption selectivity than their disubstituted analogue viz., DBPBI-BuI and DBzPBI-BuI which devoid of IL character [Kumbharkar (2010)]. This supports our proposition of introducing IL character in the glassy polymer backbone to sorb CO_2 preferentially. This would improve the CO_2 based sorption selectivity and hence CO_2 separation performance. Owing to the glassy nature of present PILs, S_{CO_2}, S_{CO_2}/S_{N_2} and S_{CO_2}/S_{H_2} at low pressures were considerably higher (Fig. 4.14-4.17), which is in accordance with the dual mode nature of the CO_2 sorption isotherm.

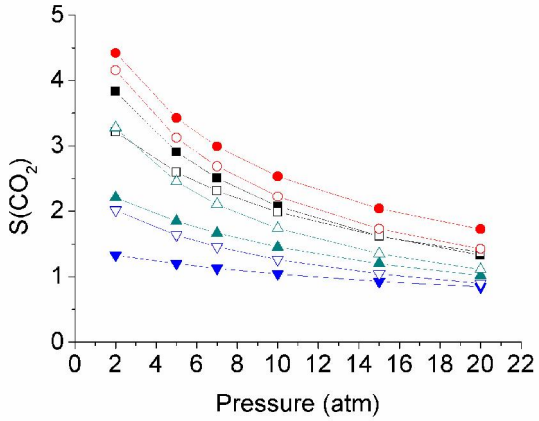

Fig. 4.14. CO_2 solubility coefficient of PBI-BuI based PIL at 35 ºC (■: [DBDMPBI-BuI][I],●: [DBDMPBI-BuI][BF_4], ▲: [DBDMPBI-BuI][Tf_2N], ▼: [DBDMPBI-BuI][HFB], □: [DBzDMPBI-BuI][I], ○: [DBzDMPBI-BuI][BF_4], △: [DBzDMPBI-BuI][Tf_2N], ▽: [DBzDMPBI-BuI][HFB]).

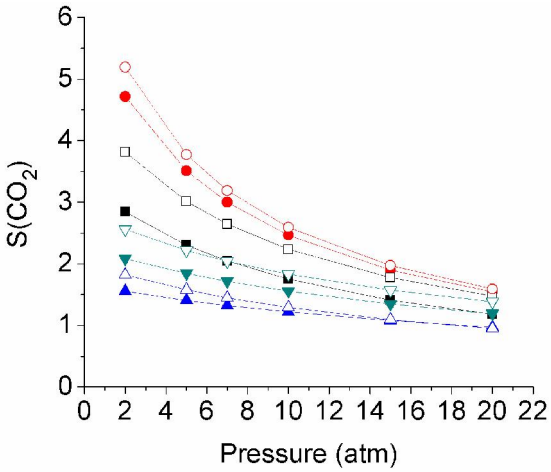

Fig. 4.15. CO_2 solubility coefficient of PBI-HFA based PIL at 35 ºC (■: [DBDMPBI-HFA][I], ●: [DBDMPBI-HFA][BF_4], ▲: [DBDMPBI-HFA][Tf_2N], ▼: [DBDMPBI-HFA][HFB],□: [DBzDMPBI-HFA][I], ○: [DBzDMPBI-HFA][BF_4], △: [DBzDMPBI-HFA][Tf_2N], ▽: [DBzDMPBI-HFA][HFB]).

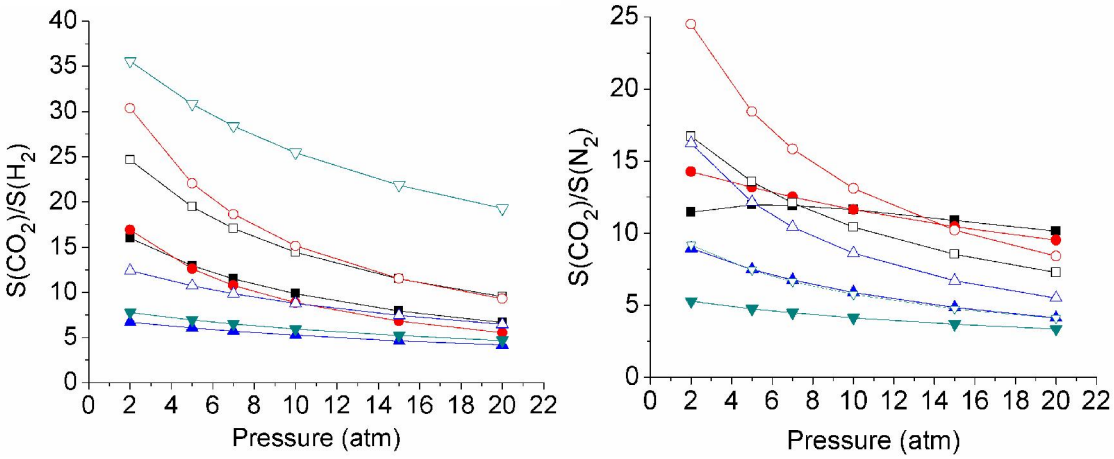

Fig. 4.16. CO_2 solubility selectivity of PBI-BuI based PIL at 35 ºC (■: [DBDMPBI-BuI][I], ●: [DBDMPBI-BuI][BF_4], ▲: [DBDMPBI-BuI][Tf_2N], ▼: [DBDMPBI-BuI][HFB], □: [DBzDMPBI-BuI][I], ○: [DBzDMPBI-BuI][BF_4], △: [DBzDMPBI-BuI][Tf_2N], ▽: [DBzDMPBI-BuI][HFB]).

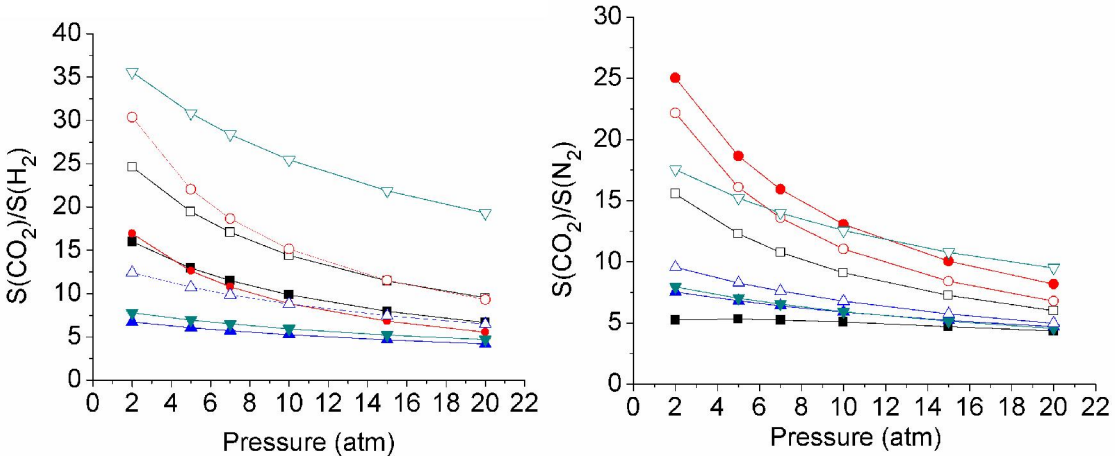

Fig. 4.17. CO_2 solubility selectivity of PBI-HFA based PIL at 35 ºC (■: [DBDMPBI-HFA][I], ●: [DBDMPBI-HFA][BF_4], ▲: [DBDMPBI-HFA][Tf_2N], ▼: [DBDMPBI-HFA][HFB], □:[DBzDMPBI-HFA][I], ○: [DBzDMPBI-HFA][BF_4], △: [DBzDMPBI-HFA][Tf_2N], ▽: [DBzDMPBI-HFA][HFB]).

4.5 Gas permeation properties

Permeation analysis of PIL based membranes was carried out in order to analyze effects of polymer backbone, substituent present on them and an anion they hold. The pure gas permeability for He, H_2, N_2, CO_2 and ideal selectivity data for various gas pairs are given in Table 4.5. A large variation in the gas permeability of PILs with the variation in PBI backbone, its substituents or anion was observed, as discussed below.

4.5.1 Effects of variation in *N*-substituent

It could be seen from data in Table 4.5 that PILs with both the backbones showed significant variations in permeability with variation in the substituent. It was observed that PILs possessing 4-*tert*-butylbenzyl group exhibited higher permeability for various gases and slightly lower CO_2 based selectivity over N_2 and H_2; than that for PILs with *n*-butyl substituents based on the same backbone. This could be correlated to the size of substituent, which governs the chain packing as evidenced from the WAXD and density analysis. The higher d_{sp} and lower density of PILs possessing 4-*tert*-butylbenzyl group was an indication of looser chain packing in their matrix. As an effect of lower chain packing, these PILs have higher diffusivity coefficients than their counterparts possessing *n*-butyl substituent (Table 4.6). The Fractional Free Volume (FFV) of present PILs would

have been further useful in these interpretations, but the same could not be estimated due to unavailability of group contribution parameters for quaternary nitrogen atom.

Table 4.5. Permeability coefficient (P)[a] and permselectivity (P_A/P_B) of PILs

PILs	P_{He}	P_{H_2}	P_{N_2}	P_{CO_2}	P_{He}/P_{H_2}	P_{He}/P_{N_2}	P_{CO_2}/P_{N_2}	P_{CO_2}/P_{H_2}
PBI-BuI based PILs								
[DBDMPBI-BuI][I]	6.23	4.6	0.21	5.5	1.3	31.1	27.5	1.20
[DBDMPBI-BuI][BF_4]	6.8	6.2	0.26	8.8	1.1	22.7	33.8	1.42
[DBDMPBI-BuI][Tf_2N]	22.0	16.2	0.71	20.3	1.3	31.4	29.0	1.25
[DBDMPBI-BuI][HFB]	21.5	19.7	0.76	21.3	1.1	26.9	28.0	1.08
[DBzDMPBI-BuI][I]	12.6	10.7	0.51	11.3	1.2	25.2	22.6	1.06
[DBzDMPBI-BuI][BF_4]	16.4	16.3	0.61	18.7	1.0	27.3	31.2	1.15
[DBzDMPBI-BuI][Tf_2N]	28.3	20.6	0.90	24.5	1.4	31.4	27.2	1.19
[DBzDMPBI-BuI][HFB]	24.4	23.6	0.95	24.9	1.0	27.1	26.2	1.06
PBI-BuI[b]	10.1	10.7	0.06	1.9	1.0	168.0	32.0	0.18
PBI-HFA based PILs								
[DBDMPBI-HFA][I]	8.8	5.5	0.30	7.1	1.6	29.3	23. 7	1.29
[DBDMPBI-HFA][BF_4]	11.6	10.6	0.51	13.9	1.1	23.2	27.8	1.31
[DBDMPBI-HFA][Tf_2N]	20.0	16.2	0.71	18.1	1.2	28.6	25.9	1.12
[DBDMPBI-HFA][HFB]	21.6	16.2	0.70	18.9	1.3	30.9	27.0	1.17
[DBzDMPBI-HFA][I]	13.5	10.2	0.50	11.0	1.3	27.0	22.0	1.08
[DBzDMPBI-HFA][BF_4]	15.4	13.8	0.70	16.7	1.1	22.0	23.9	1.21
[DBzDMPBI-HFA][Tf_2N]	24.9	20.3	1.00	22.2	1.2	24.9	22.2	1.09
[DBzDMPBI-HFA][HFB]	24.7	20.5	1.01	23.2	1.2	27.4	22. 9	1.13
PBI-HFA[b]	12.9	12.2	0.10	2.9	1.0	129.0	29.0	0.24

[a]: Determined at 20 atm upstream pressure, expressed in Barrer (1 Barrer = 10^{-10} cm^3 (STP).cm.cm^{-2}.s.cm Hg), [b]: Data taken from Ref. [Kumbharkar (2006)].

In addition to the substituent, anion of a PIL also plays a crucial role in governing its gas permeability. The substituent effect is predominantly seen in case of PILs with I^- and BF_4^- anions than those with Tf_2N^- and HFB^- anions (Table 4.5). The effect of substituent in the latter cases could be masked due to higher bulk of the anion, as represented in Fig. 4.18. In case of PILs possessing BF_4^- as a common anion but different substituent, a gradual increase in permeability is clearly seen with variation in the bulk of anion (methyl < *n*-butyl < 4-*tert*-butylbenzyl). On the other hand, PILs with same substituent but Tf_2N^- anion, such effect is not that noteworthy.

Table 4.6. Diffusivity coefficient (D)[a] and diffusivity selectivity (D_A/D_B) of PBI based PILs

PILs	D_{H_2}	D_{N_2}	D_{CO_2}	D_{H_2}/D_{N_2}	D_{CO_2}/D_{H_2}	D_{CO_2}/D_{N_2}
PBI-BuI based PILs						
[DBDMPBI-BuI][I]	23.3	1.2	3.1	20.0	0.13	2.7
[DBDMPBI-BuI][BF_4]	58.9	1.4	4.6	41.3	0.08	3.2
[DBDMPBI-BuI][Tf_2N]	123.1	2.1	15.1	57.9	0.12	7.1
[DBDMPBI-BuI][HFB]	99.8	2.4	19.3	41.0	0.19	7.9
[DBzDMPBI-BuI][I]	45.2	2.0	6.3	22.6	0.14	3.1
[DBzDMPBI-BuI][BF_4]	154.9	2.7	9.3	57.7	0.06	3.5
[DBzDMPBI-BuI][Tf_2N]	142.3	3.4	16.8	41.6	0.12	4.9
[DBzDMPBI-BuI][HFB]	119.6	3.1	21.0	38.5	0.17	6.8
PBI-BuI	24.4	0.08	0.65	306.0	0.03	8.0
PBI-HFA based PILs						
[DBDMPBI-HFA][I]	23.2	0.8	4.6	27.5	0.20	5.4
[DBDMPBI-HFA][BF_4]	28.8	2.0	6.9	14.4	0.24	3.4
[DBDMPBI-HFA][Tf_2N]	53.5	3.0	14.5	18.1	0.27	4.9
[DBDMPBI-HFA][HFB]	82.0	2.7	13.2	30.9	0.16	4.9
[DBzDMPBI-HFA][I]	51.7	1.5	5.6	34.0	0.11	3.7
[DBzDMPBI-HFA][BF_4]	61.7	2.3	8.0	26.7	0.13	3.4
[DBzDMPBI-HFA][Tf_2N]	102.8	4.0	17.9	25.7	0.17	4.5
[DBzDMPBI-HFA][HFB]	86. 6	2.7	13.4	31.6	0.15	4.9
PBI-HFA[b]	30.6	0.16	1.1	188.0	0.03	6.9

[a]: Expressed in 10^{-8} $cm^{2.}$ S^{-1}, [b]: Data taken from Ref. [Kubharkar (2006)].

4.5.2 Effects of variation in anion

It was observed that the nature of anion had a considerable effect on governing the gas permeability of present PILs (Table 4.5). While keeping the substituent (*n*-butyl or 4-*tert*-butylbenzyl) or backbone (PBI-BuI or PBI-HFA) the same, permeability of all gases was generally increased in the order of increasing bulk of an anion, based on their van der Waal's volume (V_w, expressed in $cm^3.mol^{-1}$, V_w of $I^- = 19.5 < BF_4^- = 30.1 < Tf_2N^- = 88.5 \leq HFB^- = 86.5$) [Bondi (1964), Beichel (2013), Park (1997)]. This follows the order of increasing bulk of the anion. Table 4.6 also shows that for a particular polycation and a substituent, the diffusivity coefficient for CO_2 was increased with the variation of anion as $I^- < BF_4^- < Tf_2N^- \leq HFB^-$, indicating bulk of the anion contributed in governing the CO_2 diffusivity, and thus the gas permeability in PILs.

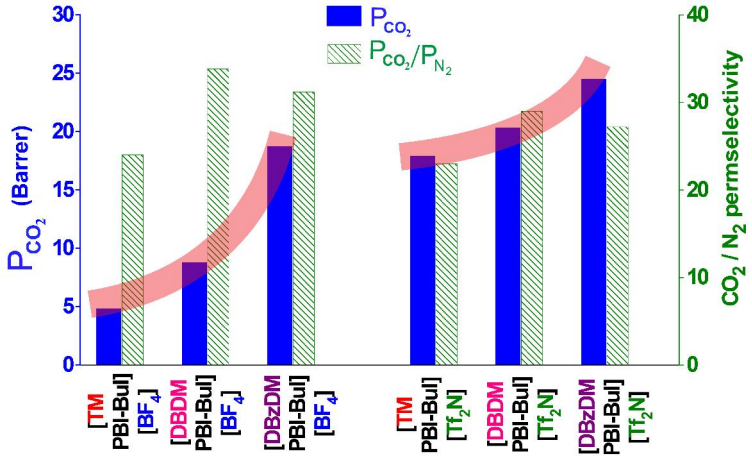

Fig. 4.18. CO_2 permeability (Barrer) and permselectivity over N_2 of the present and methyl substituted PILs [Bhavsar (2014b)] based on PBI-BuI

Fig. 4.18 shows the effect of anions in governing CO_2 permeability and its permselectivity over N_2 for PILs based on BF_4^- and Tf_2N^- anion. It is seen that for all three substituents (viz., methyl, *n*-butyl and 4-*tert* butylbenzyl), PILs with Tf_2N^- anion not only possessed high permeability, but also maintained comparable selectivity as that of PILs possessing BF_4^- anion. This conveys that Tf_2N^- anion has better ability (than that of other anions) to offer not only higher permeability, but also appreciable selectivity, wherein the role of substituent remained subordinate. As could be seen from Table 4.5, present PILs, especially those with BF_4^-, Tf_2N^- and HFB^- anions possessed considerably higher CO_2 permeability and P_{CO_2}/P_{H_2} selectivity than that of usual glassy polymers (increase in P_{CO_2} for Matrimid: ~2 times, PSF: ~4 times and polyetherimide: ~19 times) [Shao (2009)]. Only marginal lowering was observed in the case of P_{CO_2}/P_{N_2} selectivity. The elevation in permeability is possible due to presence of the bulky substituents group.

4.6 Effect of asymmetric substitution on gas permeation properties

In the case of glassy polymers, gas transport occurring through a solution-diffusion mechanism although provides a room to tune diffusivity (by modifying the polymer chain/subgroup flexibility and free volume present in the polymer matrix);

tuning solubility by manipulation of gas-polymer interaction has comparatively a less scope. Present methodology of PBI based polymeric ionic liquids (PILs) provides a possibility for tuning not only the diffusivity as they are based on rigid PBI backbone, but also the solubility of CO_2 due to the presence of IL character in them. Asymmetric nature of substitution might be of further help, as discussed below.

Structural tuning of PBI by *N*-substitution leading to PIL formation can be done by choosing both the groups (to be substituted on two 'N' of an imidazole) either the same or different. It would be worth to compare effects of symmetric substitution [Bhavsar (2014b)] with that of asymmetric one, as studied here. The maximum enhancement in P_{CO_2} achieved was ~ 6 folds (for PIL: [DBzDMPBI-BuI][I], as compared to the methyl substituted symmetric PIL: [TMPBI-BuI][I]). This was contributed by larger enhancement in the diffusion coefficients for CO_2 (~ 10 folds increase), which was counterbalanced by some lowering in the solubility coefficient. This lowering could be attributed to the decreased IL character (ratio of number of IL groups in repeat unit and the molecular weight of the repeat unit); that is decreased due presence of the bulky group in asymmetrically substituted PILs, in place of just methyl group in symmetrically substituted PILs. However, when the CO_2 sorption is expressed in mol% of the present PILs (Fig 4.19), it could be seen that the sorption was comparable for both the types of PILs it was actually slightly higher for asymmetrically substituted PILs, at lower pressures. On the other hand, CO_2 based sorption selectivity (S_{CO_2}/S_{H_2} and S_{CO_2}/S_{N_2}) for asymmetrically substituted PILs possessing I^- and BF_4^- are higher than that of symmetrically substituted PILs, possessing the same anion. The asymmetric *N*-substitution on PBI led to PILs with higher permeability and better/similar CO_2–philic character over their symmetric counterparts bearing same anion.

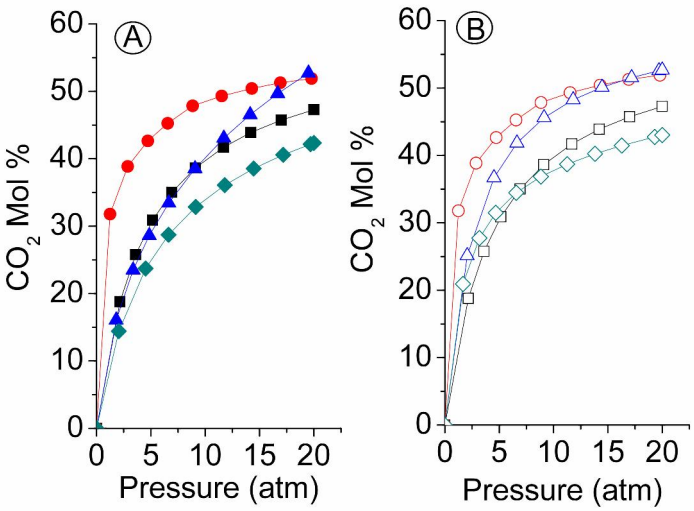

Fig. 4.19. CO_2 solubility expressed in mol% for (a) asymmetrically substituted PILs (■: [DBzDMPBI-BuI][I], ●: [DBzDMPBI-BuI][BF_4],▲: [DBzDMPBI-BuI][Tf_2N], ◆: [DBzDMPBI-HFA][HFB]), and (b) symmetrically substituted PILs (□: [TMPBI-BuI][I], ○:[TMPBI-BuI][BF_4], △: [TMPBI-BuI][Tf_2N], ◇: [TMPBI-HFA][HFB]).

It may be worth to note the appearance of present PILs on Robeson's upper bound [Robeson (2008)], along with PILs known in the literature and commonly used polymers, such as Matrimid, PSF, and PC [Shao (2009)]. It could be evident from Fig. 4.20 that although present PILs are superior to Matrimid, PSF, and PC, they are placed either below or along with PILs known in the literature. It may be noted that the permeability of known PILs is reported at lower pressure (of ~ 40 psi to 10 atm), while present PILs are investigated at 20 atm. It is well known that CO_2 permeability and hence CO_2 based selectivity is reduced with the applied pressure [Hu (2003)]. Secondly, present PILs possess rigid PBI-based backbone than the aliphatic and flexible backbone of known PILs. These two features may be responsible for the appearance of present PILs along with those reported. The performance of present PILs in terms of improving CO_2 permeation properties can be better evident based on their P_{CO_2} and P_{CO_2}/P_{H_2} (Fig. 4.21). Even after the pressure differential of permeation analysis of present PILs with that of reported ones remains, as discussed above; this Figure shows that present PILs offer additional benefits towards improving CO_2 permeation characteristics.

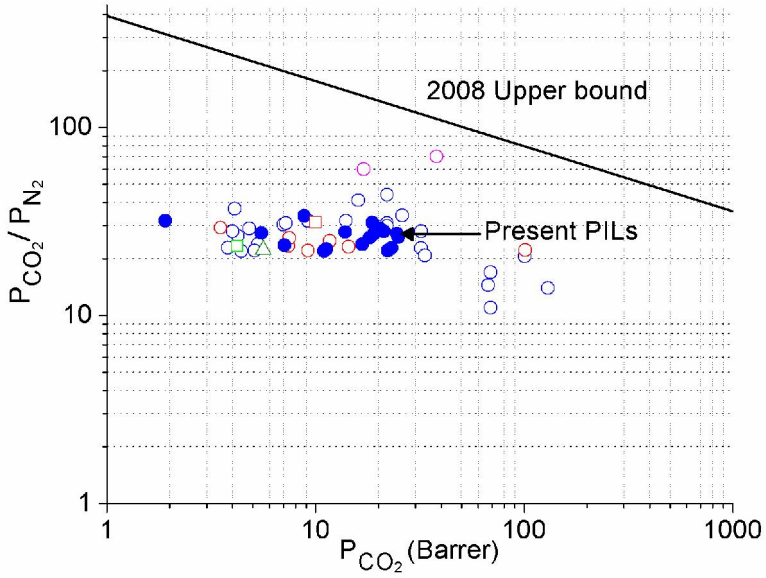

Fig. 4.20. Comparison of present PILs on the Robeson's Upper bound, along with reported PILs (upstream pressure ○: 40 psi, ○: 2 atm ○: 10 atm, ●: present PILs (20 atm) and common polymers, viz., □: Matrimid, △:PSF, □: PC.

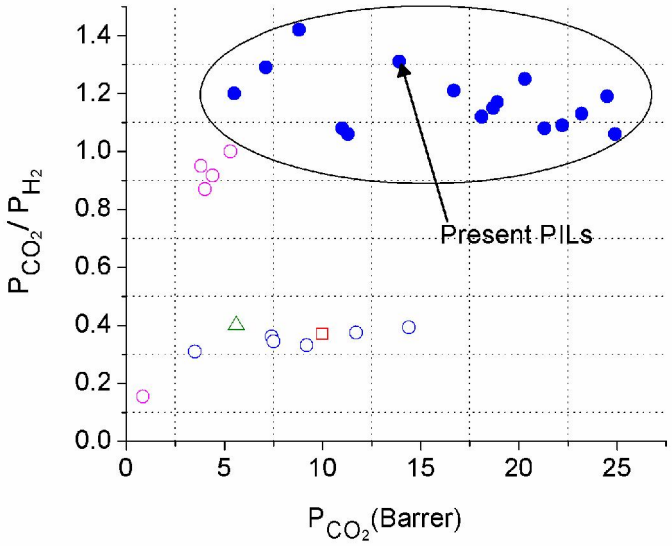

Fig. 4.21. Comparison of present PILs for CO_2/H_2 separation (○: reported PILs with upstream pressure 2 atm, ○: 10 atm, ●: present PILs (20 atm) and common polymers, viz., □: Matrimid, △: PSF

An enhancement in P_{CO_2}, which is approaching towards P_{H_2} (reverse selectivity) seems to be a major outcome of asymmetrically substituted PILs, in addition to their improved

permeability caused by attempted structural architecture (Fig. 4.22). Although the contribution of *'bulky'* 4-*tert*-butylbenzyl group towards increasing permeability could not be overlooked, the asymmetric type of substitution by two different alkyl groups seems to offer advantage towards offering better CO_2 based ideal selectivity over other gases. The analysis on diffusivity and solubility coefficients conveys that there is still opportunity to enhance diffusivity of CO_2, so that better benefits of enhanced CO_2 solubility can be exploited to elevate the CO_2 based selectivities. This could be made possible by further tuning in the structure of substituent and appropriate selection of anion, combinely. An increase in the bulk of substituent and / or anion is still a room available towards elevating diffusivity. These efforts are described in next chapters.

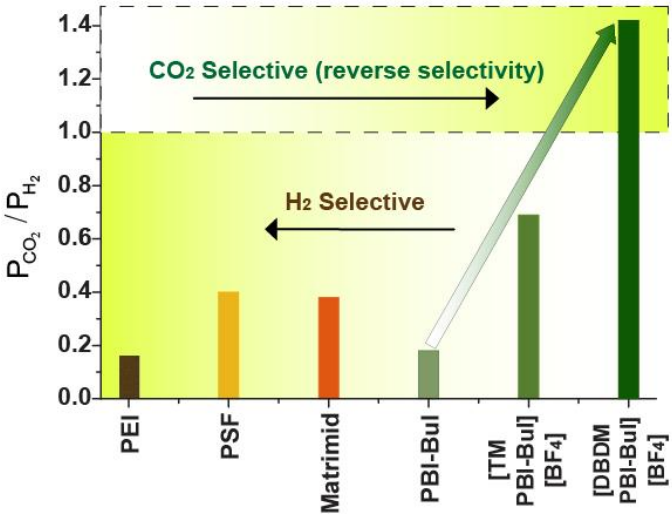

Fig. 4.22. CO_2/H_2 permselectivity of PBI-BuI based PILs and other common polymers [Shao (2009)].

4.7 Conclusions

Film-forming PILs with substitution asymmetry were synthesized successfully in two steps, *N*-substitution followed by *N*-quaternization of PBI-BuI and PBI-HFA in high yields. This was followed by exchange of iodide with chosen anions (BF_4^-, Tf_2N^- and HFB^-) with high yield of anion exchange. Some of these PILs showed enhanced solvent solubility in common low boiling solvents such as acetone, acetonitrile, and methanol; an assertive feature towards their easy processability. In addition, their amorphous nature

and high CO_2 permeability coupled with appreciable selectivity position them as attractive materials for gas separation; especially, CO_2. For PILs based on a particular backbone (either PBI-BuI or PBI-HFA) and a substituent (4-*tert*-butylbenzyl or *n*-butyl), CO_2 sorption generally increased in the order of anion variation as $HFB^- \leq Tf_2N^- < I^- < BF_4^-$. The PILs with Tf_2N^- and HFB^- as an anion showed higher gas permeability than those based on other anions. Among the two substituents, 4-*tert*-butylbenzyl containing PILs exhibited higher permeability than those containing *n*-butyl group. It was found that both, nature of the substituent as well as anion play a niche role in governing gas diffusion and sorption, thus overall permeability. The asymmetric type of substitution seems to be a constructive proposition towards enhancing permeability (e.g. P_{CO_2} in [DBzDMPBI-BuI][I] was 6 times higher than symmetrically substituted [TMPBI-BuI][I]).

As evident from eccentricities of tuning gas diffusivity as well as solubility simultaneously by variations of anions and substituent present in PILs based on PBI, this methodology provides an attractive approach for tuning permeation properties of glassy polymers in a promising manner. This is evident from higher CO_2 permeability of many of the PILs than that of H_2, in spite of their glassy nature. The combination of CO_2 specific anion coupled with loose chain packing in PILs offered higher CO_2 permeability and comparable permselectivity with that of common glassy polymers, e.g. Matrimid, PSF, PC, etc.

Chapter 5

Incorporation of rigid polyaromatic substituents in PBI based PILs: Effects on gas permeation and nitroexplosive detection properties

5.1. Introduction

There are several reports in the literature describing promising effects of incorporation of polycyclic aromatic hydrocarbons (PAHs) into polymer backbone on their gas permeation properties [Chung (2003), Rabbani (2012), Sekizkardes (2014), Tom (2015), UKK (1998)]. For instance, the naphthalene ring containing polyimides and polyarylates showed enhancement in permselectivity for various gas pairs, which was associated with some lowering in permeability [Chung (2003), Kharul (1998)]. The incorporation of pyrene in benzimidazole-linked nanofibers exhibited high CO_2/N_2 sorption selectivity of ~128 [Rabbani (2012)]. Similarly, pyrene-based benzimidazole-linked polymer showed higher CO_2 binding affinity and its uptake over CH_4 (CO_2/CH_4=11) and N_2 (CO_2/N_2 =103) under pressure and vacuum swing adsorption conditions [Sekizkardes (2014)]. The intermolecular interactions between the 'polymer of intrinsic microporosity', PIM-1 and polycyclic aromatic hydrocarbon (PAH), pyrene, were investigated recently by Tom et al. [Tom (2015)]. Blending PIM-1 with pyrene and 1-aminopyrene (11% of pyrene incorporation) displayed improved gas sorption selectivities for CO_2 over N_2 as compared to unmodified PIM-1 film.

In the present work, we selected pyrenyl and anthryl groups for *N*-substitution of thermally and mechanically stable PBI. Further, *N*-quaternization was performed using 4-*tert* butylbenzyl group in order to obtain PILs. The halide anion of these PILs was further exchanged with two chosen anions, viz., Tf_2N^- and BF_4^-. The choice of these anions was based on their attractive CO_2 sorption-permeation properties. [Bhavsar (2014b), Chapter 4]. The obtained PILs were characterized by requisite physical properties, pure gas sorption and permeation properties.

Pyrene is also known for its preferential binding with nitroaromatics (NACs) *via* electron donation and acceptation interaction [Gang (2011)]. The pyrene excimer

emission is known to be rapidly quenched by its exposure to NACs based on electron-transfer between pyrene and NAC molecules [Beyazkilic (2014), Wang (2012), Demirel (2013), Goodpaster (2002), Guo (2014)]. Fluorescent anthracene derivatives though have seen widely demonstrated for cation and anion sensing due to their well-known photophysical properties and commercial availability [Manez (2003), Shellaiah (2013)], only few reports are available on their use towards the detection of explosives [Ponnu (2010), Gole (2011)].

From the viewpoint of practical use, thin-film sensors are more suitable for field test [Shanmugraju (2011), Desmonts (2007)]. Advantages of film sensors over solution based sensors are reusability and easy possibility for device making [Gole (2011)]. Therefore, thin films possessing excimer emission are very promising materials as fluorescence sensors for numerous vapor phase detection. However, preparation of thin films with strong excimer emission is challenging. Physical entrapment of the fluorescent probe in a polymer matrix is though reported; this methodology produces inhomogeneity in the material and leads to stability issues due to the leaching of the fluorescent probe. This reduces the lifetime and reproducibility of the sensor [Desmonts (2007)].The most preferred method to prevent decay of excimer emission is the covalent attachment of fluorophore in the polymer matrix [Beyazkilic (2014), Desmonts (2007)]. It is known that poor excimer emission signal can be observed even for the covalently bonded pyrene molecules [Beyazkilic (2014), Li (2011)]. Furthermore, covalent attachment of pyrene derivatives requires tedious, costly synthetic steps and usually results in low yields of the target products [Beyazkilic (2014)].

To circumvent this, pyrene and anthracene substituted PILs (intentionally synthesized for elevating gas permeation properties) possessing excellent film forming properties were also investigated for their nitro-explosive detection. This work demonstrates an efficient way of incorporation of polycyclic aromatic pyrene and anthracene fluorophores in a proportion (almost two fluorophore per repeat unit) into a film forming polymer. Moreover, present approach of post-modification of PBI allows the polymer (PBI) molecular weight to be independently optimized.

5.2. Synthesis of PILs and their characterization by spectroscopic techniques

The *N*-substitution of PBI-BuI was carried out by preparing their sodium salt in dry DMSO, followed by reaction with either *9*-(chloromethyl)anthracene (An) or *2*-(bromomethyl)pyrene (Py), as detailed in Chapter 3. The purified *N*-substituted polymer was then alkylated by *4-tert*-butylbenzyl bromide (Bz) in the next step in order to obtain PILs with asymmetric *N*-substitution. They were further purified and characterized by ^{1}H NMR and IR spectroscopy.

An exchange of iodide anion from above PILs was performed using sodium tetrafluoroborate (BF_4), lithium trifluoromethane sulphonimide (Tf_2N) in DMF. This solvent was chosen owing to good solubility of the present PILs as well as chosen salts in it. In the cases of exchange by BF_4^- and Tf_2N^- anions, formed byproduct (LiI or NaI) was separated from the polymer by precipitating the reaction mixture in water followed by repeated water wash to the precipitated polymer.

In ^{1}H-NMR spectra of PILs (Fig 5.1), a peak in the range of δ 13-14, attributable to the 'imidazole' N-H protons of PBI-BuI disappeared completely. This was a primary indication of almost quantitative nature of the substitution reaction.

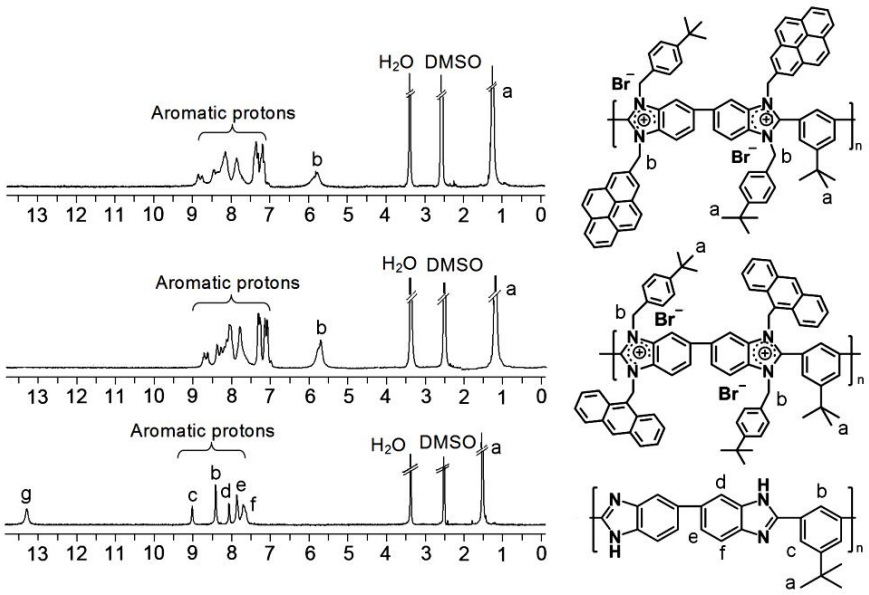

Fig. 5.1. ^{1}H-NMR spectra of pyrene and anthracene substituted PILs.

An assessment of degree of quaternization was done by Volhard's method [Jeffery (1989)]. In case of [DPyDBzPBI-BuI][Br], the degree of substitution was 87%, while in case of [DAnDBzPBI-BuI][Br], it was 84%.

For all PILs, FTIR spectra scanned at the ambient temperature showed a broad band at ~3610 cm^{-1} (Fig 5.2). This is attributable to the sorbed moisture, as was observed for PBIs and PILs based on them [Bhavsar (2014b), Kumbharkar (2009a)].

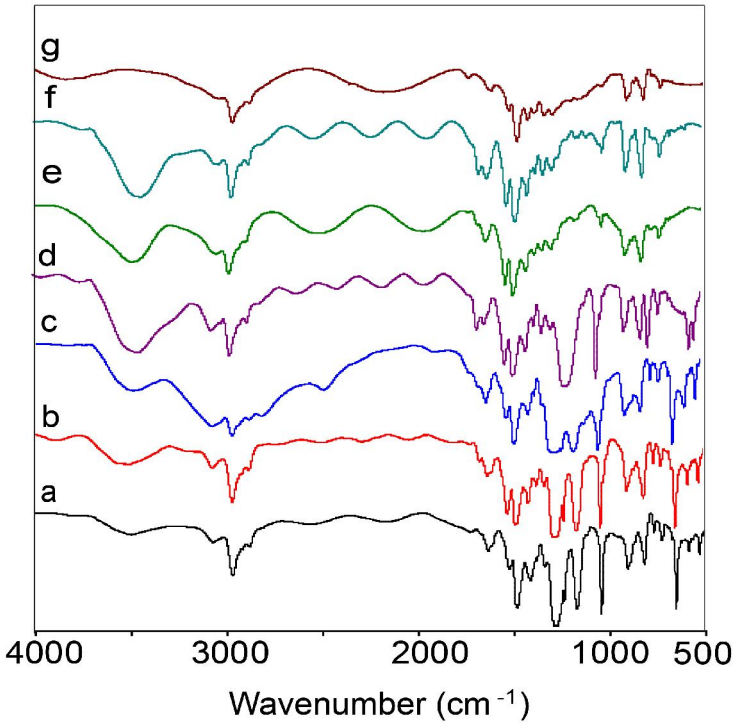

Fig. 5.2. FT-IR spectra of PILs based on PBI-BuI (a: PBI-BuI, b: [DPyDBzPBI-BuI][Br], c:[DPyDBzPBI-BuI][BF_4], d: [DPyDBzPBI-BuI][Tf_2N], e: [DAnDBzPBI-BuI][Br],f: [DAnDBzPBI-BuI][BF_4], g: [DAnDBzPBI-BuI][Tf_2N]).

The characteristic bands for benzimidazole at ~1500-1650 cm^{-1} (attributable to C=C/C=N ring vibration) are originated from the PBI backbone [Musto (1993)]. FTIR analysis supported the exchange of bromide by a particular anion (Fig. 5.2), which showed appearance of new peaks attributable to the respective anion. In PILs possessing BF_4^- anion, a band at ~1080 cm^{-1} is attributable to the B-F stretching vibrations [Suarez

(1996)]. Bands in the range of 1100-1230 cm^{-1} are attributable to C-F stretching of Tf_2N anion [Silverstein (1981)].

5.3. Physical Properties

5.3.1 Solvent solubility, WAXD analysis and density

The solubility of PILs in organic solvents is summarized in Table 5.1. PILs possessing bromide anion were soluble in polar high boiling solvents such as DMAc, DMF, NMP and DMSO and low boiling solvent, acetonitrile. The solubility was enhanced when the bromide ion was exchanged by another anion. As observed in chapter 4 PILs with Tf_2N^- and BF_4^-as anions were soluble even in acetone at the ambient temperature. All these PILs were insoluble in water and alcohols examined. Above results indicated that the solvent solubility of PBI which is known to be poor [Kumbharkar (2009)], was substantially improved after its conversion to the PIL. As discussed in chapter 4 such improvement in the solubility of polybenzimidazole based PILs can be attributed to the presence of ionic character as well as *N*-substitution.

Table 5.1. Solubility of PILs in various solvents

PILs	DMF	DMSO	DMAc	NMP	Acetone	CH_3CN	MeOH
[DPyDBzPBI-BuI][Br]	+	+	+	+	−	+	−
[DPyDBzPBI-BuI][BF_4]	+	+	+	+	+	+	±
[DPyDBzPBI-BuI][Tf_2N]	+	+	+	+	+	+	±
[DAnDBzPBI-BuI][Br]	+	+	+	+	−	+	−
[DAnDBzPBI-BuI][BF_4]	+	+	+	+	+	+	−
[DAnDBzPBI-BuI][Tf_2N]	+	+	+	+	+	+	±

+: Soluble at ambient temperature, ±: partially soluble, −: insoluble after 6 h heating near boiling point of the solvents.

In Table 5.2, d_{sp} obtained from WAXD spectra are given. WAXD patterns of these PILs indicated their amorphous nature (Fig. 5.3). Marginal variations in the *d*-spacing of PILs were correlated to both, substituent bulk and nature of the anion. For example, the d_{sp} of PILs having pyrenyl group were higher than PILs possessing anthryl group. It may be due to higher van der Waal volume of pyrenyl group (V_w = 116.75 $cm^3.mol^{-1}$), as compared to that of anthryl group (V_w = 99.21 $cm^3.mol^{-1}$) [Bondi (1964)] and would

inhibit close chain packing. In all PILs with a given substituent, d_{sp} increased in the order of anion variation as $Br^- < BF_4^- < Tf_2N^-$. This shows that bulk of the substituent as well as anion play a role in governing the chain packing in the PIL matrix.

Table 5.2. Physical properties of PILs

PILs	Bromide exchange[a] (mol %)	d_{sp}[b] (Å)	ρ[c] ($g.cm^{-3}$)	TG analysis		T_g[f] (ºC)
				IDT[d] (ºC)	W_{900}[e] (%)	
[DPyDBzPBI-BuI][Br]	0	5.14	1.318	213	32.3	ND
[DPyDBzPBI-BuI][BF_4]	85	5.26	1.169	380	25.5	242
[DPyDBzPBI-BuI][Tf_2N]	86	5.54	1.249	426	24.6	272
[DAnDBzPBI-BuI][Br]	0	4.60	1.396	210	35.4	ND
[DAnDBzPBI-BuI][BF_4]	85	4.92	1.194	330	37.1	ND
[DAnDBzPBI-BuI][Tf_2N]	82	5.04	1.275	370	33.1	265
[DBzPBI-BuI][g]	-	5.22	1.097	370	53.0	ND

[a]: Determined by Volhard's method, [b]: d-Spacing obtained from WAXD spectra, [c]: density at 35 ºC, [d]: initial decomposition temperature, [e]: char yield at 900°C, [f]: glass transition temperature, [g]: data taken from Ref [Kumbharkar (2010)], ND: could not be detected.

The density of PILs is summarized in Table 5.2. The Effects of substituent on the PIL backbone as well as anion were evident in governing the density. The density was lower in cases of PILs with pyrenyl as a substituent, than those based on anthryl group. This could be due to the bulkier nature of pyrenyl group that would loosen chain packing, as also supported by the WAXD analysis. The density within a series of PILs based on a particular *N*-substituent increased in the order of anion variation as: $BF_4^- < Tf_2N^- \approx Br^-$ (Table 5.2). It may be noted that present PILs showed lower density as compared to earlier reported methyl substituted asymmetric PILs based on PBI-BuI backbone [Bhavsar (2014a). However densities were comparable with *4-tert*-butylbenzyl substituted PBI-BuI based PILs [Chapter 4]. These results again indicated the role of a substituent and an anion in governing chain packing in PILs.

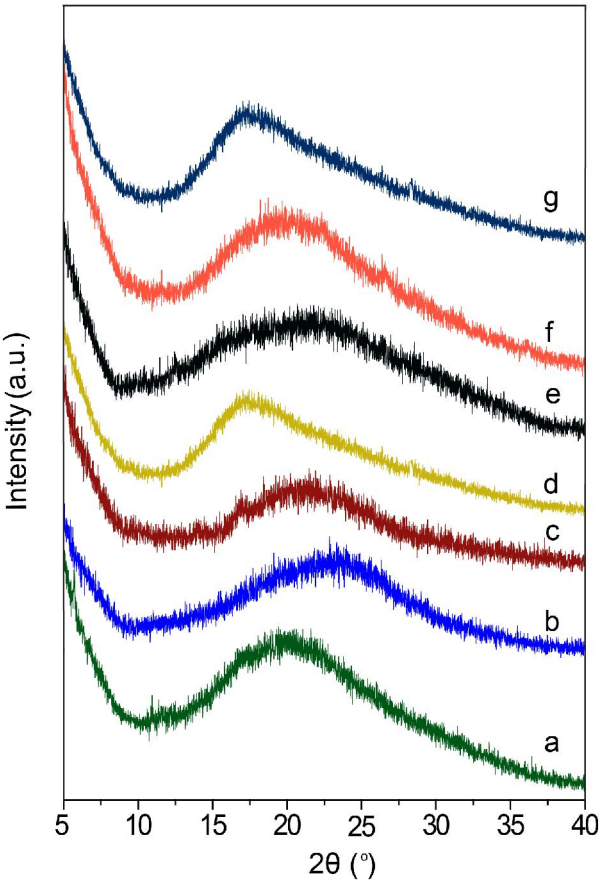

Fig. 5.3. XRD curves of PBI-BuI and PILs (a: PBI-BuI, b: [DPyDBzPBI-BuI][Br], c:[DPyDBzPBI-BuI][BF_4], d: [DPyDBzPBI-BuI][Tf_2N], e: [DAnDBzPBI-BuI][Br], f: [DAnDBzPBI-BuI][BF_4], g: [DAnDBzPBI-BuI][Tf_2N]).

5.3.2 Thermal stability of PILs

Initial degradation temperature (IDT) of present PILs are given in Table 5.2 and TG curves are shown in Fig. 5.4. The IDT of present PILs was in the range of 210-426 °C. For a common anion, PILs possessing pyrenyl as a substituent showed higher thermal stability than that of anthryl substituent. The higher thermal stability of pyrene substituted imidazoles as compared to their anthracene substituted analogues is reported [Dhirendra (2011)]. In case of PILs with the similar substituents but with varying anion, thermal stability of PILs increased with the order of anion variation as $Br^- < BF_4^- < Tf_2N^-$. Similar effects of anion variation on governing thermal stability were seen in earlier study of PILs based on PBI [Chapter 4, Bhavsar (2014a), Shaligram (2015)], indicating a

crucial role of substituent and anion in governing their thermal stability. Some of the present PILs showed a small weight loss at ~ 100 ºC. Such behaviour was observed in previous cases of PBI based PILs and was ascribed to the absorption of moisture as confirmed by IR at different temperatures [Bhavasar (2014a)].

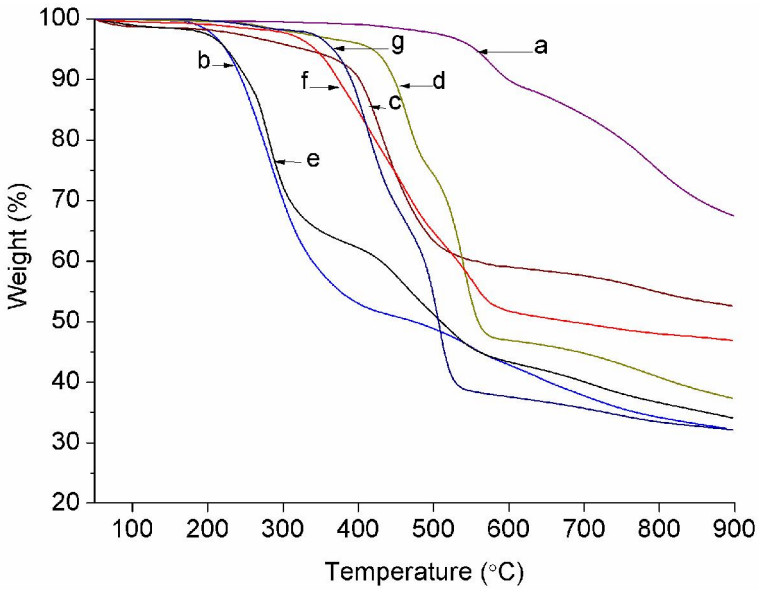

Fig. 5.4. TG curves of PBI-BuI and PILs (a: PBI-BuI, b: [DPyDBzPBI-BuI][Br], c:[DPyDBzPBI-BuI][BF_4], d: [DPyDBzPBI-BuI][Tf_2N], e: [DAnDBzPBI-BuI][Br], f: [DAnDBzPBI-BuI][BF_4], g: [DAnDBzPBI-BuI][Tf_2N]).

Glass transition temperature (T_g) of present PILs could not be detected in the DSC thermogram, even after repeated cycles of heating and cooling. Dynamic mechanical analysis (DMA) was performed and some of the PILs exhibited tan δ transition (Fig. 5.5), which is usually ascribed to the chain segmental motions, i.e. T_g. High T_g values of these PILs establish their glassy nature. For some of the PILs, tan δ could not be observed. They can be presumed to be glassy polymers since they possess similar rigid aromatic PBI backbone and similar substituents.

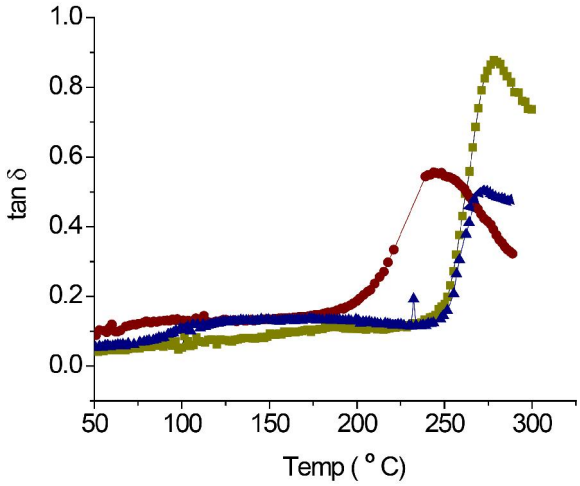

Fig. 5.5. The tan δ curves from dynamic mechanical analysis (DMA) of PILs (■: [DPyDBzPBI-BuI][Tf_2N], ●: [DPyDBzPBI-BuI][BF_4], ▲: [DAnDBzPBI-BuI][Tf_2N]

Part A: Gas permeation properties

5.4a Gas sorption

Equilibrium sorption isotherms of H_2, N_2, CH_4 and CO_2 in present PILs exhibited typical dual-mode nature (Fig. 5.6a), as usually observed for glassy polymers [Koros (1976), SCK (2010)]. The gas sorption parameters (k_D, b and C'_H) are given in Table 5.3a. In all present PILs, C'_H was higher for CO_2 than for other gases, attributable to the higher condensability of this gas [Kanehashi (2005)]. This is in accordance with the gas sorption behavior observed for most of the common glassy polymers [McHattie (1992), Barbari (1988), Kumbharkar (2006), Karadkar (2007)] that possessed higher C'_H for CO_2 than for other gases. It may be noted that C'_H for CO_2 in PILs possessing BF_4^- anion was higher than that of PILs based on other anions; conveying better CO_2-philic nature of this anion than that of others. The Langmuir affinity constant 'b' was negligible for H_2, N_2 and CH_4, but was relatively higher in case of CO_2. This could be considered as an indication of preferred CO_2 sorption in PILs containing BF_4^- anion. Table 5.4a presents the solubility coefficient (S) and solubility selectivity (S_A/S_B) for different PILs at 20 atm.

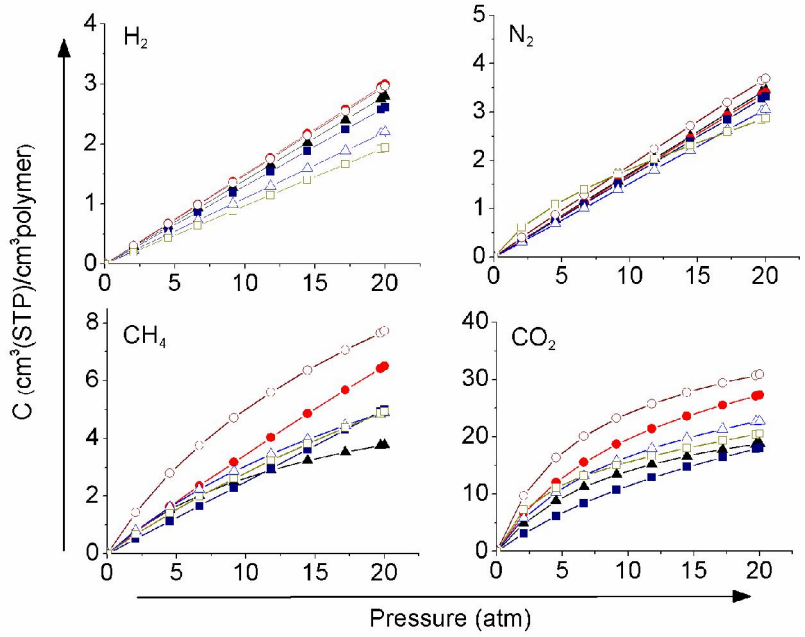

Fig. 5.6a. Gas sorption isotherms for PILs based on PBI-BuI at 35 ºC (△: [DPyDBzPBI-BuI][Br], ○: [DPyPBI-BuI][BF_4], □: [DPyDBzPBI-BuI][Tf_2N], ▲: [DAnDBzPBI-BuI][Br], ●: [DAnDBzPBI-BuI][BF_4], ■: [DAnDBzPBI-BuI][TF_2N]).

The solubility coefficient for different gases in all PILs increased in the order: $H_2 < N_2 < CH_4 < CO_2$; which followed the order of increasing inherent condensability of these gases (Fig. 5.7a) [Kumbharkar (2010), Li (2009), Kanehashi (2005)]. This behavior holds true irrespective of the *N*-substituent (pyrenyl or anthryl) of a PIL and the anion they hold. In case of PILs with the *pyrenyl* as substituent, CO_2 solubility coefficient was slightly higher than for their counterparts bearing *anthryl* substituent and the same anion. The higher sorption coefficient in these PILs could be correlated to the comparatively looser packing in earlier cases of PILs, as discussed above. It was observed that for a particular substituent, CO_2 sorption coefficient generally increased in the order of anion variation as $Tf_2N^- < Br^- < BF_4^-$, which led to enhanced CO_2 based sorption selectivity in case of PILs possessing BF_4^- as the anion (Table 5.4a). It may be noted that PILs possessing BF_4^- as anion also exhibited higher C'_H and b than for PILs with other anions. The favored CO_2 interactions for BF_4^- anion can be correlated to its higher basicity in comparison to other anions (pka of conjugate acid: HBr (−6.00) > $HNTf_2$ (−4.00) > HBF_4 (−0.44) [MacFarlane (2006)]. In our earlier study on PDADMA based PILs, it was shown that the CO_2 sorption increased with increase in the basicity of anion [Bhavsar (2012)].

Table 5.3a. Dual-mode sorption parameters[a] obtained for PILs

PILs	H_2			N_2			CH_4			CO_2		
	k_D	C'_H	b	k_D	C'_H	B	k_D	C'_H	b	k_D	C'_H	b
[DPyDBzPBI-BuI][Br]	0.11	0.68	5.52×10^{-5}	0.13	2.19	2.83×10^{-5}	0.05	3.74	0.17	0.09	23.92	0.11
[DPyDBzPBI-BuI][BF_4]	0.14	1.56	3.58×10^{-6}	0.15	2.44	4.41×10^{-5}	0.25	2.22	0.01	0.23	32.90	0.11
[DPyDBzPBI-BuI][Tf_2N]	0.13	0.17	5.80×10^{-2}	0.17	2.24	2.43×10^{-5}	0.26	3.83	3.44×10^{-5}	0.20	26.50	0.06
[DAnDBzPBI-BuI][Br]	0.15	1.56	4.94×10^{-5}	0.16	3.29	2.23×10^{-5}	0.04	9.95	6.70×10^{-2}	0.22	25.4	0.13
[DAnDBzPBI-BuI][BF_4]	0.15	0.14	2.50×10^{-3}	0.16	1.12	3.23×10^{-2}	0.12	11.83	3.70×10^{-2}	0.20	33.60	0.20
[DAnDBzPBI-BuI][Tf_2N]	0.10	0.12	1.96×10^{-5}	0.16	0.24	1.01×10^{-5}	0.15	4.69	3.70×10^{-2}	0.40	14.62	0.25
[DBzPBI-BuI][b]	0.17	2.64	1.1×10^{-3}	0.24	3.46	0.011	0.27	8.59	0.144	0.46	24.66	0.21

[a]: k_D is expressed in cm^3(STP).cm^{-3}polymer.atm, C'_H is expressed in cm^3(STP).cm^{-3}polymer, while b is expressed in atm^{-1}, [b:] Data taken from Ref [Kumbharkar (2010)].

Table 5.4a. Solubility coefficient (S^a) and solubility selectivity (S_A/S_B) of PILs at 20 atm

PILs	S_{H_2}	S_{N_2}	S_{CH_4}	S_{CO_2}	S_{N_2}/S_{CH_4}	S_{CO_2}/S_{H_2}	S_{CO_2}/S_{N_2}	S_{CO_2}/S_{CH_4}
[DPyDBzPBI-BuI][Br]	0.11	0.11	0.18	0.94	0.63	8.95	8.24	5.15
[DPyDBzPBI-BuI][BF_4]	0.15	0.17	0.32	1.36	0.53	9.19	7.89	4.19
[DPyDBzPBI-BuI][Tf_2N]	0.11	0.17	0.26	0.93	0.68	8.26	5.33	3.63
[DAnDBzPBI-BuI][Br]	0.11	0.17	0.31	1.14	0.56	10.25	6.56	3.69
[DAnDBzPBI-BuI][BF_4]	0.16	0.19	0.32	1.44	0.58	9.61	8.31	4.84
[DAnDBzPBI-BuI][Tf_2N]	0.10	0.16	0.26	0.80	0.62	8.27	4.98	3.11
[DBzPBI-BuI][b]	0.17	0.27	0.59	1.45	0.45	8.52	5.53	5.37

[a]: Expressed in cm^3 (STP).cm^{-3}polymer.atm, [b:] Data taken from Ref [Kumbharkar (2010)].

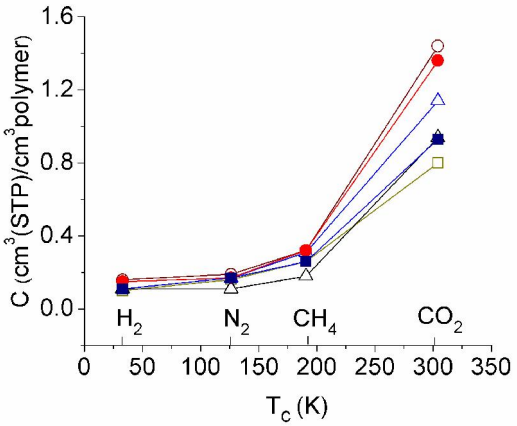

Fig. 5.7a. Gas solubility in PILs as a function of critical temperature of gases (△: [DPyDBzPBI-BuI][Br], ○: [DPyPBI-BuI][BF_4], □: [DPyDBzPBI-BuI][Tf_2N], ▲: [DAnDBzPBI-BuI][Br], ●: [DAnDBzPBI-BuI][BF_4], ■: [DAnDBzPBI-BuI][TF_2N]).

As could be seen from the results in Table 5.4a, variation in the anion has more pronounced effect on governing CO_2 sorption coefficient, while role of the bulk of substituent remains subordinate. The effect of substituent and anion was not significant in governing solubility of other gases (H_2, N_2 and CH_4). Therefore, with these structural variations, no specific trend could be seen in case of S_{N_2}/S_{H_2} and S_{N_2}/S_{CH_4} selectivity. They probably are governed by properties associated with the glassy nature.

5.5a Gas permeability

The pure gas permeability data for He, H_2, N_2, CH_4, CO_2 and ideal selectivity for various gas pairs are given in Table 5.5a. Considerable variations in the gas permeability of PILs with the variation in substituent or anion were observed, as discussed below.

5.5.1a Effects of variation in *N*-substituent

It was observed that PILs possessing pyrenyl group exhibited higher permeability for various gases and slightly lower CO_2 based selectivity over N_2, CH_4 and H_2; than that for PILs with anthryl substituent based on the same anion (4-*tert*-butylbenzyl group being common in both the PILs). This could be correlated to the size of substituent (van der Waal volume), which governs the chain packing as evidenced from WAXD and density measurements. The higher d_{sp} and lower density of PILs possessing pyrenyl group supported looser chain packing in their matrix. Effect of this chain loosening is reflected

on gas diffusivity coefficients (Table 5.6a). As an effect of lower chain packing, PILs possessing pyrenyl substituent and the same anion exhibited higher diffusivity coefficients than their counterparts possessing anthryl substituent (Table 5.6a).

As could be anticipated, permselectivity for various gas pairs (Table 5.5a) was higher for anthryl substituted PILs possessing the common anion. Variations in the gas permeation properties caused by substituent were more pronounced in the case of PILs possessing Br^- as an anion, than those possessing BF_4^- and Tf_2N^- as anion. This indicates that the effect of substituent in latter cases is shadowed by the higher bulk of the anion. As could be seen from the Fig. 5.8a, the diffusivity coefficient was found to correlate well with the kinetic diameter of gases. Similarly, Fig. 5.9a shows that the diffusivity of gases can be roughly correlated with the d_{sp} of PILs. These observations are typical for the glassy polymers [(Karadkar (2007), Bhavsar (2014b)].

Table 5.5a. Permeability coefficient (P [a]) and permselectivity (P_A/P_B) of PILs

PILs	P_{He}	P_{H_2}	P_{N_2}	P_{CH_4}	P_{CO_2}	P_{He}/P_{N_2}	P_{He}/P_{CH_4}	P_{H_2}/P_{N_2}	P_{H_2}/P_{CH_4}	P_{H_2}/P_{CO_2}	P_{CO_2}/P_{N_2}	P_{CO_2}/P_{CH_4}	P_{N_2}/P_{CH_4}
[DPyDBzPBI-BuI][Br]	25.7	24.8	1.11	0.82	23.9	23.2	31.3	22.3	30.2	1.04	21.5	29.1	1.35
[DPyDBzPBI-BuI][BF_4]	32.1	29.8	1.32	0.92	30.0	24.3	34.9	22.6	32.4	0.99	22.7	32.6	1.43
[DPyDBzPBI-BuI][Tf_2N]	38.8	36.5	1.81	1.25	36.2	21.4	31.0	20.2	29.2	1.01	20.0	29.0	1.45
[DAnDBzPBI-BuI][Br]	16.6	15.3	0.62	0.49	15.0	26.8	33.9	24.7	31.2	1.02	24.2	30.6	1.27
[DAnDBzPBI-BuI][BF_4]	25.9	23.3	0.92	0.75	25.1	28.2	34.5	25.3	31.1	0.93	27.3	33.5	1.23
[DAnDBzPBI-BuI][Tf_2N]	29.7	28.7	1.43	1.04	30.9	20.8	28.6	20.1	27.6	0.93	21.6	29.7	1.38
[DBzPBI-BuI][b]	-	46.4	1.51	1.37	21.3	-	-	30.7	33.9	2.18	14.1	15.5	1.10

[a]: Determined at 20 atm upstream pressure, expressed in Barrer (1 Barrer = 10^{-10} cm^3 (STP).cm.cm^{-2}.s.cm Hg), [b:] Data taken from Ref [Kumbharkar (2010)].

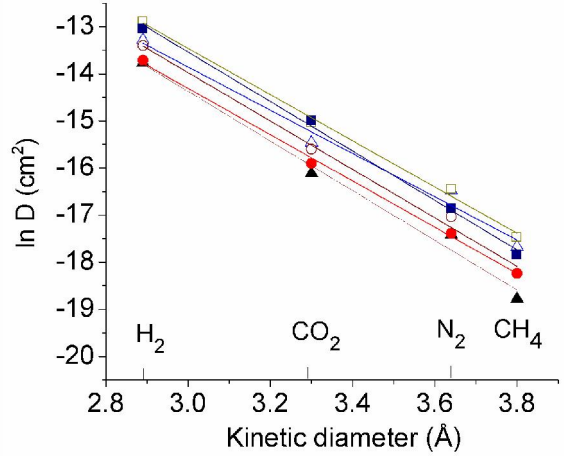

Fig. 5.8a. Correlation of diffusion coefficient with kinetic diameter (Å) of gases in PILs at 35 °C (△: [DPyDBzPBI-BuI][Br], ○: [DPyPBI-BuI][BF_4], □: [DPyDBzPBI-BuI][Tf_2N], ▲: [DAnDBzPBI-BuI][Br], ●: [DAnDBzPBI-BuI][BF_4], ■: [DAnDBzPBI-BuI][TF_2N]).

Table 5.6a. Diffusivity coefficient (D^a) and diffusivity selectivity (D_A/D_B) of PILs estimated at 20 atm

PILs	D_{H_2}	D_{N_2}	D_{CH_4}	D_{CO_2}	D_{H_2}/D_{N_2}	D_{H_2}/D_{CO_2}	D_{N_2}/D_{CH_4}	D_{CO_2}/D_{N_2}	D_{CO_2}/D_{CH_4}
[DPyDBzPBI-BuI][Br]	171.3	7.6	3.4	19.3	22.5	8.9	2.24	2.5	5.7
[DPyDBzPBI-BuI][BF_4]	151.0	5.9	2.1	16.8	25.6	9.0	2.81	2.8	8.0
[DPyDBzPBI-BuI][Tf_2N]	252.2	8.0	3.6	29.6	31.5	8.5	2.22	3.7	8.2
[DAnDBzPBI-BuI][Br]	105.7	2.7	1.2	10.0	39.1	10.6	2.25	3.7	8.3
[DAnDBzPBI-BuI][BF_4]	110.7	3.7	1.8	13.2	29.9	8.4	2.06	3.6	7.3
[DAnDBzPBI-BuI][Tf_2N]	218.1	6.7	3.0	29.3	32.6	7.4	2.23	4.4	9.8
[DBzPBI-BuI][b]	206.3	4.2	1.8	11.2	49.1	18.4	2.33	2.7	6.2

[a]: Expressed in 10^{-8} cm^2/s, [b]: Data taken from Ref [Kumbharkar (2010)].

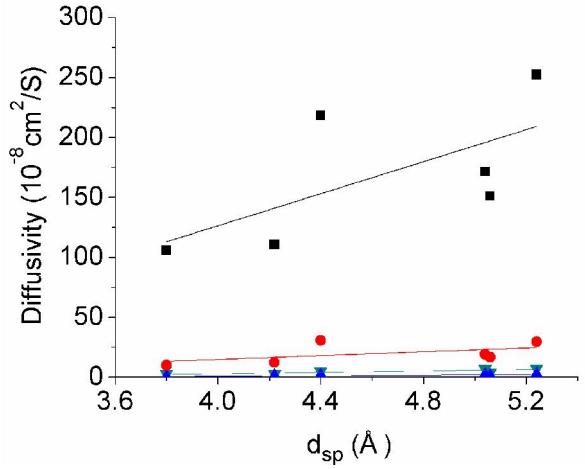

Fig. 5.9a. Variation of diffusion coefficient with d_{sp} of PILs (■: H_2, ▼: N_2, ▲: CH_4, ●: CO_2)

5.5.2a Effects of variation in the anion

As could be seen from results in Table 5.5a, while keeping substituent (pyrenyl or anthryl) the same, the permeability for all gases generally increased in the order of increasing bulk of anions as Br^- (V_w =15.9 $cm^3.mol^{-1}$) < BF_4^- (V_w = 30.1 $cm^3.mol^{-1}$) < Tf_2N^- (V_w = 88.5 $cm^3.mol^{-1}$) [Beichel (2013)]. Table 5.6a shows that for a particular substituent, the diffusivity coefficient for CO_2 was increased in the variation of anion as Br^- < BF_4^- < Tf_2N^-, indicating bulk of the anion contributed in governing the CO_2 diffusivity, and thus its permeability in PILs. Fig. 5.10a shows effect of anion variation in governing CO_2 permeability and its permselectivity over N_2. It is seen that for both the

substituents (pyrenyl and anthryl), PILs with Tf_2N^- anion possessed higher permeability with marginal lowering in CO_2 based selectivity as compared to those possessing BF_4^- anion. The higher P_{CO_2}/P_{N_2} and P_{CO_2}/P_{CH_4} selectivity for PILs with BF_4^- as an anion can be attributed to the favourable interactions of this anion with CO_2. These observations convey that Tf_2N^- anion has a better ability to elevate permeability of a PIL, while BF_4^- anion better contributes towards elevating CO_2 based permselectivity.

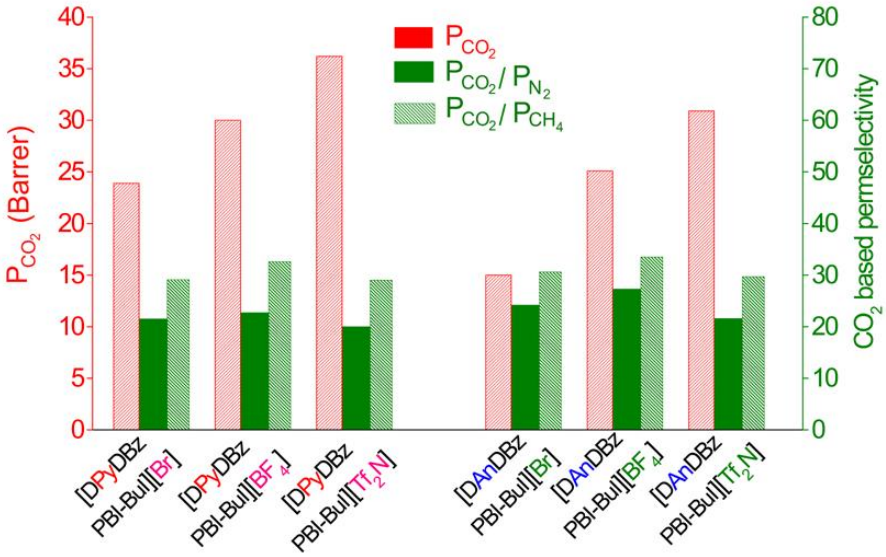

Fig. 5.10a. CO_2 permeability and CO_2 based permselectivity of PILs.

5.5.3a Comparison with PBI based PILs and other common polymers

In order to understand efficacy of having rigid polyaromatic hydrocarbons substituted in PBI based PILs, it would be worth to compare their permeation properties with that of recently reported PBI based PILs and conventional polymers. It could be seen from Fig. 5.11a that present PILs possessed considerably higher CO_2 permeability as compared to previously as reported PBI-based PILs. The enhancement in P_{CO_2} achieved was ~6 fold for present PIL, [DPyDBzPBI-BuI][Br], vis-à-vis its methyl substituted analogue, [TMPBI-BuI][I] that could be treated as the base case for PBI-based PILs. Such enhancement with respect to the recently reported *asymmetrically substituted* PIL, [DBzDMPBI-BuI][I] was also substantial (~2 fold) [Chapter 4]. It is seen that, this enhancement in permeability was majorly contributed by the diffusion coefficients for

CO_2, rather than the sorption coefficients. These variations in permeability can be correlated to the size of substituent present on the PBI backbone.

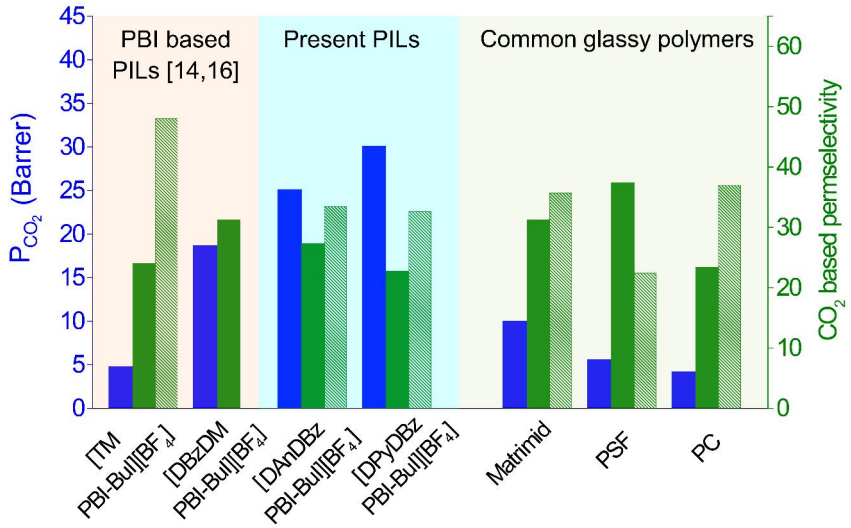

Fig. 5.11a. CO_2 permeability (▬) and CO_2 based permselectivity (▬: P_{CO_2}/P_{N_2}, ▨: P_{CO_2}/P_{CH_4}) of some common glassy polymers and PBI based PILs.

In order to further understand the role of polyaromatic hydrocarbon in governing permeability, packing density parameters WAXD, density and permeation properties of these PILs need to be compared with their disubstituted analogue, i.e., DBzPBI-BuI reported earlier [Kumbharkar (2010)]. It is seen from Table 5.2, all PILs (except [DPyDBzPBI-BuI][Tf_2N]) exhibited lower d-spacing and thus tighter chain packing than that of [DBzPBI-BuI]. This could be possible due to the accommodation of flat anthracene and pyrene groups in initially available free space of [DBzPBI-BuI], leading to closer chain packing. As a result, present PILs exhibited lower permeability for gases (H_2, N_2 and CH_4), with an exception for CO_2; than that of [DBzPBI-BuI]. Such a reduction in permeability by substitution of an alkyl group in the polymer chain by virtue of accommodating its bulk in available free space is known in the literature (Yampolskii (2001), Mchattie (1990)]. Although such reduction in permeability is anticipated; effects of 'ionic liquid character' present in PILs are distinctly visible. This can be explained based on increase in both, CO_2 permeability and its selectivity over N_2 and CH_4 especially when permeability of other gases is decreased than that of [DBzPBI-BuI]. As

an example, [DPyDBzPBI-BuI][Tf_2N] showed 21% decrease in H_2 permeability, but 41% enhancement CO_2 permeability than that of [DBzPBI-BuI]. This supports our proposition of increasing CO_2 based permeation characteristics by introducing bulky substituent and IL character in the glassy PBI backbone, simultaneously. Other aspects, such as enhanced solvent solubility and strong film forming ability that could easily withstand high applied pressure, are added advantages of the present methodology.

As could be seen from Fig 5.9a, present PILs (with BF_4^- anions) possessed considerably higher CO_2 permeability than that of conventional glassy polymers (Matrimid: ~2 times, PSF: ~4 times and PC: ~9 times [Shao (2009), Barbari (1989)]. This elevation in CO_2 permeability is coupled with either similar or marginal lowering in its selectivity (P_{CO_2}/P_{N_2} and P_{CO_2}/P_{CH_4}).

5.6a Conclusions

Pyrenyl and anthryl functionalized PILs based on PBI-BuI were successfully synthesized, followed by exchange of bromide with chosen anions BF_4^- and Tf_2N^-. For PILs based on a particular substituent, *viz.* pyrenyl or anthryl, CO_2 sorption generally increased in the order of anion variation as $Tf_2N^- < Br^- < BF_4^-$. Those with Tf_2N^- as an anion showed higher gas permeability, while those possessing BF_4^- was dominating towards elevation in selectivity. Among the two substituents, pyrenyl group containing PILs exhibited higher permeability than those based on anthryl group containing PILs. It was found that both, the nature of the substituent as well as anion play a key role in governing gas diffusion and sorption, thus overall permeability.

As evident from eccentricities of tuning gas diffusivity as well as solubility simultaneously by variations of anions and substituent of PILs, this methodology provides an attractive approach for systematic tuning of permeation properties (especially for CO_2) of glassy polymers in a promising manner. This is easily evident from the higher CO_2 permeability of many of the PILs than that of H_2, in spite of them being glassy in nature. The combination of CO_2 specific anion coupled with higher free volume in PILs offered higher CO_2 permeability and comparable permselectivity than their structural analogue 'without IL functionality', DBzPBI-BuI and conventional glassy polymers such as Matrimid, aromatic polysulfone and polycarbonate.

Part B: Detection of Nitroexplosive

5.4b. Optical properties

5.4.1b UV spectra

The covalent attachment of the pyrene and anthracene moieties in PILs significantly affected the UV-absorption and fluorescence properties of the parent PBI-BuI. It could be seen from Fig. 5.6b that the parent PBI-BuI showed strong UV absorption band at 347 nm due to the presence of benzimidazole group in it. The pyrene containing PIL, [DPyDBzPBI-BuI][Br] exhibited strong absorption bands at 347, 330 and 282 nm, which could be correlated with the vibration bands of pyrene [Dhirendra (2011)]. On the other hand, anthracene containing PIL, [DAnDBzPBI-BuI][Br] showed a wider UV absorption in the range 340–420 nm. These bands correlate with the vibrational characteristic of isolated anthracene chromophore [Dhirendra (2011)]. This data confirms that after covalent bonding of these fluorophores with PBI-BuI, UV-absorption characteristics of resulting PILs exhibit added features of UV-absorption due to the presence of these fluorophore.

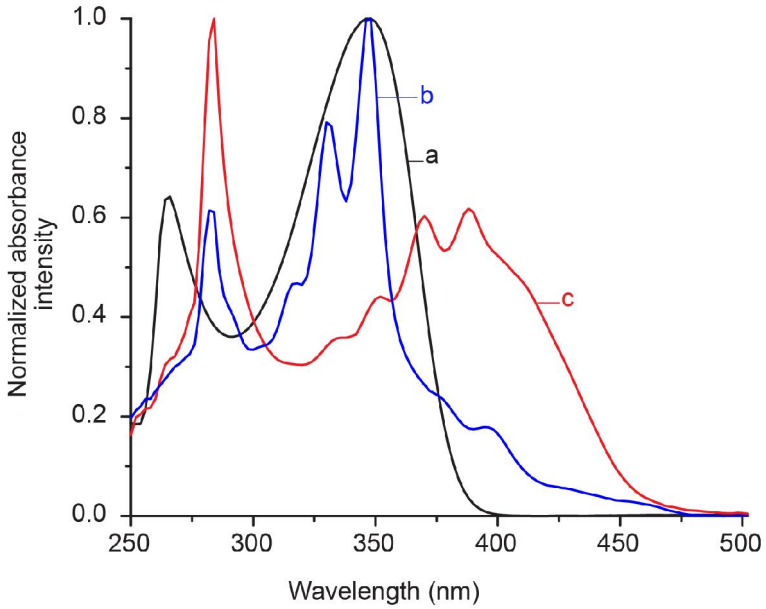

Fig. 5.6b. UV-Visible spectra of a: PBI-BuI, b: [DPyDBzPBI-BuI][Br] and c: [DAnDBzPBI-BuI][Br].

5.4.2b Fluorescence measurements

Fig. 5.7b shows fluorescence emission spectra of PBI-BuI and PIL solutions. In contrast to the UV-excitation spectra (that showed well defined characteristic features due to chromophores), the fluorescence emission spectra of PILs were quite different. Both PILs exhibited slightly broader and featureless excimer emission centered at 518-520 nm. For pyrene monomer emission is reported to be ~ 370-400 nm [Kalyanasundaram (1977) and for anthracene it is ~ 415 nm.

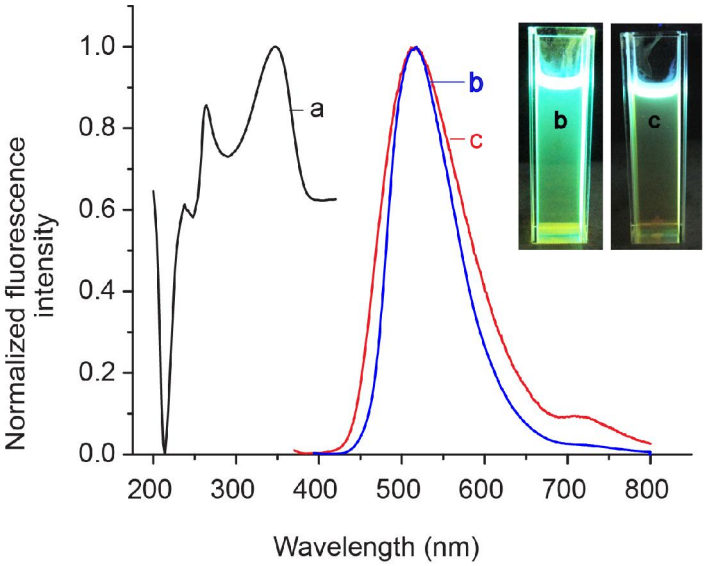

Fig. 5.7b. Fluorescence emission of a: PBI-BuI, b: [DPyDBzPBI-BuI][Br] and c: [DAnDBzPBI-BuI][Br] in DMSO (λ_{ex} = 350 nm).

The shifting of fluorescence emission to a larger wavelength (visible range) in PILs reveals the successful covalent attachment of chromophores to the fully aromatic backbone of PILs. It is known that at the low concentration of pyrene, monomer emission is dominant and no excimer emission is observed due to lack of close association; however at their high concentrations, an excimer formation is feasible where the intermolecular interaction of excited molecules with the ground state structures gives excimer emission [Winnik (1993)]. The high degree of substitution (~ 2 per repeat unit) obtained in both the present cases of PILs is thus one of the important feature, which ensures availability of high enough concentration of fluorophore in the polymer chain. The rigid, aromatic polycation and electron rich nature of fluorophore would thus provide

ideal situation for inter/intramolecular stacking between them and thus offer bright excimer emission.

5.5b Solution state sensing properties of nitroaromatics

In order to investigate the interactions of PILs with NACs, nitrobenzene (NB) was chosen as a model analyte. It is seen [Fig. 5.8b] that the initial emission intensity of both PIL solutions was quenched rapidly upon gradual addition of NB into the solution. This reduction in emission intensity of PILs is ascribed to the formation of a non-fluorescent charge-transfer (CT) complex between the electron donor (pyrene/ anthracene) and the electron acceptor (NB). After getting promising results from NB, fluorescence quenching with TNT and PA was studied [Fig. 5.9b and 5.10b].

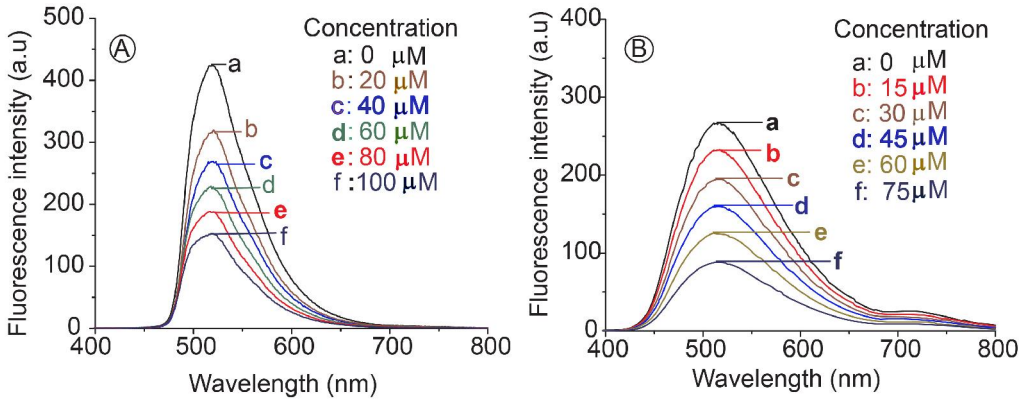

Fig.5.8b. Fluorescence emission spectra of PILs A: [DPyDBzPBI-BuI][Br], B: [DAnDBzPBI-BuI][Br] in the presence of different concentrations of nitrobenzene in DMSO (λ_{ex} = 350 nm).

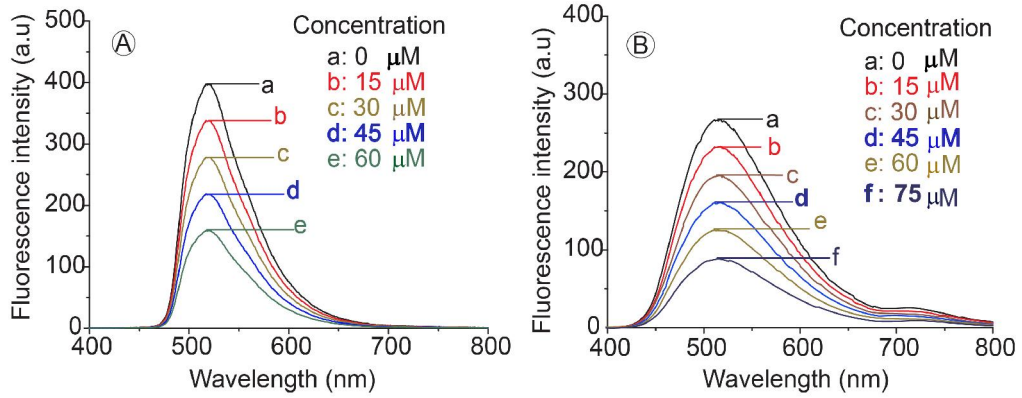

Fig.5.9b. Fluorescence emission spectra of PILs A: [DPyDBzPBI-BuI][Br], B: [DAnDBzPBI-BuI][Br] in the presence of different concentrations of TNT in DMSO (λ_{ex} = 350 nm).

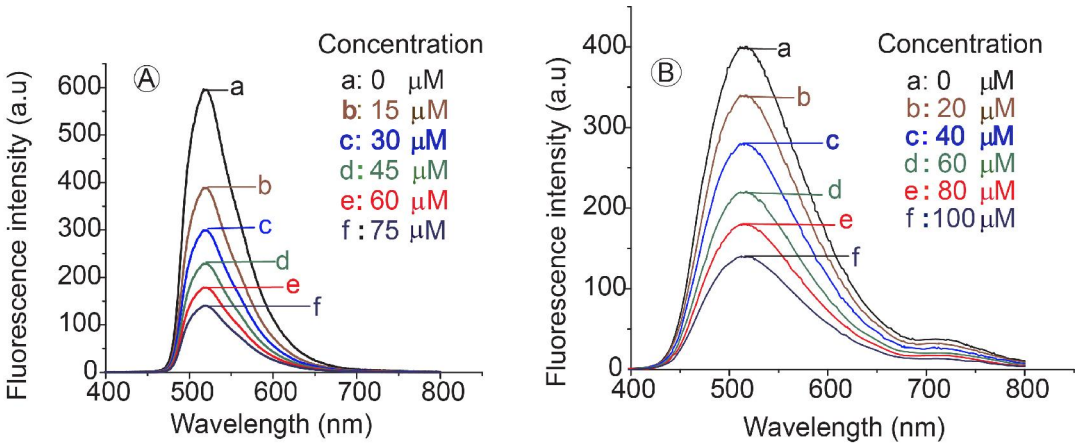

Fig.5.10b. Fluorescence emission spectra of PILs A: [DPyDBzPBI-BuI][Br], B: [DAnDBzPBI-BuI][Br] in the presence of different concentrations of PA in DMSO (λ_{ex} = 350 nm).

TNT showed the high quenching response as compared to the NB. PA showed even higher quenching of fluorescence. The higher fluorescence quenching by PA could be due to its strong hydrogen bonding interactions with PILs. Similar findings were reported for ionic liquid, [BMIM][PF_6] that exhibited high affinity towards NACs [Forzani (2009)]. The quenching efficiency of analyte is usually evaluated by Stern-Volmer relationship [Naddo (2007)]:

$$K_{sv} \times [Q] = \frac{I_0}{I} - 1$$

where, 'I_0' and 'I' are the fluorescence intensities of the polymer solution in the absence and presence of NACs, respectively, [Q] is the concentration of the NACs, and K_{sv} is the Stern-Volmer constant. For three different NACs, the obtained K_{sv} are given in Table 5.3b. The pyrene containing PIL, [DPyDBzPBI-I][Br] was found to be more efficient in quenching the fluorescence of all the three NACs than by anthracene containing PIL, [DAnDBzPBI-I][Br]. This could be due to the large delocalized π system and well matched orbital energy levels of pyrene with the NACs. The better quenching efficiency of [DPyDBzPBI-I][Br] can also be evident from [Fig 5.11b (a-d)], wherein the % quenching was calculated as:

$$\% \text{ quenching} = \frac{I_0 - I}{I_0} \times 100$$

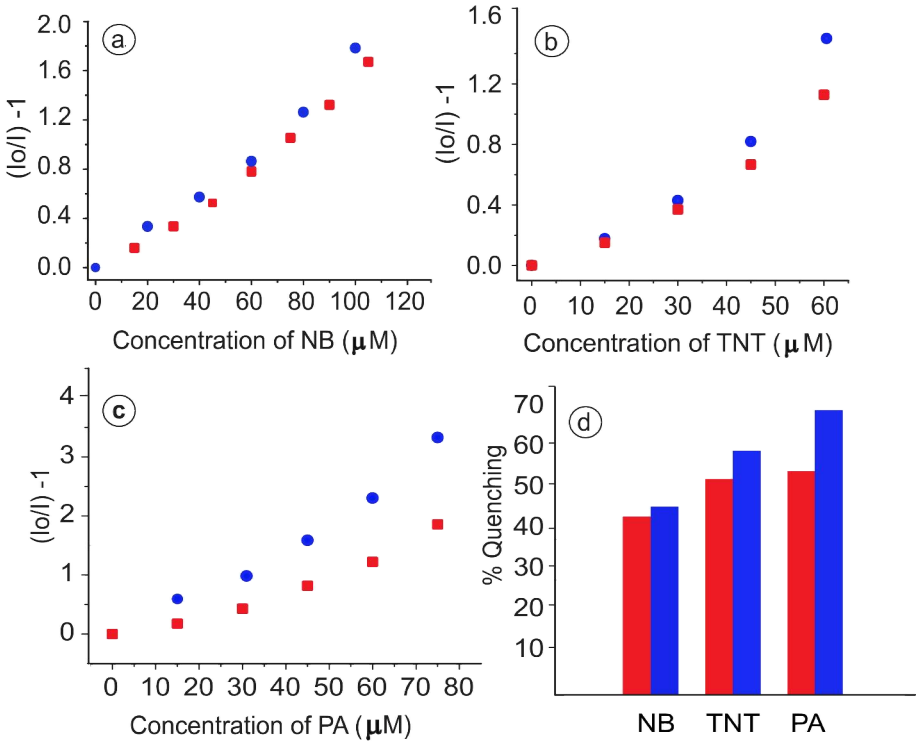

Fig. 5.11b. Stern-Volmer plots for [DPyDBzPBI-BuI][Br] (●) and [DAnDBzPBI-BuI][Br] (●) using different NAC solutions; a: NB, b: TNT and c: PA; while d: percent quenching for [DPyDBzPBI-BuI][Br] (■) and [DAnDBzPBI-BuI][Br] (■) at 60 µM concentration of NACs.

At 60 µmol/L concentration of NACs [Fig. 5.11b (d)], reduction in fluorescence intensity in case of pyrene containing PIL was 70%, 60% and 46% for PA, TNT and NB; respectively. On the other hand, anthracene containing PIL, these efficiencies were slightly lower (55%, 53% and 44%, respectively). This efficient quenching of fluorescence by all the three NACs can be attributed to the π-π interaction between the quencher and the pyrene or anthracene moieties in the respective PIL. A conjugated planar structure of pyrene and anthracene makes it easier to bind NACs *via* π-π interactions. The observed high solution state fluorescence quenching of PILs prompted us to further explore their use in the solid state.

Table. 5.3b. Stern-Volmer constants (K_{sv}[a]) of PILs

PILs	NB	TNT	PA
[DPyDBzPBI-BuI][Br]	1.78	2.50	4.15
[DAnDBzPBI-BuI][Br]	1.59	1.88	2.03

[a]: Expressed in 10^4 M^{-1}

5.6b Solid state sensing properties of nitroaromatics

5.6.1b Fluorescence quenching in thin films

From a practical standpoint, solid film-based sensing is a more convenient means of analyte detection than solution state. This is especially true in the current context, where detection of NACs in vapors may be required to detect a hidden improvised explosive device (IED) or landmine. The fluorescence quenching of PILs by saturated vapors of representative NACs ($4x10^5$ ppb for NB, $5.5x\ 10^{-6}$ torr for TNT and $7.48x10^{-7}$ torr for PA [Ostmark (2011)] was also investigated (Fig. 5.12b and 5.13b). Remarkable quenching efficiency was observed for all NAC vapors. It was observed that for various duration of film exposure to NAC vapors, the position of peak maxima in the florescence spectra did not change with time. With an exposure time of 500 s, pyrene containing PIL, [DPyDBzPBI-BuI][Br] showed 87%, 76.8% and 71.6% quenching for NB, TNT and PA, respectively. On the other hand for anthracene based PIL, [DPyDBzPBI-BuI][Br], the quenching was 80.3%, 73.5% and 67.5% for NB, TNT and PA, respectively.

For both cases of PIL films, quenching performance followed the order: NB> TNT >PA. The lowering of sensing performance for TNT and PA than that of NB can be attributed to lower vapor pressures of earlier cases. The higher fluorescence quenching efficiency in case of pyrene containing [DPyDBzPBI-I][Br] could be attributed to its electron rich nature than that of anthracene based [DAnDBzPBI-I][Br], leading to better interactions of the earlier with NACs. Selectivity is a crucial criterion for the practical detection of NACs by fluorescence quenching of films. It is thus of great interest to study the response of present PIL films to the potential chemical agents that would interfere detection of NACs by fluorescence quenching. The fluorescent quenching obtained using benzoquinone (BQ), toluene, THF and $NaNO_3$ (SN) as potential interfering agents [Gang (2011)] is shown in Fig. 5.12b and 5.13b, for both the PIL films.

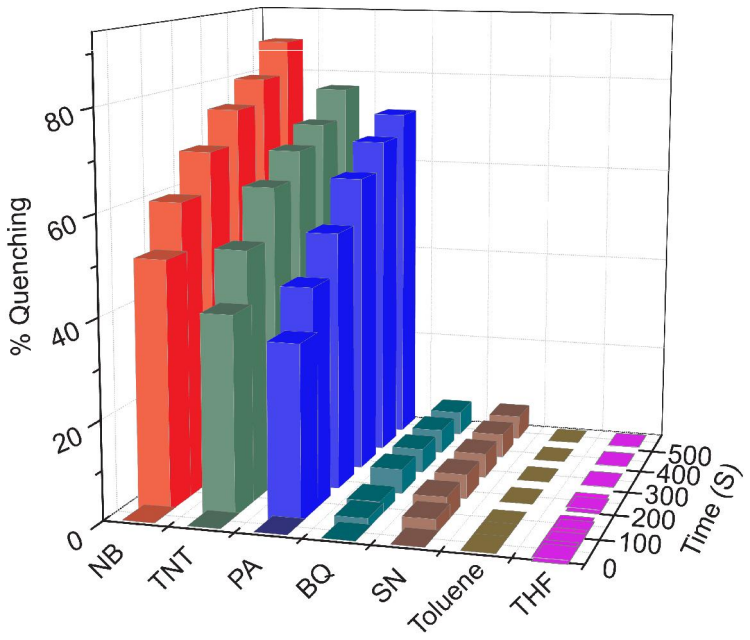

Fig. 5.12b. Time dependent quenching of [DPyDBzPBI-BuI][Br] upon exposure to the saturated vapors of NACs and common interferents.

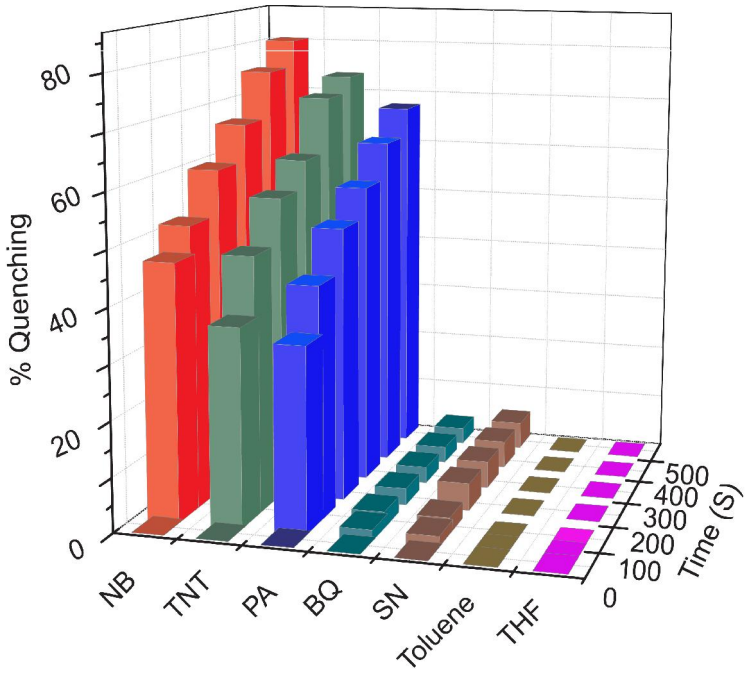

Fig. 5.13b. Time dependent quenching of [DAnDBzPBI-BuI][Br] upon exposure to the saturated vapors of NACs and common interferents.

It is seen that the fluorescence emission of PILs is rarely affected by the presence of any of the potential interfering agents. Exposure to SN did not cause significant quenching of any of the PIL film. This implies the possibility to differentiate NACs from commonly used nitrogen fertilizers. Moreover, strong electron-acceptors such as BQ did not result in significant quenching of either film, indicating possible differentiation of strong oxidants from NACs. Volatile solvents (toluene and THF) also did not show any quenching of PIL-film fluorescence. Thus, present PIL films could be said to be selective to fluorescence quenching by NACs.

The fluorescence quenching of thick film (~ 40 μm) of pyrene containing PIL by NB was also studied. The quenching after 50 s was 11% and after 300 s it reached to 30% (Fig. 5.14b).

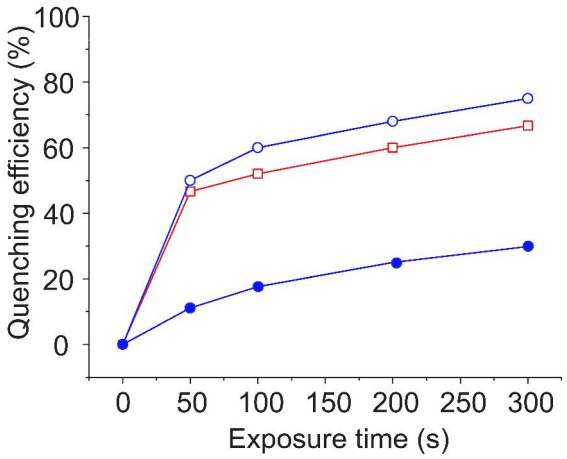

Fig. 5.14b. Time dependent quenching of the PIL films ○: [DPyDBzPBI-BuI][Br] (12 μm), □: [DAnDBzPBI-BuI][Br] (12 μm) and ●: [DPyDBzPBI-BuI][Br] (40 μm) upon exposure to the saturated vapors of NB.

The lowering in fluorescence quenching may be due to the effect of film thickness on the rate by which the NB permeates into the film. Such lowering in quenching efficiency by various NACs due to increase in film thickness of pentiptycene-derived phenyleneethynylene has been observed earlier [Yang (1998)].

5.6.2b Reversibility of the quenching process

The fluorescence regaining ability of PIL films was evaluated by exposing the film to NB vapors for 300 s, washing with methanol at ambient for 10 minutes, followed by drying in an oven at 60 ºC for 30 minutes. As could be seen from Fig. 5.15b, initial emission intensity of the film was almost recovered by a simple washing protocol followed for this purpose. Over numbers of cycles, the quenching efficiency of the film decreased gradually, presumably because the methanol could not be able to remove all the NB molecules associated with PIL film. Although this protocol can further be optimized while tuning the washing solvent/duration/temperature in order to remove the observed drift, it was outside the scope of present study. Similar drift was observed by the pH sensitive radiometric fluorophore 8-hydroxypyrene-1,3,6-trisulfonic acid (HPTS) immobilized in ethyl-cellulose, where time dependent calibrations were used to eliminate the drift [Hakonen (2008)]. Thin films of present PILs showing reversible sensing can be used for NAC detection. More significantly, the regaining of initial fluorescence intensity over repeated cycles implies the high stability of these films that could be useful for their long time infield explosive screening applicability.

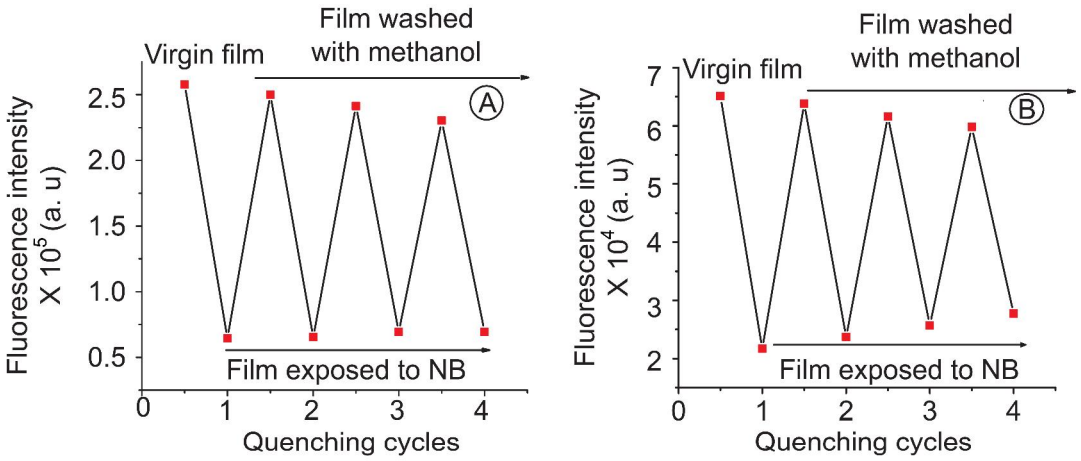

Fig. 5.15b. Regaining of quenching efficiency of PIL films; A: [DPyDBzPBI-BuI][Br], B: [DAnDBzPBI-BuI][Br] after exposure to saturated vapors of NB.

5.7b Conclusions

Pyrene and anthracene as a commonly found superior low-molecular-mass fluorophores were successfully introduced into rigid, thermo-chemically and mechanically stable polybenzimidazole (PBI). The resultant PILs showed bright excimer emission, which was found to be quenched by electron deficient NACs such as NB, TNT and PA in solution state. Fluorescence-quenching studies using self standing, solution-cast solid film of the PILs showed almost instantaneous and selective detection of the saturated vapors of NACs at ambient temperature and pressure. Fluorescence emission of PILs was rarely affected by the presence of commonly found interferences. This property is highly useful for constructing a working device for explosive vapor detection in presence of interfering agents. Pyrene containing PIL showed generally higher fluorescence quenching than the anthracene containing PIL, reflecting an improved affinity of the more electron-rich pyrene with NACs. Furthermore, fluorescence intensity could be recovered after the quenching, enabling the reuse of these films for NACs detection. The results suggest that both PILs are potential candidates for NACs sensing in presence of potential interferents of different nature.

Chapter 6

Effect of bulky anions on physical and gas permeation properties of PILs based on PBI

6.1 Introduction

The literature reports on polymeric ionic liquids (PILs) for studying CO_2 sorption properties is mostly focused on anions such as BF_4, Tf_2N and PF_6, dca, OTf, and SbF_6 [Bara (2008b)]. The previous work from our laboratory dealt with poly(diallyldimethylammonium chloride) wherein effect of systematic variation of anions categorized into carboxylates, sulphonates and inorganic type was investigated [Bhavsar (2012)]. Recently, Tomé *et al.* reported use of pyrrolidinium-PILs with cyano anions to prepare high performance PIL–IL composite membranes for post-combustion flue gas treatment (CO_2/N_2 separation) [Tome (2015)]. All these studies indicated the strong dependence of anion on CO_2 sorption-permeation properties.

In the present work, we have chosen five different anions, which are bulky in nature and are substituted analogues of BF_4^- anion. The BF_4^- anion is well known to offer better CO_2 sorption-permeation properties than other anions [Tang (2005b), Bhavsar (2014b)]. PBI based PIL [DBzDMPBI-BuI][I] investigated in chapter 4 was chosen for the present work. Its iodide anion was exchanged with the chosen bulky anions. The structures of these anions are given in Chapter 3. The obtained PILs were characterized by requisite physical properties. The effect of systematic structural variation of bulk of anions on gas sorption-permeation properties was studied for the first time.

6.2. Synthesis of PILs and their characterizations

Synthesis of parent PIL [DBzDMPBI-BuI][I] is described in Chapter 3 and its characterization by IR, NMR is given in chapter 4. An exchange of iodide anion from above PILs was performed using potassium or sodium salt of chosen anions in DMF. This solvent was chosen owing to good solubility of the parent PIL as well as chosen salts in it. The formed byproduct (KI or NaI) was separated from the polymer by

precipitating the reaction mixture in water followed by repeated water wash in order to remove the salt. Analysis of iodide (if remained unexchanged) in these 'anion exchanged' PILs was performed by Volhard's method. The extent of iodide exchanged was appreciable (80 to 85%). FTIR spectra (Fig. 6.1) showed appearance of new bands attributable to the respective anion. PILs possessing anions with B-F bond showed stretching vibration at ~1080 cm^{-1} [Suarez (1996)]. Bands in the range of 1440 and 1430 cm^{-1} are attributable to B-Aryl bond [Bellamy (1958)].

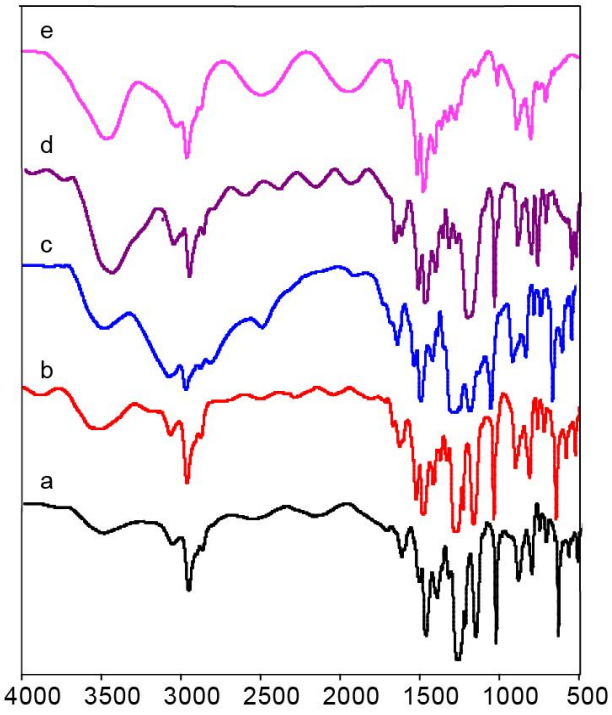

Fig. 6.1. IR spectra of PILs (a: [DBzDMPBI-BuI][$(CH_3)_3$C-Ph-BF_3],b: [DBzDMPBI-BuI][$(CF_3)_2$Ph-BF_3], c:[DBzDMPBI-BuI][Im_4B], d: [DBzDMPBI-BuI][Ph_4B], e: [DBzDMPBI-BuI][$(CF_3)_8Ph_4B$].

6.3. Physical properties

6.3.1 Solvent solubility, WAXD analysis and density

PILs based on all five anions exhibited good solvent solubility (Table 6.1) and thus easy processability. PILs with iodide anion were soluble in acetonitrile, in addition to the high boiling solvents such as DMF and NMP. The solubility of PILs was further enhanced when the iodide anion was exchanged by requisite anion. For example, all PILs

with chosen anions became soluble even in acetone and methanol at the ambient temperature, which are usually non-solvents for many of the aromatic polymers. Such improvement in the solubility of polybenzimidazole based PILs can be attributed to the presence of ionic character as well as the bulky anions used. The latter would disturb the chain packing in the polymer matrix, contributing to the enhancement in solvent solubility.

Table 6.1. Solubility of PILs in various solvents

PILs	DMF	DMSO	DMAc	NMP	Acetone	CH_3CN	MeOH
[DBzDMPBI-BuI][$(CH_3)_3$C-Ph-BF_3]	+	+	+	+	+	+	+
[DBzDMPBI-BuI][$(CF_3)_2$Ph-BF_3]	+	+	+	+	+	+	+
[DBzDMPBI-BuI][Im_4B]	+	+	+	+	+	+	+
[DBzDMPBI-BuI][Ph_4B]	+	+	+	+	+	+	+
[DBzDMPBI-BuI][$(CF_3)_8Ph_4B$]	+	+	+	+	+	+	+
[DBzDMPBI-BuI][I][a]	+	+	+	+	−	+	±

+: Soluble at room temperature; ±: partially soluble or swelling after heating at 80 ºC;
−: insoluble.

WAXD patterns of these PILs indicated their amorphous nature (Fig. 6.2). An average intersegmental *d*-spacing (d_{sp}) of PILs as obtained from the amorphous peak maxima are given in Table 6.2. The d_{sp} value for all PILs (with the exception of [DBzDMPBI-BuI][Im_4B]) was higher than that of the base case, viz., [DBzDMPBI-BuI][I]. Generally, it is increased with the size of anion. The order of variation in d_{sp} of PILs with the chosen anions was Im_4B^- < I^- < $(CH_3)_3$C-Ph-BF_3^-< $(CF_3)_2$Ph-BF_3^- < Ph_4B^- < $(CF_3)_8Ph_4B^-$. In case of Im_4B^- anion, the intermolecular forces between imidazole ring of the anion and PBI could have increased the chain packing in polymer matrix resulting in lowering of the d_{sp} of the corresponding PIL. This showed that bulk of the anion as well its chemical interaction with polymer had contribution in governing the chain packing in PIL matrix.

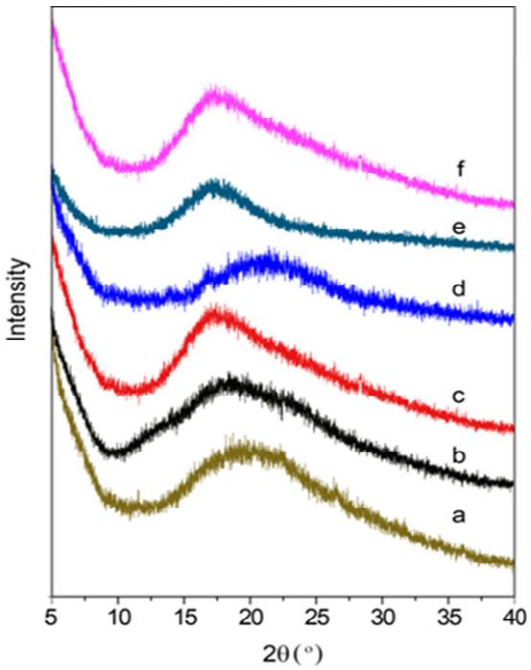

Fig. 6.2. WAXD spectra of PILs (a: [DBzDMPBI-BuI][I], b: [DBzDMPBI-BuI][$(CH_3)_3$C-Ph-BF_3],c: [DBzDMPBI-BuI][$(CF_3)_2$Ph-BF_3],d:[DBzDMPBI-BuI][Im_4B], e: [DBzDMPBI-BuI][Ph_4B] f: [DBzDMPBI-BuI][$(CF_3)_8Ph_4B$].

Table 6.2. Physical properties of PILs

PILs	Iodide exchange [a] (mol %)	d_{sp} [b] (Å)	ρ [c] (g/cm^3)	TGA analysis		T_g [f]
				IDT[d](°C)	W_{900} [e] (%)	
[DBzDMPBI-BuI][$(CH_3)_3$C-Ph-BF_3]	85	5.10	1.159	384	44	217
[DBzDMPBI-BuI][$(CF_3)_2$Ph-BF_3]	86	5.28	1.190	430	53	ND
[DBzDMPBI-BuI][Im_4B]	90	4.96	1.304	213	41	ND
[DBzDMPBI-BuI][Ph_4B]	85	5.22	1.093	335	34	237
[DBzDMPBI-BuI][$(CF_3)_8Ph_4B$]	82	5.35	1.028	373	46	277
[DBzDMPBI-BuI][I][f]	0	5.04	1.199	205	35	ND

[a]: Determined by Volhard's method, [b]: d-spacing obtained from WAXD, [c]: density measured at 35 ºC, [d]: initial decomposition temperature, [e]: char yield at 900°C, [f]: Glass transition temperature obtained from dynamic mechanical analysis, [g]: Data taken from chapter 4., ND: could not be observed.

Density of PILs is given in Table 6.2. The bulk of anion hold by the PIL seems to govern its density. The density of PILs decreased in the order of $Im_4B^- > I^- > (CH_3)_3$ C-

$Ph\text{-}BF_3^-$ > $(CF_3)_2Ph\text{-}BF_3^-$ > Ph_4B^- > $(CF_3)_8Ph_4B^-$. The order was almost opposite to that observed in case of variation in d_{sp} of these PILs while changing the anion. In other words, both the finding indicated that bulk of anions disturbed the chain packing which led to lowering in the density and increase in d_{sp}. It may be noted that present PILs except PIL possessing Im_4B^- anion showed lower density as compared to the PILs based on same PBI backbone but different anion as investigated in chapters 4 and 5. The lowering in density is better obeyed by PILs with tetra-aryl substituted boron containing anions. This analysis indicated role of both, the bulk of anion and its interaction with polymer in governing chain packing in PILs.

6.3.2. Thermal stability of PILs

Initial degradation temperature (IDT) of present PILs is given in Table 6.2 and TG curves are shown in Fig. 6.3. Thermal stability of present PILs was higher than their parent PIL with iodide as anion, in spite of their bulky nature. It was highest for $[(CF_3)_2Ph\text{-}BF_3]$ anion. Thermal stability of ionic liquids is known to increase with decreasing basicity of anion [MacFarlane (2006)]. Lower basicity of $[(CF_3)_2Ph\text{-}BF_3]$ anion could be due to presence of electron withdrawing –F atoms and aryl groups on boron and may be a reason for higher thermal stability of the PIL.

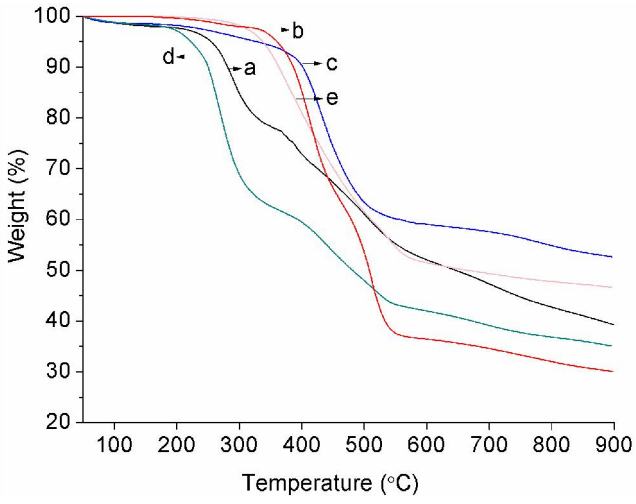

Fig. 6.3. TG curves of PILs (a: [DBzDMPBI-BuI][$(CH_3)_3C$-Ph-BF_3],b: [DBzDMPBI-BuI][$(CF_3)_2Ph\text{-}BF_3$],c:[DBzDMPBI-BuI][Im_4B], d: [DBzDMPBI-BuI][Ph_4B], e: [DBzDMPBI-BuI][$(CF_3)_8Ph_4B$].

The dynamic mechanical analysis (DMA) of PILs was performed and some of the PILs exhibited tan δ transition, as shown in Fig. 6.4. This transition is usually ascribed to the chain segmental motions, i.e. T_g. High T_g values of these PILs establish their glassy nature. For some of the PILs, tanδ could not be observed. It may be possible that their T_g is beyond their degradation temperature.

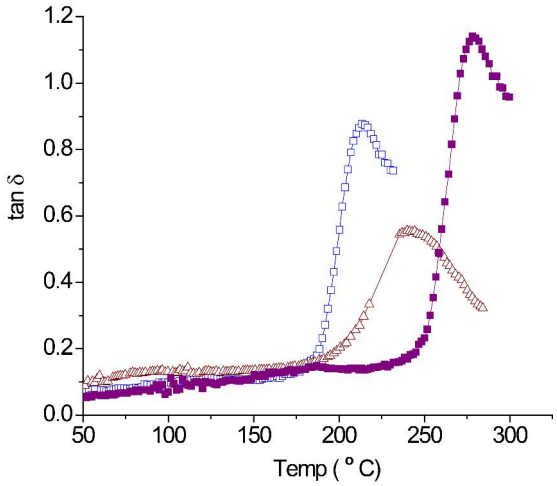

Fig. 6.4 DMA curves (tan δ) of PILs as function of temperature (□: [DBzDMPBI-BuI][$(CH_3)_3$C-Ph-BF_3], △: [DBzDMPBI-BuI][Ph_4B], ■: [DBzDMPBI-BuI][$(CF_3)_8Ph_4B$].

6.4 Gas sorption properties

6.4.1 Sorption parameters

Equilibrium sorption isotherms of H_2, N_2, CH_4 and CO_2 in present PILs exhibited typical dual-mode nature (Fig. 6.5). The gas sorption parameters (k_D, b and C'_H) are given in Table 6.3. It could be seen that Henry's solubility coefficient, k_D which is ascribed to the gas dissolution in rubbery state for all gases was considerably lower than C'_H. This behavior is attributable to the glassy nature of PILs. In all PILs, C'_H was higher for CO_2 than that of other gases. This is in accordance with the gas sorption behavior observed for most of the common glassy polymers, including PILs [Bhavasar (2014b), Kumbharkar (2006), Kanehashi (2005), Barbari (1989)]; possessing higher C'_H for CO_2 than that for other gases owing to the higher condensability of this gas [McHattie (1992)]. This parameter was negligible for H_2 and N_2 in comparison to CO_2. The C'_H and b values of present PILs are lower than that of PIL with BF_4^- anion.

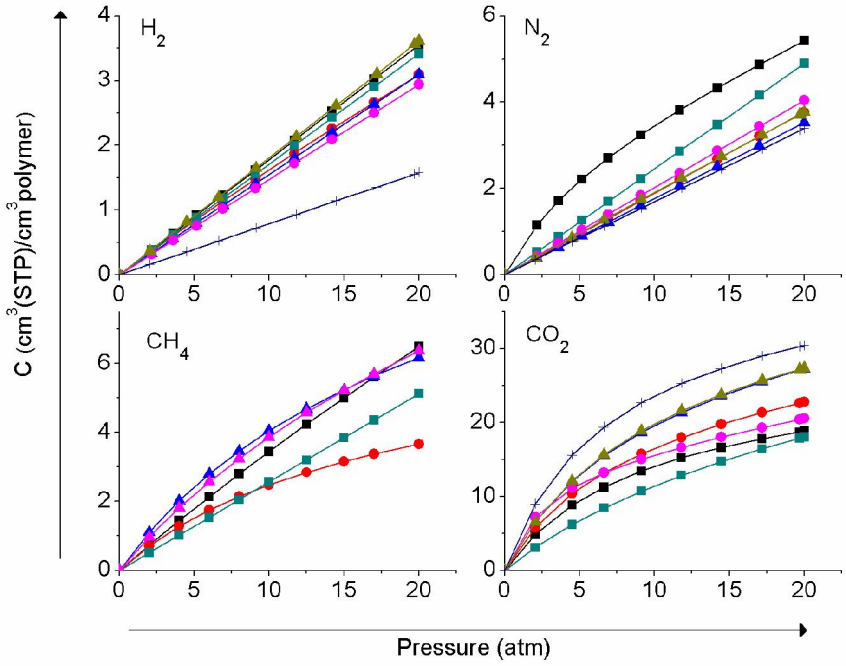

Fig. 6.5. Gas sorption isotherms of PILs at 35 ºC (▲: [DBzDMPBI-BuI][I], +: [DBzDMPBI-BuI][BF_4] ■: [DBzDMPBI-BuI][$(CH_3)_3$C-Ph-BF_3], ●: [DBzDMPBI-BuI][$(CF_3)_2$Ph-BF_3], ▲: [DBzDMPBI-BuI][Im_4B], ■: [DBzDMPBI-BuI][Ph_4B], ●: [DBzDMPBI-BuI][$(CF_3)_8Ph_4B$].

6.4.2 Sorption coefficients

Table 6.4 presents the solubility coefficient (S) and solubility selectivity (S_A/S_B) for different PILs at 20 atm. The solubility coefficient for different gases in all PILs at 20 atm increased in the order: $H_2 < N_2 < CH_4 < CO_2$ as discussed in earlier chapters. CO_2 sorption coefficient in PILs generally increased in the order of anion variation as $BF_4^- > Im_4B^- > I^- > (CF_3)_2$Ph-$BF_3^- > (CH_3)_3$C-Ph-$BF_3^- > (CF_3)_8Ph_4B^- > Ph_4B^-$. This indicates that the specific interaction of anion with CO_2 plays a primary role in governing its sorption while the bulk on anion plays a secondary role. This led to lowering of S_{CO_2}/S_{H_2}, S_{CO_2}/S_{N_2} and S_{CO_2}/S_{CH_4} sorption selectivity in present PILs than the PIL possessing BF_4^- anion. It may be recalled that PILs with BF_4^- anion also exhibited higher C'_H than for those PILs with present anions. This indicated that BF_4^- is a better anion for obtaining preferential CO_2 sorption in PILs. In case of other gases, solubility coefficient was increased with the bulk of anion.

Table 6.3. Dual-mode sorption parameters[a] obtained during gas sorption in PILs

PILs	H_2			N_2			CH_4			CO_2		
	k_D	C'_H	B	k_D	C'_H	B	k_D	C'_H	b	k_D	C'_H	b
[DBzDMPBI-BuI][$(CH_3)_3$C-Ph-BF_3]	0.15	1.74	$4.2x10^{-4}$	0.17	1.90	0.01	0.16	2.93	0.178	0.22	25.40	0.13
[DBzDMPBI-BuI][$(CF_3)_2$Ph-BF_3]	0.15	1.35	$7.0x10^{-5}$	0.19	3.59	1.64×10^{-5}	0.17	3.99	2.74×10^{-5}	0.09	23.92	0.11
[DBzDMPBI-BuI][Im_4B]	0.17	1.61	1.7×10^{-5}	0.18	0.96	2.62×10^{-4}	0.24	4.21	0.032	0.20	33.60	0.20
[DBzDMPBI-BuI][Ph_4B]	0.14	1.35	1.4×10^{-5}	0.24	0.56	1.48×10^{-4}	0.02	5.74	0.066	0.40	14.62	0.25
[DBzDMPBI-BuI][$(CF_3)_8Ph_4B$]	0.18	1.80	$5.0 x10^{-4}$	0.20	2.49	$9.38 x10^{-5}$	0.04	9.95	0.057	0.20	26.50	0.06
[DBzDMPBI-BuI][I][b]	0.15	1.74	$4.2x10^{-4}$	0.07	1.54	0.27	ND	ND	ND	0.05	34.90	0.14
[DBzDMPBI-BuI][BF_4][b]	0.08	1.63	$3.5x10^{-5}$	0.17	3.99	$2.7x10^{-5}$	ND	ND	ND	0.10	38.29	0.15

[a]: k_D is expressed in cm^3(STP)/cm^3polymer.atm, C'_H is expressed in cm^3(STP)/cm^3polymer, while b is expressed in atm^{-1}, [b]: Data taken from chapter 4.

Table 6.4. Solubility coefficient (S)[a] and solubility selectivity (S_A/S_B) of PILs at 20 atm

PILs	S_{H_2}	S_{N_2}	S_{CH_4}	S_{CO_2}	S_{N_2}/S_{CH_4}	S_{CO_2}/S_{H_2}	S_{CO_2}/S_{N_2}	S_{CO_2}/S_{CH_4}
[DBzDMPBI-BuI][$(CH_3)_3$C-Ph-BF_3]	0.15	0.17	0.33	1.03	0.52	6.86	6.05	3.16
[DBzDMPBI-BuI][$(CF_3)_2$Ph-BF_3]	0.13	0.17	0.25	1.11	0.66	8.49	6.68	4.43
[DBzDMPBI-BuI][Im_4B]	0.11	0.15	0.24	1.14	0.63	10.35	7.45	4.66
[DBzDMPBI-BuI][Ph_4B]	0.15	0.19	0.39	0.90	0.48	6.09	4.88	2.34
[DBzDMPBI-BuI][$(CF_3)_8Ph_4B$]	0.10	0.14	0.25	0.94	0.58	9.71	6.55	3.82
[DBzDMPBI-BuI][I][b]	0.18	0.19	ND	1.37	ND	9.6	7.2	ND
[DBzDMPBI-BuI][BF_4][b]	0.08	0.17	ND	1.52	ND	19.2	9.0	ND

[a]: Expressed in cm^3 (STP)/cm^3polymer.atm, [b]: Data taken from chapter 4.

6.5 Gas permeation properties

Permeation analysis of only three PILs could be carried out as PILs with $(CF_3)_8Ph_4B^-$ and Ph_4B^- anions led to brittle films and could not withstand with the applied pressure. The pure gas permeability for He, H_2, N_2, CH_4 and CO_2 and ideal selectivity data for various gas pairs of the three PILs with $Im4B^-$, $(CF_3)_2Ph\text{-}BF_3^-$ and $(CH_3)_3C\text{-}Ph\text{-}BF_3^-$anions are given in Table 6.5. A large variation in the gas permeability of PILs with the variation in bulk and nature of anion was observed.

Table 6.5. Permeability coefficient (P)[a] and permselectivity (P_A/P_B) of PILs

PILs	P_{He}	P_{H_2}	P_{N_2}	P_{CH_4}	P_{CO_2}	P_{He}/P_{N_2}	P_{H_2}/P_{N_2}	P_{H_2}/P_{CO_2}	P_{CO_2}/P_{N_2}	P_{CO_2}/P_{CH_4}
[DBzDMPBI-BuI] [$(CH_3)_3C\text{-}Ph\text{-}BF_3$]	24.6	24.0	1.09	0.78	22.6	22.6	22.0	1.06	20.7	28.9
[DBzDMPBI-BuI] [$(CF_3)_2Ph\text{-}BF_3$]	51.8	51.0	2.40	1.65	34.9	21.6	21.3	1.46	14.5	21.2
[DBzDMPBI-BuI] [Im_4B]	15.7	15.6	0.65	0.51	17.9	24.2	24.0	0.87	27.5	35.1
[DBzDMPBI-BuI] [I][b]	12.6	10.7	0.51	ND	11.3	24.7	21.0	0.95	22.2	ND
[DBzDMPBI-BuI] [BF_4][b]	16.4	16.3	0.61	ND	18.7	26.9	26.7	0.87	30.7	ND

[a]: Determined at 20 atm upstream pressure, expressed in Barrer (1 Barrer = 10^{-10} cm^3 (STP).cm/cm^2.s.cm Hg), [b]: Data taken from chapter 4

In case of all three PILs, increase in permeability for all gases was observed than tht of precursor PIL, viz., [DBzDMPBI-BuI][I]. An extent of increase in permeability was dependent on the anion they hold. The order of increase in permeability in PILs with the variation in anion was: $Im_4B^- < I^- < BF_4 < (CH_3)_3C\text{-}Ph\text{-}BF_3^- < (CF_3)_2Ph\text{-}BF_3^-$. The maximum increase in permeability was 5 times for H_2 and 3 times for CO_2 for PIL containing $(CF_3)_2Ph\text{-}BF_3^-$ anion, than the precursor PIL with I^- anion (Fig 6.6). Similar increase with respect to BF_4^- anion containing PIL was 3 times for H_2 and 2 times for CO_2. This could be correlated to the bulk of this anion, which governs the chain packing as evidenced from the WAXD and density analysis. The higher d_{sp} and lower density of

PILs possessing $(CH_3)_3C$-Ph-BF_3^- and $(CF_3)_2$Ph-BF_3^- was an indication of looser chain packing in their matrix.

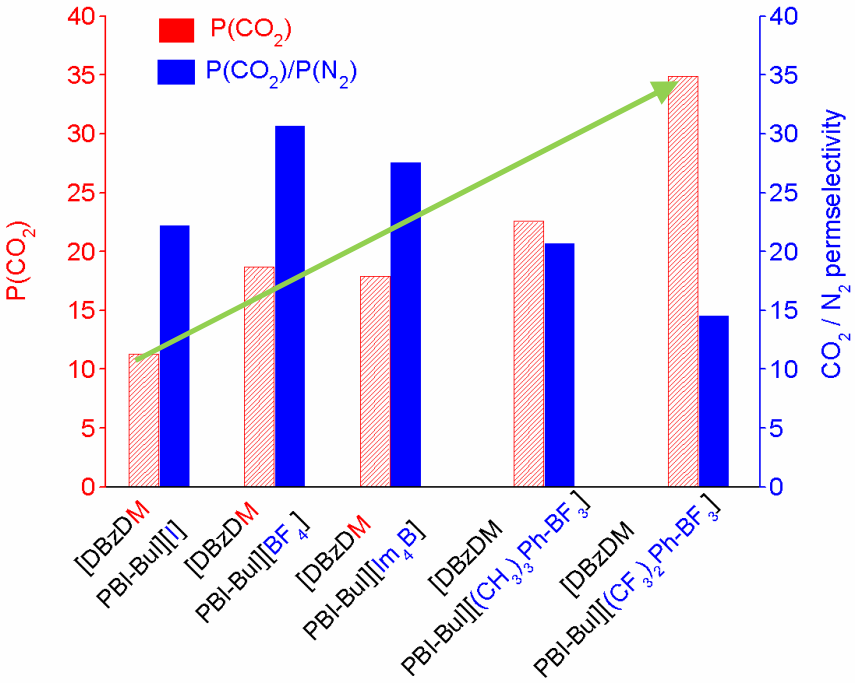

Fig. 6.6. CO_2 permeability and permselectivities of PBI based reported and present PILs.

Fig. 6.7 shows the variation of H_2 and CO_2 permeability as a function of d_{sp}. It was observed that the permeability for both gases increased with the d_{sp}. This was also supported by higher diffusivity coefficients of these anion containing PILs than their counterparts (Table 6.6). For example PIL with $(CF_3)_2$Ph-BF_3^- anion showed 8 times increase in the diffusivity coefficients for H_2 and 3 times for CO_2 in PIL containing $(CF_3)_2$Ph-BF_3^- anion than the precursor PIL possessing I^- anion. The increase in permeability of these PILs was associated with some drop in the selectivity. Among the three anions, Im_4B^- anion containing PIL showed higher selectivity for light gases as well as for CO_2. The He/N_2 and H_2/N_2 selectivities decreased in order of variation of anions as, $Im_4B^- > I^- >$ $(CH_3)_3C$-Ph-BF_3^- > $(CF_3)_2$Ph-BF_3^-. Although permeability measurements for PILs containing $(CF_3)_8Ph_4B^-$ and Ph_4B^- anions could not be made

possible due to their brittle nature, based on the available data on d_{sp} and density it is reasonable to presume that these PILs would have possessed high permeability.

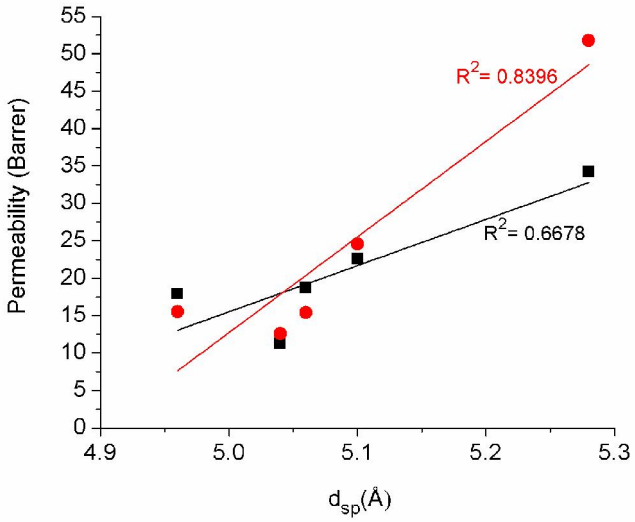

Fig. 6.7. Variation in CO_2 (■) and H_2 (●) permeability with d_{sp} of present PILs.

Table 6.6. Diffusivity coefficient (D)[a] of gases in PILs and diffusivity selectivity (D_A/D_B) estimated at 20 atm.

PILs	D_{H_2}	D_{N_2}	D_{CH_4}	D_{CO_2}	D_{H_2}/D_{N_2}	D_{H_2}/D_{CO_2}	D_{N_2}/D_{CH_4}	D_{CO_2}/D_{N_2}	D_{CO_2}/D_{CH_4}
[DBzDMPBI-BuI] [$(CH_3)_3$C-Ph-BF_3]	302.3	9.5	4.5	27.1	31.8	11.1	2.1	2.9	6.1
[DBzDMPBI-BuI] [$(CF_3)_2$Ph-BF_3]	379.3	15.3	7.3	31.5	24.8	12.0	2.1	2.1	4.3
[DBzDMPBI-BuI] [Im_4B]	117.0	3.7	1.2	10.4	31.9	11.2	3.1	2.8	8.7
[DBzDMPBI-BuI] [I][b]	45.2	2.0	ND	6.3	22.6	7.17	ND	3.1	ND
[DBzDMPBI-BuI] [BF_4][b]	154.9	2.7	ND	9.3	57.7	14.21	ND	3.5	ND

[a]: Expressed in 10^{-8} $cm^2 \cdot S^{-1}$, [b]: Data taken from chapter 4

6.6 Conclusions

PBI based PILs with new bulky anions were synthesized with high yield of anion exchange. All PILs showed enhanced solvent solubility in common low boiling organic

solvents such as acetone, acetonitrile, and methanol; an attractive feature towards their easy processability. In addition to their amorphous nature, these PILs showed higher d_{sp} and lower density than their precursor PIL. The thermal stability of present PILs was higher than that of the precursor PIL. For present PILs, CO_2 sorption generally increased in the order of anion variation as Im_4B^-> $(CF_3)_2Ph\text{-}BF_3^-$ > $(CH_3)_3C\text{-}Ph\text{-}BF_3^-$> $(CF_3)_8Ph_4B^-$ > Ph_4B^-. The solubility coefficients were lower than their unsubstituted fluorinated anion BF_4^-. Permeation analysis of only three PILs could be carried out as PILs with $(CF_3)_8Ph_4B^-$ and Ph_4B^- formed brittle films and could not withstand with the applied pressure. The maximum increase in permeability was 5 times for H_2 and 3 times for CO_2 for PIL containing $(CF_3)_2Ph\text{-}BF_3^-$ anion than the precursor PIL with I^- anion. This was also supported by higher diffusivity coefficients of these anion containing PILs than their counterparts.

Chapter 7

PBI based Polymeric ionic liquid (PIL) membranes for separation of olefin/paraffin

7.1 Introduction

The transport of gases in dense polymeric films can be described by the solution–diffusion model [Wijmans (1995)]. The variations in diffusivity and solubility of individual gases from their mixture determine the separation factor which is an intrinsic property of the polymer. In order to obtain sufficiently high gas permeance, the polymer membrane thickness should be as low as possible. On the other hand, low membrane thickness causes poor mechanical stability and/or membrane handling difficulties. These issues could be overcome by using composite membranes consisting of a thin selective dense layer supported on a microporous layer [GE USP 3874986, Peter (2009)].

The potential of supported ionic liquid membranes for propane-propylene separation is reported in the literature. Higher sorption of propylene over propane was observed by Lee et al. [Lee (2012)]. In case of polymeric ionic liquid (poly([pyr][NTf_2]), gas permeation properties for ethane/ethylene were investigated [Tome (2014)], which showed maximum permselectivity of 2.93 for this pair. Polymer–ionic liquid composite membranes for propane/propylene separation by facilitated transport were also evaluated by Fallanza *et al.* [Fallanza (2013)]. To the best of our knowledge, viability of PIL membranes for propane/propylene separation has not been explored.

The present work investigates gas permeance and selectivity of TFC membranes prepared using polysulfone (PSF) based ultrafiltration (UF) membrane as a structural support and polymeric ionic liquid (PIL) as a selective layer. PIL, [DBzDMPBI-BuI][BF_4] was selected to prepare TFC membranes due to its better intrinsic permeation properties and solubility in low boiling organic solvents (Chapter 4). Effects of concentration of dope solution used to cast porous PSF support and concentration of the coating solution were evaluated by analyzing pure and mixed gas permeance and selectivity of different gas pairs in the formed TFC membranes. To the best of our

knowledge, this is the first attempt concerning investigations on the permeation properties of TFC membranes with the PIL as a selective layer.

7.2. Dense membrane properties

The sorption characteristics for H_2, N_2 and CO_2 in present PIL are discussed in chapter 4. The gas sorption data for CH_4, C_2H_4, C_2H_6, C_3H_6 and C_3H_8 is presented in this chapter. The sorption isotherms of these gases in PIL as shown in Fig. 7.1 exhibited typical dual-mode nature, as usually observed for glassy polymers [Bhavsar (2014b), Kumbharkar (2006), Koros (1976)]. The gas sorption parameters (k_D, b and C'_H) are given in Table 7.1. It could be seen that Henry's solubility coefficient, k_D (ascribed to the gas dissolution in rubbery state) for all gases was considerably lower than that of C'_H. This behavior is attributable to the glassy nature of PILs. The C'_H is considered as the hole-filling constant in the glassy state, which was slightly higher for C_2H_4 and C_3H_6 than C_2H_6 and C_3H_8, respectively, due to the fact that they are more condensable and compact, therefore can access the microvoids more readily.

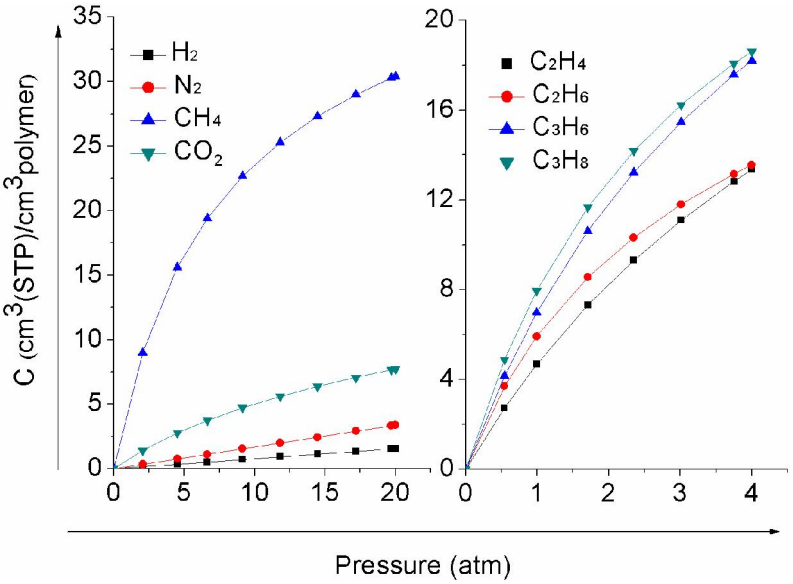

Fig. 7.1. Gas sorption isotherms of PIL at 35 ºC

Table 7.2 presents the solubility coefficient (S) and solubility selectivity (S_A/S_B) for different PILs. The solubility coefficient for different gases in all PILs increased in

the order: H_2 [*Chapter 4*] < N_2 [*Chapter 4*] < CH_4 < CO_2 [*Chapter 4*] < C_2H_4< C_2H_6 < C_3H_6 < C_3H_8; which followed the order of increasing inherent condensability of these gases as shown in Fig 7.2 [Bhavsar (2014a), Li (2009)]. The solubility coefficient show minimal differences in the concentrations of C_2H_4 and C_2H_6 as well as C_3H_6 and C_3H_8 in the PIL. The C_2H_4 and C_3H_6 were sorbed slightly more than that of C_2H_6 and C_3H_8. This results in solubility selectivities of close to one, which is in good agreement with the previous literature report [Swaidan (2015a,b)]. Therefore, the separation of C_2H_4 from C_2H_6 and C_3H_6 from C_3H_8 is expected to be essentially diffusion-based.

Table 7.1. Dual-mode sorption parameters[a] for PILs

Gas	k_D	C'_H	b
C_2H_4	0.290955	30.23	0.169
C_2H_6	0.266185	28.81	0.410
C_3H_6	0.20296	36.17	0.231
C_3H_8	0.072314	32.77	0.314

[a:] k_D is expressed in cm^3(STP).cm^{-3}polymer.atm, C'_H is expressed in cm^3(STP).cm^{-3} polymer, while b is expressed in atm^{-1}

Table 7.2. Sorption, permeation and diffusion properties of [DBzDMPBI-BuI][BF_4]

Gas	Solubility coefficient (S) and solubility selectivity	Permeability coefficient (P^b) and permselectivity	Diffusivity coefficient (D^d) and diffusivity selectivity
CH_4[c]	0.38	0.46	1.56
C_2H_4	3.34	2.03	4.61
C_2H_6	3.39	0.5	1.12
C_3H_6	4.55	0.31	0.05
C_3H_8	4.65	ND	ND
$\alpha(CO_2/CH_4)$	3.94	40.09	5.99
$\alpha(C_2H_4/C_2H_6)$	0.98	4.06	4.12
$\alpha(C_3H_6/C_3H_8)$	1.02	ND	ND

[a:] Expressed in cm^3 (STP).cm^{-3}polymer.atm, [b]: determined at 4 atm upstream pressure, [c]: determined at 20 atm upstream pressure, expressed in Barrer (1 Barrer = 10^{-10} cm^3 (STP).cm.cm^{-2}.s.cm Hg, [d:] expressed in 10^{-8} $cm^{2.}$ S^{-1}, ND: could not be determined.

The permeation characteristics for He, H_2, N_2 and CO_2 in dense membrane of PIL [DBzDMPBI-BuI][BF_4] were discussed in Chapter 4. The permeation analysis for CH_4,

C_2H_4, C_2H_6, C_3H_6 and C_3H_8 is presented in this chapter (Table 7.2). The diffusivity analysis shows that for given gases diffusivity coefficient decreased with the critical volume of gas, which is anticipated in case of glassy polymers (Fig. 7.3).

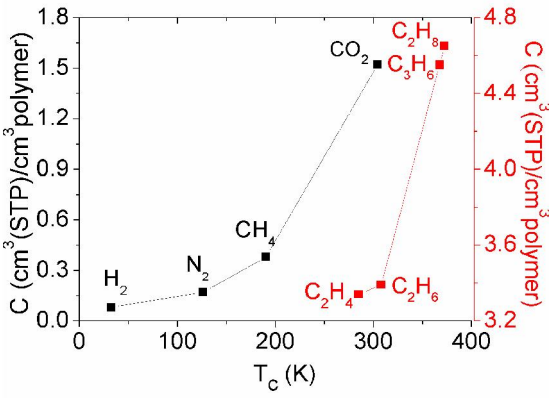

Fig. 7.2. Solubility coefficients of different gases in PIL [DBzDMPBI-BuI][BF_4] as a function of critical temperatures (T_c) of gases

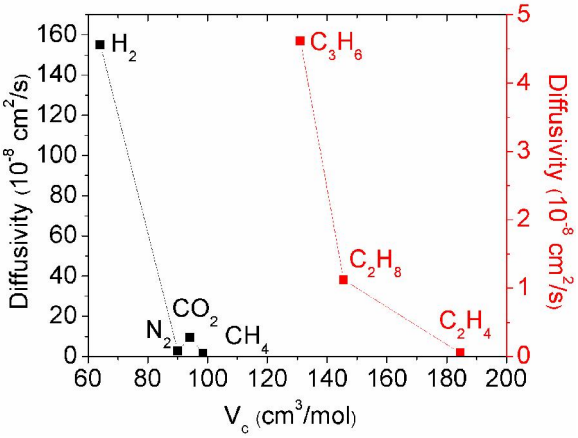

Fig. 7.3. Diffusivity of different gases in PIL as a function of critical volume (V_c) of gases.

It is seen from Table 7.2 that for ethane-ethylene, permselectivity is 4.06. The permselectivity is clearly diffusion based, as the estimated diffusivity selectivity for the same pair was 4.12. The permselectivity for propane-propylene could not be determined due to very low flux of propane gas. Thus the preparation of TFC membrane was anticipated to offer a measurable flux in the case of low permeating propane. Following sections are devoted on analysis with the TFC membranes.

7.3. UF membrane properties

Selection of a porous support is crucial for the preparation of durable and effective thin film composite (TFC) membrane. PSF based UF membranes were prepared by phase inversion method with water as the non-solvent. The membranes PSF_{22} and $PSF_{20,}$ where, the suffix denotes the concentration of polymer in the dope solution. These UF membranes exhibited average water flux of 36 and 12 $l.m^{-2}.h^{-1}$, respectively and ~ 90% rejection of PEG of MW 33 kDa and 10 kDa, respectively (Table 7.3). The gas permeance of support PSF membranes was taken for He and N_2 which was in the range of 1700-2400 GPU indicating typical ultrafiltration membrane properties

Table 7.3. Characteristics of UF membranes

UF membrane	Water flux ($l.m^{-2}.h^{-1}$)	MW of PEG with rejection of 90%	Permeance[a]	
			He	N_2
PSF_{20}	35.9	33.7 kDa	2372	2008
PSF_{22}	12.2	10.0 kDa	2167	1700

[a] Expressed in GPU (1GPU = 1×10^{-6} cm^3(STP).($cm^{-2}.s^{-1}.cm^{-1}$.Hg)

7.4. Properties of thin film composite (TFC) membranes

The formation of defect-free TFC membranes based on PIL was evaluated by comparing their permselectivity with the 'intrinsic permselectivity' of the dense membrane. The reduction in effective membrane thickness and acceptable membrane stability against applied pressure was the basis for making TFC membranes.

7.4.1 Effect of UF support properties on gas permeance of TFC membrane

The variation of permeance and selectivity of TFC membranes prepared using two different UF supports and concentrations of PIL coating solution are tabulated in Table 7.4 and Tables 7.5. The permeance of TFC membranes with PSF_{20} support was higher than that of PSF_{22}, which was accompanied with some drop in the selectivity. This was also the order of decreasing water and gas flux, as revealed by UF membrane analysis (Table 7.3).

Table 7.4. Permeance (P)[a] selectivity of TFC membranes (dip time = 30 sec) prepared with PSF based UF supports.

TFC membrane	P_{H_2}	P_{N_2}	P_{CH_4}	P_{CO_2}	$P_{C_2H_4}$	$P_{C_2H_6}$	$P_{C_3H_6}$	$P_{C_3H_8}$
PSF_{20}-PIL_6	12.6	0.47	0.34	12.7	0.71	0.22	0.20	0.020
PSF_{20}-PIL_4	16.2	0.61	0.42	15.4	0.89	0.28	0.40	0.040
PSF_{22}-PIL_6	11.7	0.42	0.31	11.7	0.69	0.21	0.21	0.020
PSF_{22}-PIL_4	12.9	0.51	0.34	12.9	0.76	0.24	0.25	0.025

[a]: Expressed in GPU (1GPU = 1×10^{-6} $cm^3(STP).(cm^{-2}\ s^{-1}cm^{-1}$ Hg)

Table 7.5. Permselectivity of TFC membranes (dip time = 30 sec) prepared with PSF based UF supports.

P_{H_2}/P_{N_2}	P_{CO_2}/P_{N_2}	P_{CO_2}/P_{CH_4}	$P_{C_2H_4}/P_{C_2H_6}$	$P_{C_3H_6}/P_{C_3H_8}$
26.81	27.02	37.35	3.23	10.00
26.56	25.18	36.57	3.17	9.90
27.86	27.86	37.74	3.33	10.77
25.24	25.24	37.74	3.14	10.04

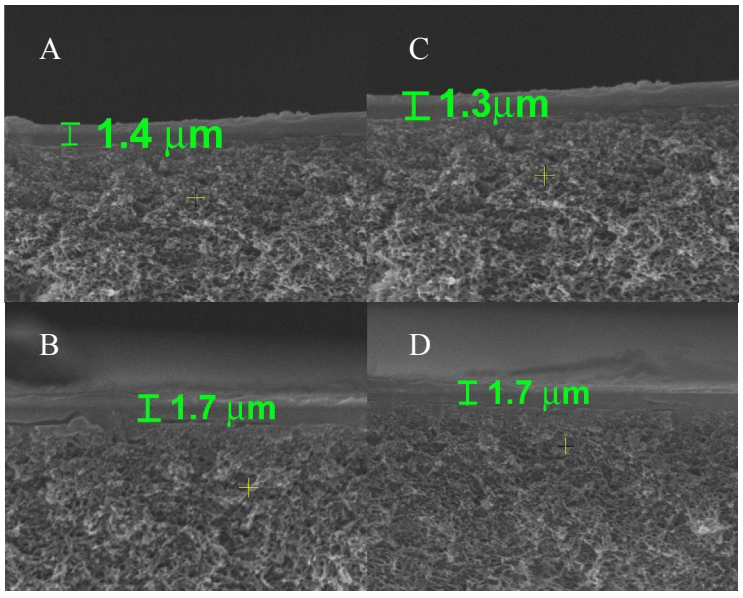

Fig. 7.4. SEM images of TFC membranes a: PSF_{20}-PIL_4, b: PSF_{20}-PIL_6, c: PSF_{22}-PIL_4, d: PSF_{22}-PIL_6

It is known that for UF support with lower molecular weight cut off (i.e. lower pore size) would lead to a lower pore intrusion by the coating solution and thus lower resistance to the gas flow and vice versa [Chung (1996)]. Also, this cannot be an independent phenomenon as polymer solution intrusion in pores of UF support need to be considered in conjugation with the concentration of polymer solution used for coating, as elaborated in the section 7.4.2.

7.4.2 Effect of coating solution concentration

The scanning electron microscope (SEM) images of the TFC membranes are as shown in Fig. 7.4. The higher thickness of coating layer was noticed for TFC membranes obtained with 6% coating solution concentration than that with 4%, as anticipated. This effective thickness accounts for both, the skin layer thickness as well as thickness due to intrusion of the polymer in the pores of the UF support. The permeation through the TFC membrane is inversely proportional to the resistance offered by the skin layer as well as the penetration of the polymer solution in the pores. The extent of pore penetration depends on the viscosity of the polymer solution, surface porosity and pore size of UF support. Higher the viscosity, lesser is the possibility of the solution penetration into the pores and visa versa. In view of hydrophobic nature of PSF and lower porosity, it seems unlikely that PIL with its ionic nature would penetrate deeper into the small pores of PSF support. Thus, an increase in effective layer thickness could be attributed to the increase in skin layer thickness, rather than originated from the pore penetration. As could be seen from Table 7.4 the permeace for all gases was higher in case of 4% coating solution concentration which was accompanied with some drop in selectivity. This could be ascribed to insufficient coating at the lower coating solution concentration.

Fig 7.5 shows the effect of porous support and coating layer concentration on permeance and permselectivity of C_2H_4, C_2H_6, C_3H_6, and C_3H_8. The maximum selectivity of 3.6 and 10.5 was observed for ethane-ethylene and propane-propylene gas pairs.

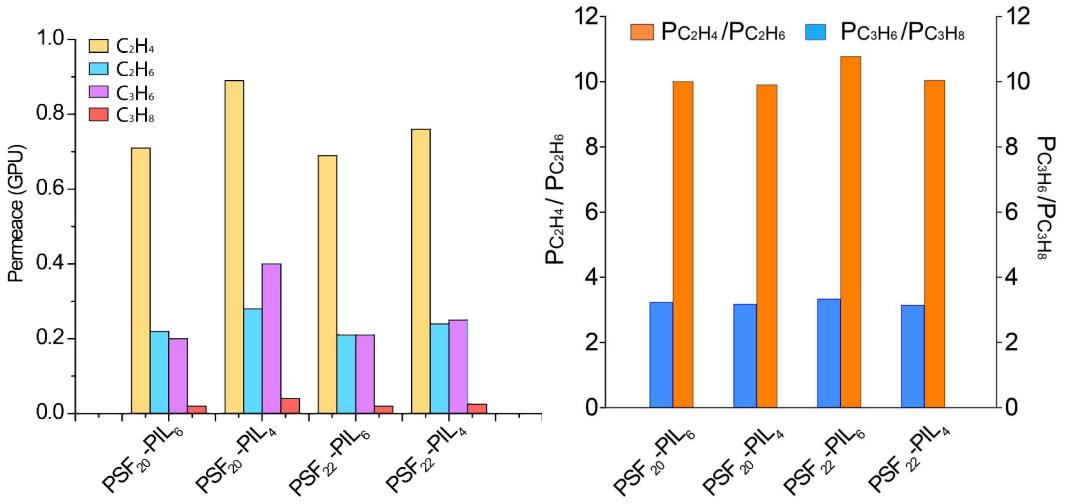

Fig. 7.5. Permeance and permselectivity of different gases in TFC membranes

The permeance of different gases could be correlated to their kinetic diameter as shown in Fig. 7.6 which could be attributed to the glassy nature of selective PIL layer and indicates that the permeation is diffusion based.

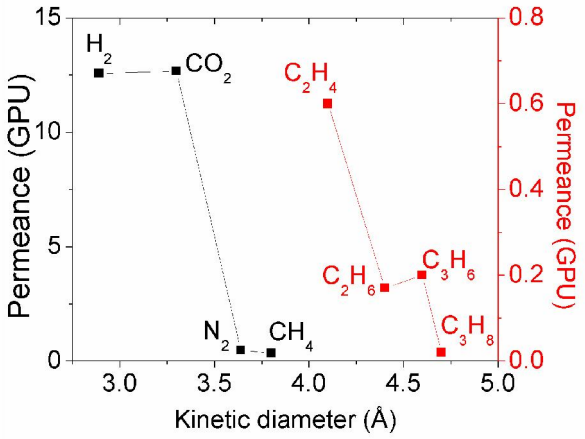

Fig. 7.6. Gas permeance of different gases in PIL as a function of kinetic diameters of gases

7.5 Mixed gas permeation analysis

Mixed gas permeability for CO_2/ CH_4 and C_3H_6/C_3H_8 were measured following the procedure described in the experimental section of Chapter 3. For both the pairs 50-

50 % (V/V) gas mixture was prepared. The selectivity of TFC membrane (PSF_{20}-PIL_4) for these gas pairs along with dense membranes are given in the Table 7.5

Table 7.5 Permselectivity of dense and TFC membranes

	P_{CO_2} / P_{CH_4}	$P_{C_3H_6} / P_{C_3H_8}$
Dense PIL[a]	25.4	6.8
PSF_{20}-PIL_4[a]	22.9	6.2

[a]: selectivity is measured for 50-50% (V/V) of CO_2-CH_4 and C_3H_6-C_3H_8

It is seen that in both the cases the mixed gas selectivity decreased almost by 40% as compared to single gas selectivity. In case of CO_2-CH_4 this could be due to the competitive sorption between two gases where CH_4 could have decreased CO_2 solubility in PIL matrix, leading to lowering in permselectivity. In case of C_3H_6-C_3H_8, since there is no solubility difference between two components, competitive diffusion between two gas components could be the reason for lowering in the selectivity.

The comparison of propane-propylene single gas permselectivity was done with common glassy polymers as shown in Fig. 7.7. It is seen that propane-propylene selectivity of present PIL was superior to common glassy polymers such as PPO, EC, CA and PSF, while it was comparable to Matrimid. These results suggest that with optimization of PIL selective layer in TFC membranes, PIL can be potential candidate in hydrocarbon separation.

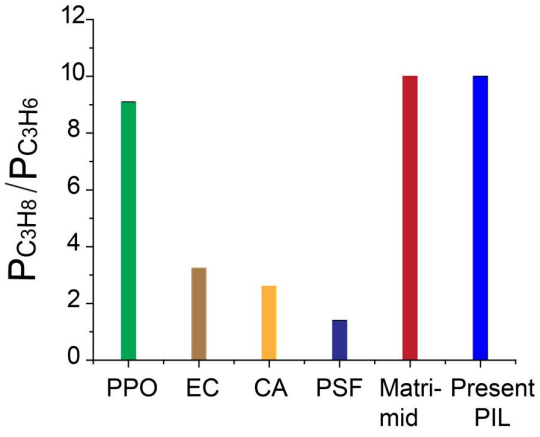

Fig. 7.7. Comparison with common glassy polymers.

7.6 Conclusions

The permeation properties of PIL dense as well as TFC membranes were studied for olefin/paraffin separations. PIL [DBzDMPBI-BuI][BF_4] was selected to prepare TFC membranes due to its better intrinsic permeation properties. The formation of defect free selective layer was confirmed by comparing selectivity data of light gases with that of dense membrane. The permeation characteristics of prepared TFC membrane for hydrocarbons such as C_2H_4, C_2H_6, C_3H_6 and C_3H_8 were studied. The effect of support layer porosity and concentration of coating layer were studied on the permeance of these membranes. The permeance of TFC membranes with PSF_{20} support was higher than that of PSF_{22} which was accompanied with some drop in the selectivity while the permeace for all gases was higher in case of 4% coating solution concentration with some drop in selectivity. The maximum selectivity of 3.6 and 10.5 was achieved for ethane-ethylene and propane-propylene gas pairs. Mix gas permselectivity measurements showed lowering in selectivity due to competitive sorption and diffusion of two components. The comparison of single gas propane-propylene permselectivity was done with common glassy polymers. It was observed that propane-propylene selectivity of present PIL was superior to common glassy polymers such as PPO, EC, CA and PSF, while it was comparable to Matrimid. These results suggest that with optimization of PIL selective layer (thickness minimization) in TFC membranes, PIL can be potential candidate in hydrocarbon separation.

Chapter 8

Conclusions

The present work deals with the investigations of PBI based polymeric ionic liquids (PILs) and their gas permeation properties. Effects of structural variation in their backbone, anion and *N*-substitution using various alkyl groups on physical and gas permeation properties were analyzed. Initially, PILs with substitution asymmetry were synthesized in two steps, *N*-substitution followed by *N*-quaternization of PBI-BuI and PBI-HFA. PILs were obtained in high yields, indicating almost quantitative substitution, which was further assessed by ^{1}H NMR and Volhard's analysis. This was followed by exchange of iodide with chosen anions (BF_4^-, Tf_2N^- and HFB^-). Most of these synthesized PILs exhibited enhanced solvent solubility in common low boiling organic solvents such as acetone, acetonitrile, and methanol; an attractive feature towards their easy processability into thin film / membrane form. As indicated by WAXD analysis, all these PILs exhibited an amorphous nature. In case of PILs with the *4-tert*-butylbenzyl as the substituent, CO_2 solubility coefficient was slightly higher than those bearing *n*-butyl substituent. This could be correlated to the comparatively looser chain packing in earlier case of PILs (judged by d_{sp} and density variations). For PILs based on a particular backbone (either PBI-BuI or PBI-HFA) and a substituent (*4-tert*-butylbenzyl or *n*-butyl), CO_2 sorption generally increased in the order of anion variation as $HFB^- \leq Tf_2N^- < I^- < BF_4^-$. The trend was correlated to the basicity of these anions. Among the two substituents, *4-tert*-butylbenzyl based PILs exhibited higher permeability than those based on *n*-butyl group. This was also explained with the chain packing as supported by d_{sp} and density. The PILs with Tf_2N^- and HFB^- as an anion showed higher gas permeability than those based on other anions. This was correlated to the Van der volume (Vw) of these anions. It was found that both, substituent as well as nature of the anion play a niche role in governing gas diffusion and sorption, thus overall permeability. The asymmetric type of substitution seems to be a welcome proposition towards enhancing permeability. The data demonstrated that P_{CO_2} in [DBzDMPBI-BuI][I] was 6 times higher than that of tetramethyl symmetrically substituted PIL, viz., [TMPBI-BuI][I].

With an objective to tune the diffusivity, and thereby permeability of these PIL family, bulky and rigid, polyaromatic hydrocarbons, viz., pyrene and anthracene were chosen with an anticipation that they would result in chain loosening of these PILs. The *N*-substitution was carried out with pyrenyl bromide/anthryl bromide, while *N*-quaternization was done with *4-tert* butyl benzyl bromide. The halide anion of these PILs was exchanged with two chosen anions, viz., Tf_2N^- and BF_4^-. The choice of these anions was based on our earlier findings of attractive CO_2 sorption-permeation properties while opting these anions. For PILs based on a particular substituent, *viz.* pyrenyl or anthryl, CO_2 sorption generally increased in the order of anion variation as $Tf_2N^- < Br^- < BF_4^-$. Those with Tf_2N^- as an anion showed higher gas permeability, while those possessing BF_4^- was dominating towards elevation in selectivity. Among the two substituents, pyrenyl group containing PILs exhibited higher permeability than those based on anthryl group containing PILs. It was found that both, the nature of the substituent as well as anion play a key role in governing gas diffusion and sorption, thus overall permeability. The combination of CO_2 specific anion coupled with higher free volume in PILs offered higher CO_2 permeability and comparable permselectivity than their structural analogue 'without IL functionality', viz., DBzPBI-BuI.

Owing to the presence of fluorescent pyrene and anthracene resultant PILs showed bright excimer emission which was found to be quenched by electron deficient nitroaromatics such as NB, TNT and PA in solution state. Fluorescence-quenching studies using self standing, solution-cast solid film of the PILs showed almost instantaneous and selective detection of the saturated vapors of NACs at ambient temperature and pressure. Fluorescence emission of PILs was rarely affected by the presence of commonly found interferences. This property is highly useful for constructing a working device for explosive vapor detection in presence of interfering agents. Pyrene containing PIL showed generally higher fluorescence quenching than the anthracene containing PIL, reflecting an improved affinity of the more electron-rich pyrene with NACs. Furthermore, fluorescence intensity could be recovered after the quenching, enabling the reuse of these films for NACs detection. The results suggest that both PILs are potential candidates for NACs sensing in presence of potential interferents of different nature.

PIL literature related to CO_2 sorption properties is frequently encountered by BF_4, Tf_2N and PF_6 as an anion. From our prior investigations, it was observed that both CO_2 specificity and bulk of the anion play important roles in governing CO_2 based transport properties. In the present work, five different anions, which are bulky in nature and are substituted analogues of BF_4^- anion were chosen for the iodide exchange in a PIL, [DBzDMPBI-BuI][I] as investigated in Scheme 1. In addition to their amorphous nature, these PILs showed higher d_{sp} and lower density than their precursor PIL. The thermal stability of present PILs was higher than that of the precursor PIL, [DBzDMPBI-BuI][I]. For present PILs, CO_2 sorption generally increased in the order of anion variation as Im_4B^-> $(CF_3)_2Ph\text{-}BF_3^-$ > $(CH_3)_3C\text{-}Ph\text{-}BF_3^-$> $(CF_3)_8Ph_4B^-$ > Ph_4B^-. The solubility coefficients were lower than their unsubstituted fluorinated anion, BF_4^-. Permeation analysis of only three PILs could be carried out as PILs with $(CF_3)_8Ph_4B^-$ and Ph_4B^- as the anion formed brittle films and could not withstand with the applied pressure. The maximum increase in permeability was 5 times for H_2 and 3 times for CO_2 for PIL containing $(CF_3)_2Ph\text{-}BF_3^-$ anion, than that of the precursor PIL possessing I^- anion. This result was also supported by higher diffusivity coefficients of these anion containing PILs, than their counterparts.

In order to increase the flux of these PIL membranes while maintaining their selectivity, Thin Film Composite (TFC) membranes were prepared. The separation performance of ethane-ethylene and propane-propylene was evaluated with both, the dense and TFC membranes. These TFC membranes were prepared using PSF based UF membrane as a structural support and polymeric ionic liquid (name here) as a selective layer. The effect of support layer porosity and concentration of coating layer were studied on the permeance of these membranes. The maximum selectivity of 3.6 and 10.5 was achieved for ethane-ethylene and propane-propylene gas pairs. Mixed gas permselectivity measurements showed lowering in selectivity due to competitive sorption and diffusion of two components. The comparison of single gas propane-propylene permselectivity was done with common glassy polymers. It was observed that propane-propylene selectivity of present PIL was superior to common glassy polymers such as polyphenylene oxide, ethyl cellulose, cellulose acetate and polysulfone; while it was comparable to the Matrimid. These results suggested that with optimization of PIL selective layer (lowering

of the thickness) in TFC membranes, PIL as a class of polymers can be potential candidate for olefin-paraffin separation.

This work initially established an understanding towards effects of substituent and anion variation on physical and gas sorption properties of PBI based PILs. In the case of glassy polymers, gas transport occurring through a solution-diffusion mechanism although provides a scope to tune diffusivity (by modifying the polymer chain/subgroup flexibility and free volume present in the polymer matrix); tuning solubility by manipulation of gas-polymer interaction has comparatively a little room. Present methodology of PBI based polymeric ionic liquids (PILs) provides a possibility for tuning not only the diffusivity (as they are based on rigid PBI backbone), but also the solubility of CO_2 due to the presence of IL character in them. This is evident from higher CO_2 permeability of many of the PILs than that of H_2, in spite of their glassy nature. The permeation properties can be further improved by judicious choice of substituent and anion, combinely. To expand applications for gas separation membranes, material research must not only identify attractive candidate polymers, but transformation of these materials into an industrially relevant form is equally important. The formation of PIL based TFC membrane thus opens up new avenue for practical applicability of these materials.

References

Aaron D., Tsouris C., *Sep. Sci. Technol.*, **2005**, 40, 321–348.

Abedini R., Nezhadmoghadam A., *Petroleum & Coal,* **2010**, 52(2) 69–80.

Aitken B.S., Lee M., Hunley M. T., Gibson H.W., Wagener K.B., *Macromolecules*, **2010,** 43, 1699–1701,

Aki S.N.V.K., Mellein B.R., Saurer E.M., Brennecke J.F., *J. Phys. Chem. B.,* **2004,** *108,* 20355–20365.

Baltus E., *Sep. Sci. Technol*, **2005,** 40, 525–541.

Bara J.E., Camper D.E., Gin D.L., Noble R.D., *Accounts Chem. Res.,* **2010,** 43, 1, 152–159.

Bara J.E., Carlisle T.K., Gabriel C.J., Camper D., Finotello A., Gin D.L., Noble R.D., *Ind. Eng. Chem. Res.,* **2009a,** 48, 2739–2751.

Bara J.E., Gabriel C.J., Hatakeyama E.S., Carlisle T.K., Lessmann S., Noble R.D., Gin D.L., *J. Membr. Sci.*, **2008b**, 321, 3–7.

Bara J.E., Gabriel C.J., Lessmann S., Carlisle T.K., Finotello A., Gin D.L., Noble R.D., *Ind. Eng. Chem Res.*, **2007a**, 46, 5380–5386.

Bara J.E., Gin D.L., Noble R.D., *Ind. Eng. Chem. Res.,* **2008d,** 47, 9919–9924.

Bara J.E., Hatakeyama E.S., Gabriel C.J., Zeng X., Lessmann S., Gin D.L., Noble R.D., *J. Membr. Sci.*, **2008a**, 316, 186–191.

Bara J.E., Hatakeyama E.S., Gin D.L., Noble R.D., *Polym. Adv. Technol.,* **2008c**, 19, 1415–1420.

Bara J.E., Lessmann S., Gabriel C.J., Hatakeyama E.S., Noble R.D., Gin D.L., *Ind. Eng. Chem. Res.* **2007b,** 46, 5397–5404.

Bara J.E., Noble R.D., Gin D.L., *Ind. Eng. Chem. Res.,* **2009b,** 48, 4607–4610.

Barbari T.A., Koros W.J., Paul D.R., *J. Membr. Sci.*, **1989**, 42, 69–86.

Barbari T.A., Koros W.J., Paul D.R., *J. Polym. Sci., Part B: Polym. Phys.,* **1988**, 26, 729–744.

Barrer R.M., *Trans Faraday Sci.*, **1939**, 35, 628–643.

Bates E.D., Mayton R.D., Ntai I., Davis J.H., *J. Am. Chem.* Soc., **2002**, 124, 926–927.

Beichel W., From the Crystal Structures of Organic Salts to Consistent Ion Volumes and their Charge Distribution, *Ph.D. dissertation*, **2013**, The Albert-Ludwigs-Universität Freiburg, Germany.

Bellamy L. J, Gerrardm W., F. Lapperta, Williams R. L. *J. Chem. Soc.,* **1958**,481, 2412-2415.

Bernardo P., Clarizia G., *Chem. Eng. Trans*., **2013**, 32, 1999–2004.

Bernardo P., Drioli E., Golemme G., *Ind. Eng. Chem. Res.* **2009,** 48, 4638–4663.

Beyazkilic P., Yildirim A., Bayindir M., *Appl. Mater. Interfaces*, **2014**, 6, 4997−5004.

Bhavsar R. S., Kumbharkar S. C., Kharul U. K., *J. Membr. Sci*., **2012,** 389, 305– 315.

Bhavsar R. S., Kumbharkar S. C., Rewar A.S, Kharul U. K., *Poly. chem*., **2014a**, 5, 4083-4096.

Bhavsar R. S., Kumbharkar S. C., Kharul U. K., *J. Membr. Sci*., **2014b**, 470,494–503

Bhole Y.S., Karadkar P.B., Kharul U.K., *Euro. Poly. Jour.,* 2007, 43, 1450–1459.

Blanchard L. A., Hancu D., Beckman E. J., Brennecke J. F., *Nature*, **1999**, 399, 28–29.

Bondi A., *J. Phys. Chem.*, **1964**, 68, 441–451.

Browall R. W., Salemme R. M., *US patent*, **1975**, USP 3874986.

Brunetti A., Scura F., Barbieri G., Drioli E., *J. Membr. Sci*., **2010**, 359, 115–125.

Cabusas M.E.Y., *Ph.D. dissertation*, 1998, Virginia Polytechnic Institute and State University, Blacksburg, Virginia.

Cadena C., Anthony J. L., Shah J. K., Morrow T. I., Brennecke J. F., Maginn E. J., *J. Am. Chem.* Soc., **2004**, 126, 5300–5308.

Car A., Stropnik C., Yave W., Peinemann K.V., *J. Membr. Sci*., **2008**, 307, 88–95.

Carlisle T.K., Bara J.E., Lafrate A. L., Gin D. L., Noble R.D., *J. Membr. Sci*., **2010**, 359, 37–43.

Carlisle T.K., Nicodemus G.D., Gin D.L., Noble R.D., *J. Membr. Sci*., **2012**, 397–398, 24–37.

Carlisle T.K., Wiesenauer E.F., Nicodemus G.D., Gin D.L., Noble R.D., *Ind. Eng. Chem. Res.,* **2013**, 52, 1023−1032.

Chen H., Kovvali A. S., Majumdar S., Sirkar K. K., *Ind. Eng. Chem. Res.* **1999,** 38, 3489-3498.

Chen H., Sun H., Zheng M., Jia Q., Wanhai Dang, *Poly. Bull.,* **2006**, 56, 221–227.

Chern R.T., Sheu F.R., Jia L., Stannett V.T. H.B. Hopfenberg, *J. Membr. Sci*., **1987,** 35,103-115.

Chi W.S., Hong S.U., Jung B., Kang S.W., Kang Y.S., Kim J. H., *J. Membr. Sci*., **2013**, 443, 54–61.

Chinn D., Vu Q., Driver, Boudreau, *US patent,* **2006**, USP 7527775B2.

Chung T.S., Ren J., Wang R., Li D.F., Liu Y., Pramoda K.P., Cao C., Loh W.W., *J. Membr. Sci.*, **2003**, 214, 57–69.

Cizek E. P., Arbor A., Mich, *US patent,* **1967**, USP 3383435.

Costello L.M., Koros W.J., *J. Polym. Sci.; Part B: Polym. Phys.*, **1994**, 32, 701–713.

D'Alessandro D.M., Smit B., Long J.R., *Angew. Chem. Int. Ed*., **2010**, 49, 6058–6082.

de Sales J.A., Patrício P.S.O., Machado J.C., Silva G.G., Windmöller D., *J. Membr. Sci.*, **2008**, 310, 129 - 140.

Demirel G. B., Daglarac B., Bayindir M., *Chem. Commun.,* **2013,** 49, 6140-6142.

Desmonts L.B., Reinhoudt D. N., Crego-Calama M., *Chem. Soc. Rev.,* **2007**, 36, 993–1017.

Dhirendra K., Justin Thomas K.R. *J. Photochem. Photobiol., A,* **2011**, 218, 162.

Donaldson T. L., Nguyen Y. N., *Ind. Eng. Chem. Fundam,*. **1980**, 19, 260-266.

Dortmundt, D. and K. Doshi, "Recent Developments in CO_2 Removal Membrane Technology," *UOP LLC*, Des Plaines, Illinois, **1999**.

Fallanza M., Ortiz A., Gorri D., Ortiz I., *J. Membr. Sci.„* **2013***,* 444, 164–172.

Fang W., Luo Z., Jiang J., *Phys. Chem. Chem. Phys.,***2013**, 15, 651–658.

Forzani E. S., Lu D., Leright M. J., Aguilar A. D., Tsow F., Iglesias R. A., Zhang Q., Lu J., Li J., Tao N., *J. Am. Chem. Soc.,* **2009**, 131, 1390-1396.

Gang H., Yan N., Yang J., Wang H., Ding L., Yin S., and Fang Y., *Macromolecules,* **2011**, 44, 4759-4766.

Ghosal K., Chern R.T., Freeman B.D., Daly W.H., Negulescu I.I., *Macromolecules,* **1996,** 29, 4360–4369.

Ghosal K., Chern R.T., Freeman B.D., *J. Polym. Sci. Polym. Phys,* **1993,** 31, 891–893.

Ghosal K., Freeman B.D., *Polym. Adv. Technol.*, **1994**, 5, 673–697.

Gole B., Shanmugaraju S., Bar A., Mukherjee P., *Chem. Commun.,* **2011**, 47, 10046.

Goldberg D.E., Genetic algorithms in search, optimization and machine learning, Addison-Wesley, Reading, MA **1989**.

Goodpaster J. V, Harrison J. F, McGuffin V. L., *J. Phys. Chem. A,* **2002**, 106, 10645.

Green O., Grubjesic S., Lee S., Firestone M.A., *J. Macromol. Sci. C. Polym. Reviews*, **2009**, 49, 339–360.

Gülmüs S.A., Yilmaz L., *J. Polym. Sci.; Part B: Polym. Phys.*, **2007**, 45, 3025–3033.

Guo L., Zu B., Yang Z., Cao H., Zheng X., Dou X., *Nanoscale*, **2014**, 6, 1467-1473.

Guo R., McGrath J. E. Aromatic polyethers, polyetherketones, polysulfides, and polysulfones. In: Matyjaszewski K, Möller M, editors. Polymer science: a comprehensive reference, vol. 5. Amsterdam: Elsevier BV; **2012**, 377-430.

Gurkan B., Goodrich B. F., Mindrup E. M., Ficke L. E., Massel M., Seo S., Senftle T. P., Wu H., Glaser M. F., Shah J. K., Maginn E. J., Brennecke J. F., Schneider W. F., *J. Phys. Chem. Lett.* **2010**b, 1, 3494–3499.

Gurkan B.E., de la Fuente J.C., Mindrup E.M., Ficke l.E., Goodrich B.F., Price E.A., Schneider W.F., Brennecke J.F., *J. Am. Chem.* Soc., **2010a**, 132, 2116–2117.

Hacarlioglu P., Toppare L., Yilmaz L., *J Appl. Polym. Sci.*, **2003**, 90, 776–785.

Hakonen A., Hulth S., *Analytica chimica acta*, **2008**, 606, 63.

Hamad F., Khulbe K. C., Matsuura T., *Desalination,* **2002,** 148, 369-375.

Hao L., Li P., Yang T., Chung T.S., *J. Membr. Sci.*, **2013**, 436, 221–231.

Hay A.S., Blanchard H.S., Endres G. F., Eustance J. W. *J. Am. Chem.* Soc, **1959**, 8, 6335-6336.

Hay A.S., Schenectaddy N. Y., *US patent,* USP 3306875.

He Y., Inoue Y., *Polym. Int.*, **2000**, 49, 623–626.

Henis J. M. S., Tripodi M. K., *US patent,* USP 4230463.

Houghton J.T., Climate Change 2001: The Scientific Basis, Cambridge University Press, Cambridge, 2001, Page No.-13.

Hu C.C., Chang C.S., Ruaan R.C., Lai J.Y., *J. Membr. Sci.*, **2003**, 226, 51–61.

Hu X., Tang J., Blasig A., Shen Y., Radosz M., *J. Membr. Sci.*, **2006**, 281, 130–138.

Huang Y., Paul D. R., *Ind. Eng. Chem. Res.* **2007,** 46*,* 2342-2347.

Hudiono Y.C., Carlisle T.K., LaFrate A.L., Gin D.L., Noble R.D., *J. Membr. Sci.*, **2011**, 370, 141–148.

Jeffery G.H., Bassett J., Mendham J., Denney R.C., Vogel's Textbook of Quantitative Chemical Analysis, *British Library Cataloguing in Publication Data*, 5th edn, **1989**.

Julian H., Wenten I.G., *IOSR Journal of Engineering,* **2012**, 2, 484-495.

Kalyanasundaram K., Thomas J. K., *J. Am. Chem. Soc,* **1977**, 99, 2039-2044.

Kanehashi S., Nagai K., *J. Membr. Sci.*, **2005**, 253, 117–138.

Karadkar P.B., Kharul U.K., Bhole Y.S., Badhe Y.B., Tambe S.S., Kulkarni B.D., *J. Membr. Sci.*, **2007**, 303, 244–251.

Kharul U. K., Kulkarni S. S., *Macromol. Chem. Phys.,* 199, **1998,** 1379-1386

Khulbe K. C., Hamad F., Feng C., Matsuura T., Gumi T., Palet C., *Sep. Pur. Technol*., **2004**, 36, 53–62.

Khulbe K. C., Matsuura T., Lamarche G., Kim H.J., *J. Membr. Sci.*, **1997**, 135, 211–223.

Kim T. H., Koros W.J., Husk G.R., *J. Membr. Sci.*, **1988**, 37, 45–62.

Kim T. H., Koros W.J., Husk G.R., *J. Membr. Sci.*, **1989**, 46, 43–56.

Koros W. J., Paul D. R., *J. Polym. Sci., Polym. Phys.,* **1976**, 14, 1903–1907.

Koros W.J., Coleman, Walker D. R. B, *Annu. Rev. Mater. Sci.,* **1992,** 22, 47-89

Koros W.J., Hellums M. W., *Fluid Phase Equilibria,* **1989**, 53, 339–354.

Koros W.J., *J. Polym. Sci., Polym. Phys*, **1985**, 23, 1612–1628.

Koros W.J., Mahajan R., *J. Membr. Sci.*, **2000**, 175, 181–196.

Kumbharkar S.C., Bhavsar R. S., Kharul U.K., *RSC Adv.,* **2014**, 4, 4500-4503.

Kumbharkar S.C., Karadkar P.B., Kharul U.K., *J. Membr. Sci.*, **2006**, 286, 161–169.

Kumbharkar S.C., Kharul U.K., *Eur. Polym. J.,* **2009b**, 45, 3363–3371.

Kumbharkar S.C., Kharul U.K., *J. Membr. Sci.*, **2010**, 357, 134–142.

Lee J. H., Kang S. W., Song D., Wond J., Kang Y. S., *J. Membr. Sci.*, **2012**, 424, 159–164.

Lee K.J., Jho J.Y., Kang Y.S., Dai Y., Robertson G.P., Guiver M.D., Won J., *J. Membr. Sci.*, **2003**, 212, 147–155.

Li J.L., Chen B.H., *Sepn. Purif. Technol.*, **2005**, 41, 109–122.

Li J.R., Kuppler R.J., Zhou H.C., *Chem. Soc. Rev*., **2009**, 38, 1477–1504.

Li P., Coleman M.R., *Eur. Polym. J*., **2013**, 49, 482–491.

Li P., Paul D.R., Chung T.S., *Green Chem*., **2012**, 14, 1052–1063.

Li P., Pramoda K.P., Chung T.S., *Ind. Eng. Chem. Res*., **2011**, 50, 9344–9353.

Li P., Zhao Q., Anderson J.L., Varanasi S., Coleman M.R., *J. Polym. Sci. A. Polym. Chem*., **2010**, 48, 4036–4046.

Liu Y., Pan C.Y., Ding M.X., Xu J.P., *J. Appl. Polym. Sci.*, **1999**, 73, 521–526.

Liu Y., Wang R., Chung T.S., *J. Membr. Sci.„* **2001***,* 189, 231–239.

Lu J., Yan F., Texter J., *Prog. Polym. Sci*., **2009**, 34, 431–448.

MacFarlane D.R., Pringle J.M., Johansson K.M., Forsyth S.A., Forsyth M., *Chem. Commun*., **2006**, 1905–1917.

MacFarlane D.R., Tachikawa N., Forsyth M., Pringle J.M., Howlett P.C., Elliott G.D., Davis J.M., Watanabe M., Simon P., Angell C.A., *Energy Environ. Sci*., **2014**, 7, 232–250.

Manez R., Sanceno´n F., *Chem. Rev.,* 2003**, 103***,* 4419.

McDonald T. O., Akhtar R., Lau C. H., Ratvijitvech T., Cheng G., Clowes R., Adams D. J., Hasella T., Coopera A. I., *J. Mater. Chem. A,* **2015**, 3, 4855-4864.

McHattie J.S., Koros W.J., Paul D.R., *Polymer*, **1991a**, 32, 840–850.

McHattie J.S., Koros W.J., Paul D.R., *Polymer*, **1991b**, 32, 2618–2625.

McHattie J.S., Koros W.J., Paul D.R., *Polymer*, **1992**, 33, 1701–1711.

Mecerreyes D., *Prog. Polym. Sci*. **2011**, 36, 1629–1648.

Metz B., Davidson O., Coninck H.D., Loos m., Meyer L., IPCC Special Report on Carbon Dioxide Capture and Storage, Cambridge University Press, Cambridge, **2005**.

Mikkola J.P., *Chem Sus Chem*, **2013**, 6, 1500–1509.

Musto P., Karaszt F.E., MacKnight W.J., *Polymer*, **1993**, 34, 14, 2934–2945.

Naddo T., Che Y., Zhang W., Balakrishnan K., Yang X., Yen M., Zhao J., Moore J., Zang L., *J. Am. Chem. Soc*., **2007**, 129, 6978-6979.

Ostmark H., Wallin S., Ang H. G., *Propellants Explos. Pyrotech.,* **2012**, 37, 12 – 23.

Park J.Y., Paul D.R., *J. Membr. Sci.„* **1997**, 125, 23–39.

Payagala T., Huang J., Breitbach Z.S., Sharma P.S., Armstrong D. W., Chem. Mater. 19 (2007) 5848–5850.

Peter J., Peinemann K.V., *J. Membr. Sci.„* **2009**, 340, 62–72.

Petkovic M., Seddon K.R., Rebeloa L.P.N., Pereira C. S., *Chem. Soc. Rev.,* **2011**, 40, 1383–1403

Ponnu A., Anslyn E., *Supramolecular Chemistry*, **2010**, 22, 65-71.

Powell C.E., Qiao G.G., *J. Membr. Sci.*, **2006,** 279, 1–49.

Privalova E.I., Karjalainen E., Nurmi M., Arvela P.M., Ernen K., Tenhu H., Murzin D.Y., Puleo A.C., Paul D.R., *J. Membr. Sci.*, **1989,** 47, 301-332.

Quéré C. Le., Earth Syst. Sci. Data, **2015**, 7, 349–396.

Rabbani M. G., Sekizkardes A. K., El-Kadri O. M., Kaafarani B. R., El-Kaderi H. M., *J. Mater. Chem.*, **2012**, 22, 25409-25417.

Rahman M. H., Siaj M., Larachi F., *Chem. Eng. Process.*, **2010**, 49, 313–322.

Ramdin M., de Loos T. W., Vlug T. J. H., *Ind. Eng. Chem. Res*., **2012**, 51, 8149–8177.

Robeson L.M., *J. Membr. Sci.*, **1991**, 62, 165–185.

Robeson L.M., *J. Membr. Sci.*, **2008**, 320, 390–400.

Rocha M. A. A., Neves C. M. S. S., Freire M.G., Russina O., Triolo A., Coutinho J. A. P., Santos M. N. B. F., J. Phys. Chem. B. 117 (2013) 10889–10897.

Sacristan J., Mijangos C., *Macromolecules,* **2010**, 43, 7357–7367.

Sanders D.F., Smith Z.P., Guo R., Robeson L.M., McGrath J.E., Paul D.R., Freeman B.D., *Polymer*, **2013**, 54, 4729–4761.

Scholes C.A., Kentish S.E., Stevens G.W., *Recent Patents on Chem. Eng.,* **2008**, 1, 52–66.

Sekizkardes A. K., ˙Islamo˘glu T., Kahveci Z., El-Kaderi H.M., *J. Mater. Chem. A*, **2014**, 2, 12492-12500.

Shaligram S. S., Wadgaonkar P. P., Kharul U. K., *J. Mater. Chem. A*, **2014**, 2, 13983-13989.

Shanmugaraju S., Joshi S. A., Mukherjee P. S., *J. Mater. Chem. A*, **2011**, 21, 9130-9138.

Shao L., Low B.T., Chung T.S., Greenberg A.R., *J. Membr. Sci.*, **2009,** 327, 18–31.

Shekhawat D., Luebke, Shiflett M.B., Kasprzak D.J., Junk C.J., Yokozeki A., *J. Chem. Thermodynamics*, **2008**, 40, 25–31.

Shellaiah M., Wu Y., Singh A., Raju M., Lin H., *J. Mater. Chem. A*, **2013**, 1, 1310-1318.

Shiflett M.B., Drew D.W., Cantini R.A., Yokozeki A., *Energy Fuels*, **2010**, 24, 5781–5789.

Shishatskii A.M., Yu. P. Yampol'skii, Peinemann K.V., *J. Membr. Sci.*, **1996,** 112, 275–285.

Silverstein R.M., Spectrometric Identification of Organic Compounds, *John Wiley and Sons Inc.,* New York, 4th edn, **1981**.

Sridhar S., Smitha B., Aminabhavi T. M., *Sep. Pur. Reviews*, **2007**, 36, 2, 113–174,

Stern S.A., Gareis P.J., Sinclair T.F., Mohr P.H., *J. Appl. Polym. Sci.*, **1963**, 7, 2035–2051.

Stern S.A., *J. Membr. Sci.,* **1994,** 94, l–65.

Stern S.A., Mi Y., Yamamoto H., St. Clair A.K., *J. Polym. Sci. Polym. Phys. Ed.*, **1989**, 27, 1887–1909.

Suarez P.A.Z., Dullius J.E.L., Einloft S., De Souza R.F., Dupont J., *Polyhedron*, **1996**, 15, 7, 1217–1219.

Supasitmongkol S., Styring P., *Energy Environ. Sci*., **2010**, 3, 1961–1972.

Swaidan R. J., Ghanem B., Swaidan R., Litwiller E., Pinnau I., *J. Membr. Sci.*, **2015,** 492, 116–122.

Swaidan R. J., Xiaohua M., Litwiller E., Pinnau I., *J. Membr. Sci.*, **2015,** 495, 235–241.

Tang H., Tang J., Ding S., Radosz M., Shen Y., *J. Polym. Sci. A. Polym. Chem*., **2005c**, 43, 1432–1443.

Tang J., Shen Y., Radosz M., Sun W., *Ind. Eng. Chem. Res.,* **2009,** 48*,* 9113–9118.

Tang J., Sun W., Tang H., Radosz M., Shen Y., *Macromolecules*, **2005e**, 38, 2037–2039.

Tang J., Tang H., Sun W., Plancher H., Radosz M., Shen Y., *Chem. Commun.*, **2005a**, 3325–3327.

Tang J., Tang H., Sun W., Radosz M., Shen Y., *J. Polym. Sci. A. Polym. Chem*., **2005b**, 43, 5477–5489.

Tang J., Tang H., Sun W., Radosz M., Shen Y., *Polymer*, **2005d**, 46, 12460–12467.

Teramoto M., Nakai K., Ohnishi N., Huang Q., Watari T., Matsuyama H., *Ind. Eng. Chem. Res.* **1996,** 35*,* 538-545.

Thomas W., *Chem Rev.*, **1999**, 99, 2071–2083.

Thran A., Kroll G., Faupel F. *J. Polym. Sci. B. Polym. Phys.*, 37, **1999**, 3344–3358.

Tome´ L.C., Freire C.S.R., Mecerreyes D., Marrucho I.M., *J. Membr. Sci.„* **2015**, 483, 155-165.

Tome´ L.C., Mecerreyes D., Freire C.S.R., Rebelo L.P.N., Marrucho I.M., *J. Membr. Sci.,* **2013**, 428, 260–266.

Tome´ L.C., Mecerreyes D., Freire C.S.R., Rebelo L.P.N., Marrucho I.M., *J. Mater. Chem. A,* **2014**, 2, 4855-4864.

Tsujita Y., *Prog. Polym. Sci.*, **2003**, 28, 1377–1401.

Victor J.G., Torkelson J.M., *Macromolecules,* **1987,** 20, 2241–2250.

Vieth W.R., Howell J.M., Hsieh J.H., *J. Membr. Sci.,* **1976**, 1, 177–220.

Wang C., Luo X., Luo H., Jiang D., Li H., Dai S., *Angew. Chem. Int. Ed.,* **2011**, 50, 4918–4922.

Wang G.N., Dai Y., Lu J.F., Xiao F., Wu Y.T., Zhang Z.B., Zhou Z., *J. Molecular Liquids*, **2012**, 168, 17–20.

Wang J. S., Naito Y., Kamiya Y., *J. Polym. Sci. B. Polym. Phys.,* **1996**, 34, 2027–2033.

Wijmans J.G., Baker R.W., *J. Membr. Sci.,* **1995**, 07, 1–21.

Wilke A., Yuan J., Antonietti M., Weber J., *ACS Macro Lett.,* **2012**, 1, 1028–1031.

Winnik F. M., *chem. Rev.,* **1993**, 93, 587-414.

Wonders A. G., Paul D.R., *J. Membr. Sci.,* **1979**, 5, 63–75.

Xiao Y., Low B. T., Hosseini S. S., Chung T. S., Paul D. R., *Prog. Polym. Sci*. **2009a**, 34, 561–580.

Xiao D., Hines Jr. L. G., Li S., Bartsch R. A., Quitevis E. L., *J. Phys. Chem. B*, **2009b,** 113 6426–6433.

Xu G., Liang F., Yang Y., Hu Y., Zhang K., W. Liu, *Energies,* **2014**, 7, 3484-3502.

Yamaguchi T., Koval C. A., Noble R. D., Bowman C. N., *Chem. Engg. Sci.,* 51, **1996,** 4781-4789.

Yampolskii Y. P., Korikov A. P., Shantarovich V. P., Nagai K., Freeman B. D., T. Masuda, Teraguchi M., Kwak G., *Macromolecules,* **2001,** 34*,* 1788-1796.

Yang J. S., Swager T. M., *J. Am. Chem. Soc.* **1998,** *120,* 11864-11873.

Yave W., Car A., Funari S.S., Nunes S.P., Peinemann K.V., *Macromolecules*, **2010**, 43, 326–333.

Yu H., Wu Y., Jiang Y., Zhou Z., Zhang Z., N. J. Chem. 33 (2009) 2385–2390.

Yuan J., Antonietti M., *Polymer*, **2011**, 52, 1469–1482.

Yuan J., Mecerreyes D., Antonietti M., *Prog. Polym. Sci.* **2013**, 38, 1009–1036.

Zampini A., Malon R. F., *US patent,* **1984,** USP 4468501.

Synopsis of the Thesis to be submitted to the Academy of Scientific and Innovative Research for Award of the Degree of Doctor of Philosophy in Chemistry	
Name of the Candidate	Ms. Sayali Vinayak Shaligram
Degree Enrolment No. & Date	Ph. D in Chemical Sciences (10CC11J26057); January 2011
Title of the Thesis	Polymeric Ionic Liquids based on Asymmetrically *N*-Substituted Polybenzimidazoles for Gas Permeation Studies
Research Supervisor	Dr. Ulhas K. Kharul (AcSIR, CSIR-NCL, Pune)

Introduction

Global warming caused by increasing amounts of greenhouse gases (GHGs) in the atmosphere is one of the major concerns for the 21st century and carbon dioxide is responsible for most of changes in the Earth's radiation balance [1]. Current technologies to separate CO_2 include adsorption, absorption, cryogenic and membrane separation. Inherent advantages of membrane based separation including low energy consumption, easy scale up, environmentally benign and ease to be incorporated with existing processes [1]. The CO_2 separation through polymeric membranes is largely governed by its interactions with the membrane material. Sanders et al. (2013), have noted that polymers offering the best combinations of gas selectivity and permeability are generally glassy in nature and have rigid structures that exhibit poor chain packing [2]. Since gas transport in polymers occurs through a solution-diffusion mechanism, diffusivity of penetrants can be tuned by modifying the polymer chain and subgroup flexibility, as well as free volume present in the polymer structure [3]. On the other hand, gas solubility can be tuned by gas-polymer interactions.

Statement of Problem

Polymeric ionic liquids (PILs) are a new class of functional materials that combine the chemistry of ionic liquids (ILs) with the macromolecular architecture of polymers [4,5], providing an opportunity to create a new platform for the design of IL-based materials for CO_2 separation membranes possessing required mechanical stability. Although high benefits are anticipated out of PILs, those possessing aliphatic backbone are mechanically weak [5,6] and are unable to be transformed into a film (membrane)

form for the practical separation purposes. To circumvent this issue, we have recently demonstrated an altogether different methodology for obtaining film forming PILs possessing rigid and fully aromatic backbone [7]. The *N*-quaternization of glassy polybenzimidazoles (PBIs) offered excellent mechanical properties to these PILs. However, in order to bring potentials of PILs to practice, there is a need of better understanding of structure-property relationship, which would offer insight towards new material development and address present drawbacks of lower permeability of this new family of materials.

Aims and objectives

The overall aim of present work was to develope an understanding towards gas sorption and permeation in PILs based on asymmetrically *N*-substituted PBI. It was addressed through following objectives while investigating their gas sorption, permeability, selectivity and physica properties that are known to affect gas permeation properties.

1) To investigate effects of systematic variations in '*N*-substituent' in PBI-based PILs..
2) To investigate effects of incorporation of rigid polyaromatic groups (pyrene, anthracene).
3) To investigate effects of bulky anions in PILs.
4) To prepare Thin Film Composite (TFC) membranes based on PILs as a selective layer.

Methodology

1) Polybenzimidazoles based on 3,3'-diaminobenzidine and suitably chosen aromatic dicarboxylic acids were synthesized by solution polycondensation method.
2) Asymmetrically *N*-substituted PILs were synthesized in two steps. The first step involved *N*-substitution by alkyl group and in second step *N*-quaternization by another alkyl group.
3) Demonstrate potentials of PILs towards practical application by making TFC membranes on porous polysulfone as the support and selected PIL as a top thin skin.

Sample results

Scheme 1: *Variations in 'N-substituent' of PILs in an asymmetric manner: Investigations on physical and gas permeation properties*

PILs with substitution asymmetry were synthesized and the iodide anion of formed PILs was exchanged with chosen anions (BF_4^-, Tf_2N^- and HFB^-). This work shed light on effects of substituents and anions on physical and gas permeation properties of PILs possessing substitution asymmetry. This proposition was found ot be highly constructive towards enhancing permeability (e.g. P_{CO_2} in [DBzDMPBI-BuI][I] was 6 times higher than symmetrically substituted [TMPBI-BuI][I]). Many of the PILs showed higher permeability for CO_2 than that of H_2, typically known as '*Reverse Selectivity*'. This was the highlighted outcome of the asymmetric type of substitution in PBI based PILs.

Scheme 2: *Incorporation of rigid polyaromatic substituents in PBI based PILs: Effects on gas permeation and nitroexplosive detection properties*

Pyrene and anthracene functionalized PILs were synthesized and effects of these rigid polyaromatic groups on gas permeation properties of formed PILs are investigated. Pyrene substituted PIL exhibits ~10 fold increase in CO_2 permeability than its precursor polybenzimidazole and ~2 fold increase than its methyl substituted analogue with appreciable CO_2 based permselectivity. Formed PILs were also evaluated for their nitrozromatic (explosive) sensing ability through quenching of fluorescence intensity. PIL films showed almost instantaneous and selective detection of the saturated vapors of NACs at ambient temperature and pressure.

Scheme 3: *Effect of bulky anions on physical and Gas Permeation Properties of PILs based on PBI*

The iodide anion of a PIL, viz., [DBzDMPBI-BuI][I] investigated in scheme 1 was exchanged with the systematically selected bulky anions, with an anticipation of increase in free volume of resulting PILs. The proposition offered increase in permeability by 5 times for H_2 and 3 times for CO_2 in a PIL containing $(CF_3)_2Ph\text{-}BF_3^-$ anion than that of the precursor PIL with I^- anion, conveying success of the adopeted methodology.

Scheme 4: *Thin Film Composite (TFC) membranes based on polymeric Ionic Liquid selective layer for gas separation*

This part of the work was aimed at investigating gas permeance and selectivity of TFC membranes prepared using PSF based UF membrane as a structural support and polymeric ionic liquid (PIL) as a selective layer. In addition to CO_2 separation, these membranes were also evaluated for their performance for olefin-paraffin separation. The selectivity of 3.6 and 10.5 was achieved for ethane-ethylene and propane-propylene gas

pairs. The propane-propylene permselectivity was superior to common glassy polymers such as PPO, EC and PSF.

References

[1] D. Shekhavat, *et al*., *a topical report*, DOE/NETL-2003/1200 (2003).
[2] D. F. Sanders, *et al*., *Polymer* **54** (2013) 4729–4761.
[3] P. Li, *et al*., *Ind. Eng. Chem. Res.* **50** (2011) 9344–9353.
[4] D. Mecerreyes, *et al*., *Progr. Polym. Sci.* **36** (2011) 1629–1648.
[5] J. Tang, *et al*., *Macromolecules* **38** (2005) 2037–2039.
[6] J. E. Bara, *et al*., *Ind. Eng. Chem. Res.* **316** (2008) 186–191.
[7] R. S. Bhavsar, *et al*., *Jour. membr. sci*, **470** (2014) 494–503.

Publications

- **Sayali Shaligram**, Prakash P. Wadgaonkar and Ulhas K. Kharul*, Fluorescent Polymeric Ionic Liquids for the Detection of Nitroaromatic Explosives, **Journal of Materials Chemistry A**, 2, 13983–13989 (2014).

- **Sayali Shaligram**, Prakash P. Wadgaonkar and Ulhas K. Kharul*, Polybenzimidazole-based polymeric ionic liquids (PILs): Effects of 'substitution asymmetry' on CO_2 permeation properties, **Journal of Membrane Science**, 493, 403–413 (2015).

- **Sayali Shaligram**, Anita Rewar, Prakash P. Wadgaonkar and Ulhas K. Kharul*, Incorporation of rigid polyaromatic groups in polybenzimidazole-based polymeric ionic liquids: Assertive effects on gas permeation properties, **Polymer,** 93, 30-36 (2016).
- Anita Rewar, **Sayali Shaligram** and Ulhas K. Kharul*, Polybenzimidazole based polymeric ionic liquids possessing partial ionic character: Effects of anion exchange on their gas permeation properties, **Journal of Membrane Science**, 497, 282–288 (2016).
- **Sayali Shaligram**, Prakash P. Wadgaonkar and Ulhas K. Kharul*, Polybenzimidazole-based polymeric ionic liquids (PILs): Effects of bulky anions on physical and gas permeation properties, *To be submitted*
- **Sayali Shaligram**, Prakash P. Wadgaonkar and Ulhas K. Kharul*, Polymeric ionic liquid membranes for separation of olefin/paraffin mixtures, *To be submitted*

Patent

- Ulhas Kharul, **Sayali Shaligram**, Prakash Wadgaonkar, Synthesis, Gas separation and Fluorescence properties in a Polybenzimidazole based Poly(ionic liquid)s with pyrene and anthracene fluorophores, Application number: PCT/IN2015/050013.

Presentations in conferences

- **Sayali Shaligram**, Prakash Wadgaonkar, Ulhas Kharul - Polymeric Ionic Liquids (PILs) possessing Substitution Asymmetry: Assertive Effects on Gas Permeation

Properties, Oral presentation at *International Conference on Membranes* held at M. G. University, Kerala; 23 -26 Aug. 2015.

- **Sayali Shaligram**, Prakash Wadgaonkar, Ulhas Kharul - Polymeric ionic liquid (PIL) films for the detection of nitroaromatic explosive vapors, *Best poster award from Royal Society of Chemistry* at International Conference on Membrane based Separations (MEMSEP-2015) held at the M. S. University of Baroda, Vadodara during March 21-23, 2015.
- **Sayali Shaligram**, Prakash Wadgaonkar, Ulhas Kharul - Polymeric Ionic Liquids (PILs) possessing Substitution Asymmetry: synthesis and gas permeation studies. Poster presentation at *International Conference on Membranes* held at M. G. University, Kerala; 3 -6 Oct. 2013.